August 2005

Prediction of climate change impacts on Alpine discharge regimes under A2 and B2 SRES emission scenarios for two future time periods

BFE
OFEN
UFE
SFOE

Auftraggeber:
Bundesamt für Energie BFE, 3003 Bern

Auftragnehmer:
EPFL, Laboratoire Hydrologie et Aménagements (HYDRAM), Lausanne

Autoren:
Pascal Horton
Bettina Schaefli
Abdelkader Mezghani
Benôit Hingray
André Musy

Diese Studie wurde im Rahmen des Forschungsprogramms „Energiewirtschaftliche Grundlagen" des Bundesamts für Energie BFE erstellt. Für den Inhalt ist allein der/die Studiennehmer/in verantwortlich.

Bundesamt für Energie BFE
Worblentalstrasse 32, CH-3063 Ittigen · Postadresse: CH-3003 Bern
Tel. 031 322 56 11, Fax 031 323 25 00 · office@bfe.admin.ch · www.ewg-bfe.ch

Executive summary

The present work analyzes the climate change impacts on the runoff regimes of mountainous catchments in the Swiss Alps having current glaciation rates between 0 and 50 %. The hydrological response of 11 catchments to a given climate scenario is simulated through a conceptual, reservoir-based precipitation-runoff transformation model called GSM-SOCONT (Schaefli, 2005). For the glacierized catchments, the glacier surface corresponding to this future scenario is updated through a conceptual glacier surface evolution model. The analyzed climate change scenarios were derived from 19 climate experiments obtained within the EU research project PRUDENCE (Christensen et al. 2002). They are the results of 9 state-to-the-art Regional Climate Models (RCMs) driven by three coupled Atmosphere-Ocean General Circulation Models (AOGCMs), respectively HadCM3/HadAM3H, ECHAM4/OPYC3 and ARPEGE. The two first families of climate change scenarios correspond to changes in seasonal temperatures and precipitations simulated for the period 2070-2099 under the two green house gas emission scenarios A2 and B2 defined by the Intergovernmental Panel on Climate Change (12 experiments are available for A2 and 7 for B2). From the 19 PRUDENCE experiments 19 climate changes scenarios were additionally developed for a transient period (2020-2049) corresponding in first approximation to a global warming scenario of +1°C.

Impacts of climate changes on annual discharges and hydrological regimes

For most climate change projections and most studied catchments, the mean annual runoff is expected to undergo a significant decrease (Table I). This is first due to the significant decrease expected for mean annual precipitation. This is next induced by the substantial increase in seasonal temperatures. As a result the glacier surfaces will decrease leading to an important increase of evapotranspiration through the increase of the catchment area subject to evapotranspiration. Regional warming of future climate additionally enforces the total evapotranspiration on ice-free areas and accordingly, all catchments are expected to show a strong increase of total evapotranspiration.

Table I: Predicted change (%) of the annual runoff for the +1°C, the B2 and the A2 scenarios. Minimum, median and maximum values of the 19, 7 respectively 12 PRUDENCE RCM experiments available for +1°C (2020-2049), B2 (2070-2099) respectively A2 (2070-2099) scenario.

Catchment	+1°C scenario			B2 scenario			A2 scenario		
	Min	Med	Max	Min	Med	Max	Min	Med	Max
Drance de Bagnes	-22	-15	-11	-36	-26	-19	-49	-30	-24
Saaser Vispa	-10	-5	-2	-21	-13	-5	-34	-17	-9
Lonza	-13	-8	-4	-19	-14	-7	-32	-16	-8
Rhone at Gletsch	-19	-12	-9	-28	-20	-15	-40	-23	-16
Weisse Lütschine	-16	-9	-6	-33	-23	-12	-47	-25	-20
Minster	-13	-5	-3	-26	-14	-6	-42	-16	-11
Tamina	-12	-5	-2	-24	-16	-5	-39	-16	-10
Vorderrhein	-12	-6	-3	-22	-12	-6	-35	-14	-8
Dischmabach	-12	-7	-3	-24	-17	-4	-39	-16	-10
Rosegbach	-16	-10	-4	-28	-18	-6	-41	-22	-13
Verzasca	-12	-6	-2	-27	-16	-3	-40	-19	-10
Min	-22	-15	-11	-36	-26	-19	-49	-30	-24
Med	-13	-7	-3	-26	-16	-6	-40	-17	-10
Max	-10	-5	-2	-19	-12	-3	-32	-14	-8

For all climate change projections and all studied catchments, the predicted climate change induces an earlier start of the snowmelt period leading to a shift of the hydrological regime and the maximum monthly discharges. For the glacierized catchments, the simulated regime modifications are mainly due to the increase of the mean temperature and corresponding impacts on the snow accumulation and melting processes. The hydrological regime of the catchments located at lower altitudes is expected to be more strongly affected by the changes in the seasonal precipitation. Table II summarizes the seasonal discharge distribution simulated for the control period and for the 3 climate change configurations.

Table II: Contribution of seasonal discharges to mean annual discharge (%) for the control period, the +1°C scenario (2020-2049) and the B2 and A2 scenarios (2070-2099). Median values from the different runs.

Catchment	Control				+1°C scenario				B2 scenario				A2 scenario			
	DJF	MAM	JJA	SON	DJF	MAM	JJA	SON	DJF	MAM	JJA	SON	DJF	MAM	JJA	SON
Drance de Bagnes	2	6	72	21	3	10	70	16	4	16	65	13	9	24	54	14
Saaser Vispa	4	9	64	23	5	11	60	23	7	16	56	22	9	23	46	22
Lonza	3	10	66	21	5	13	62	20	7	17	58	18	10	22	51	18
Rhone at Gletsch	2	8	65	25	4	11	64	21	6	16	61	18	8	22	52	18
Weisse Lütschine	9	17	53	21	9	21	51	19	11	27	46	15	16	31	40	15
Minster	11	35	36	18	14	36	32	17	20	34	22	18	25	32	26	17
Tamina	7	27	47	19	9	31	41	19	11	37	32	19	16	38	29	19
Vorderrhein	6	22	52	20	7	29	46	18	9	36	38	18	13	40	32	18
Dischmabach	4	16	60	20	5	22	54	20	6	29	46	20	10	33	40	20
Rosegbach	2	8	68	22	4	11	63	23	6	16	56	23	7	21	49	24
Verzasca	5	31	38	27	6	35	32	28	7	40	22	30	9	40	20	30

Impacts of discharge changes on hydropower production

Two main impacts may affect hydroelectricity production in the Swiss Alps. 1) a significant decrease of mean annual discharges. For hydropower production systems such as those existing today, a reduction of the mean annual hydroelectricity potential is thus expected. 2) a reduction of the amplitude between summer and winter discharges, as larger amounts of water are expected in winter and spring, whereas slightly lower discharges are expected in summer. This more regular contribution of discharges over the year is likely to make the management of water storage easier.

Consistency of projections obtained from different climate experiments

For each climate change scenario analyzed in this work, the modifications of annual discharges and hydrological regimes simulated for the different RCM runs are significantly variable. The large prediction variability induced by the 19 RCM experiments considered here is partly induced by the underlying driving AOGCMs. The results presented in this study show however clearly that the differences between different RCM experiments with the same driving AOGCM can result in comparably high impact differences as the use of different AOGCMs to drive a given RCM. This result suggests that the inter-RCM variability should always be considered in climate change impact studies. Note than despite this large variability of results, all scenarios and all models predict however changes of same trend; only amplitude and timing of these changes differ.

1 Introduction

The Alps are a key element of the hydrological regime of the Swiss river network (e.g. Braun, 1999) and they are the source of many of the Europe's major river systems. The specific mean annual discharge in mountainous areas is generally higher than in catchments located at lower altitudes in the same climatic region. This results essentially from higher precipitation amounts induced by orographic effects but also from low evapotranspiration rates induced to a large part by the relatively low mean temperatures. Additionally, the hydrological regime of such environments is strongly influenced by water accumulation in form of snow and ice and the corresponding melt processes resulting in a pronounced annual cycle of the discharge. A modification of the prevalent climate and especially of the temperature can therefore considerably affect the hydrological regime and induce important impacts on the water management (see, e.g., Burlando et al., 2002; Jasper et al., 2004; Schaefli, 2005). This could have a significant impact on water uses highly dependent on the hydrological regime, such as hydropower production and irrigation, but also increase water related risks such as flood and droughts (see, e.g., Braun, 1999; Braun et al., 2000; Willis and Bonvin, 1995). The prediction of climate change impacts has consequently an evident socio-economic interest.

The quantification of potential climate change impacts on a given water resources system is conditioned by the availability of local or regional climate change predictions of different key meteorological variables such as precipitation and temperature. Currently available regional climate change projections are mainly based on the results of coupled Atmosphere-Ocean General Circulation Models (AOGCMs) or on the results of Regional Climate Models (RCMs) driven by outputs of the former. RCMs are supposed to describe the regional climatic variables better than AOGCMs because of their higher spatial resolution (RCMs have a resolution of around 0.5° of latitude and 0.5° of longitude whereas the resolution of AOGCMS is around 2.5° of latitude and 3.75° of longitude). Regional climate change projections based on such climate model outputs are however highly uncertain, mainly due to the unknown future greenhouse gas emissions but also due to the highly simplified representation of reality encoded in these models. As a consequence, different state-of-the-art AOGCMs generally simulate different climate evolutions for the same emission scenario (see, e.g. Arnell and Hulme, 2000; Räisänen, 2001; Räisänen, 2002). For a given AOGCM experiment, the corresponding RCM experiment is also subject to these modeling uncertainties. The results of several RCM experiments based on the same AOGCM outputs can therefore also differ significantly (see, e.g., Frei et al., 2003; Räisänen et al., 2004). The uncertainty introduced by the RCM is generally considered to be substantially smaller than the one inherited by the driving AOGCM (Jenkins and Lowe, 2003). An analysis of the data of the EU project PRUDENCE (Prediction of Regional scenarios and Uncertainties for Defining EuropeaN Climate change risks and Effects, (Christensen et al., 2002) suggests however that RCM inter-model variability cannot be neglected (Hingray et al., 2005a, submitted manuscript[1]).

Climate change impacts on hydrological processes in the Swiss Alps have been assessed in different studies (e.g. Braun et al., 2000; Etchevers et al., 2002; Jasper et al., 2004; Zierl and Bugmann, 2005). All these studies show that the temperature increase strongly affects the

[1] Hingray, B., Mezghani, A. and Buishand, T.A., 2005a. Development of probability distributions for regional climate change from uncertain global mean warming and an uncertain scaling relationships. Submitted to Hydrology and Earth System Sciences.

temporal evolution of the snowpack and accordingly the runoff regimes of the studied catchments. However, only few studies exists that analyze different green house gas emission scenarios or that take into account the prediction uncertainty due to the used climate model. Jasper et al., (2004) and Zierl and Bugmann, (2005) show that for Alpine river systems, these two sources of climate change prediction uncertainty lead to a wide range of possible future states, demonstrating therefore that that the quantitative assessment of hydrological changes based on a small number of climate change scenarios may yield misleading results. It is noteworthy that these results are obtained for Alpine catchments that do not have any ice-covered areas. Braun et al. (2000) and Schaefli (2005) however showed that for glacierized catchments, the retreat of the glaciers could enhance the expected climate change induced modifications of the hydrological regime. Another important drawback of the currently available studies is that they do not consider the climate change prediction uncertainty inherent in the used RCM.

Accordingly, the present study focuses on the assessment of climate change impacts on the discharge regime of various rivers of the Swiss Alps considering the climate predictions of multiple state-of-the-art regional climate models. The set of studied catchments is composed of 11 small-scale catchments that are representative of the different hydro-climatic regions and of the hydrological regimes, and includes namely glacierized catchments. The impact of climate change on the hydrological regime of a given catchment is analyzed through the simulation of the system behavior for an observed control period (1961 to 1990) and for a future period (either 2020 to 2049 or 2070 to 2099) characterized by a modified (predicted) climate. The climate predictions are derived from the result of a suite of RCM experiments produced in the framework of the EU project PRUDENCE (Christensen et al., 2002) for the two green house gas emission scenarios A2 and B2 as defined by the Special Report on Emission Scenarios (SRES, (Nakicenovic and Swart, 2000)) of the Intergovernmental Panel on Climate Change (IPCC).

The paper starts with a description of the case studies, of the corresponding datasets and of the models used for the discharge simulation and for the production of small-scale meteorological time series scenarios (Section 2). The climate change impact prediction results are presented in Section 3 followed by a detailed discussion and the main conclusions of this study.

2 Case studies: data and models

2.1 Catchment characteristics

The analyzed catchments have been selected to represent the different hydro-climatic zones of the Swiss Alps and the different mountainous hydrological regimes occurring in these zones. A number of 7 hydro-climatic regions (Figure 1) are traditionally considered for hydro-meteorological analysis purposes in the Swiss Alps (Laternser and Schneebeli, 2002).

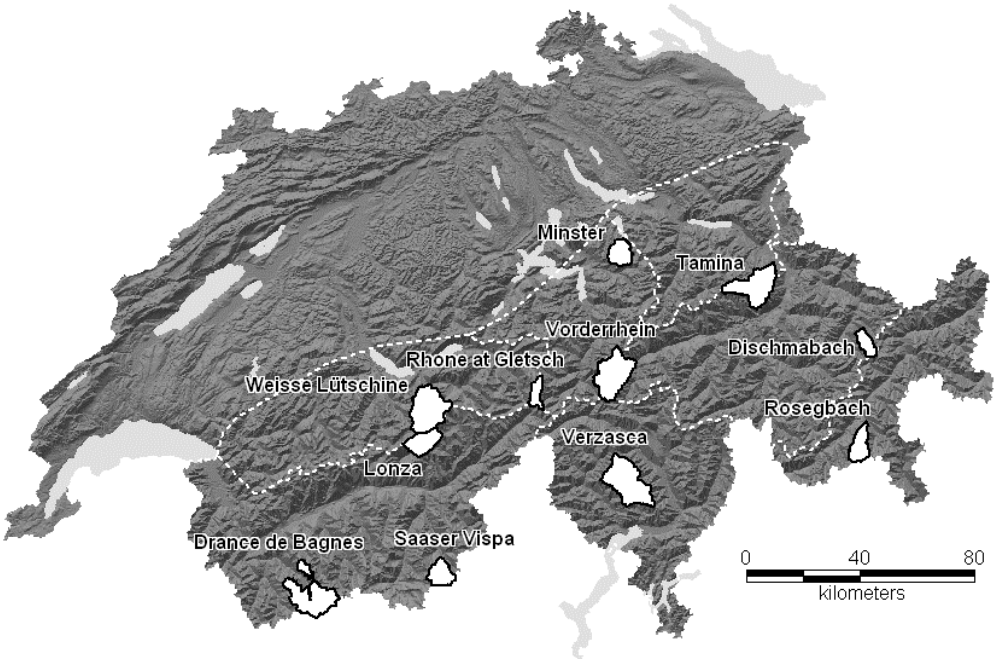

Figure 1: Location of the 11 case study catchments in the 7 hydro-climatic regions of the Swiss Alps (© Swiss Federal Office of Topography).

The choice of the case study catchments was however also conditioned by the data availability. For the context of this study, at least 30 years of observed meteorological data are required for the simulation of the reference situation (corresponding to the control period 1961 – 1990) and in addition long series of discharge measurements and corresponding meteorological data are necessary for the purposes of model calibration and validation.

Based on these considerations, 11 catchments have been selected. These catchments have different glaciation rates (between 0 and 50 %) and altitude ranges (Table 1). Their catchment areas vary between 39 to 185 km^2 and the mean altitudes vary between 1340 m a.s.l. for the Minster catchment to 2940 m a.s.l. for the Drance de Bagnes catchment.

The catchments represent a large range of hydrological regimes observed in the Swiss Alps (Table 1). The reference regime used here are the ones given by Aschwanden and Weingartner (1985). These regimes are determined based on the dimensionless Pardé coefficient (Equation 1, Pardé, 1933) that relates the mean monthly discharge of a given month to the total annual discharge.

$$PC_i = 12 \cdot \frac{Q_i}{\sum_{i=1}^{12} Q_i} \qquad (1)$$

The distribution of these coefficients over the year, their minimum and maximum values and their amplitude are the key criteria for the regime definition (Figure 2).

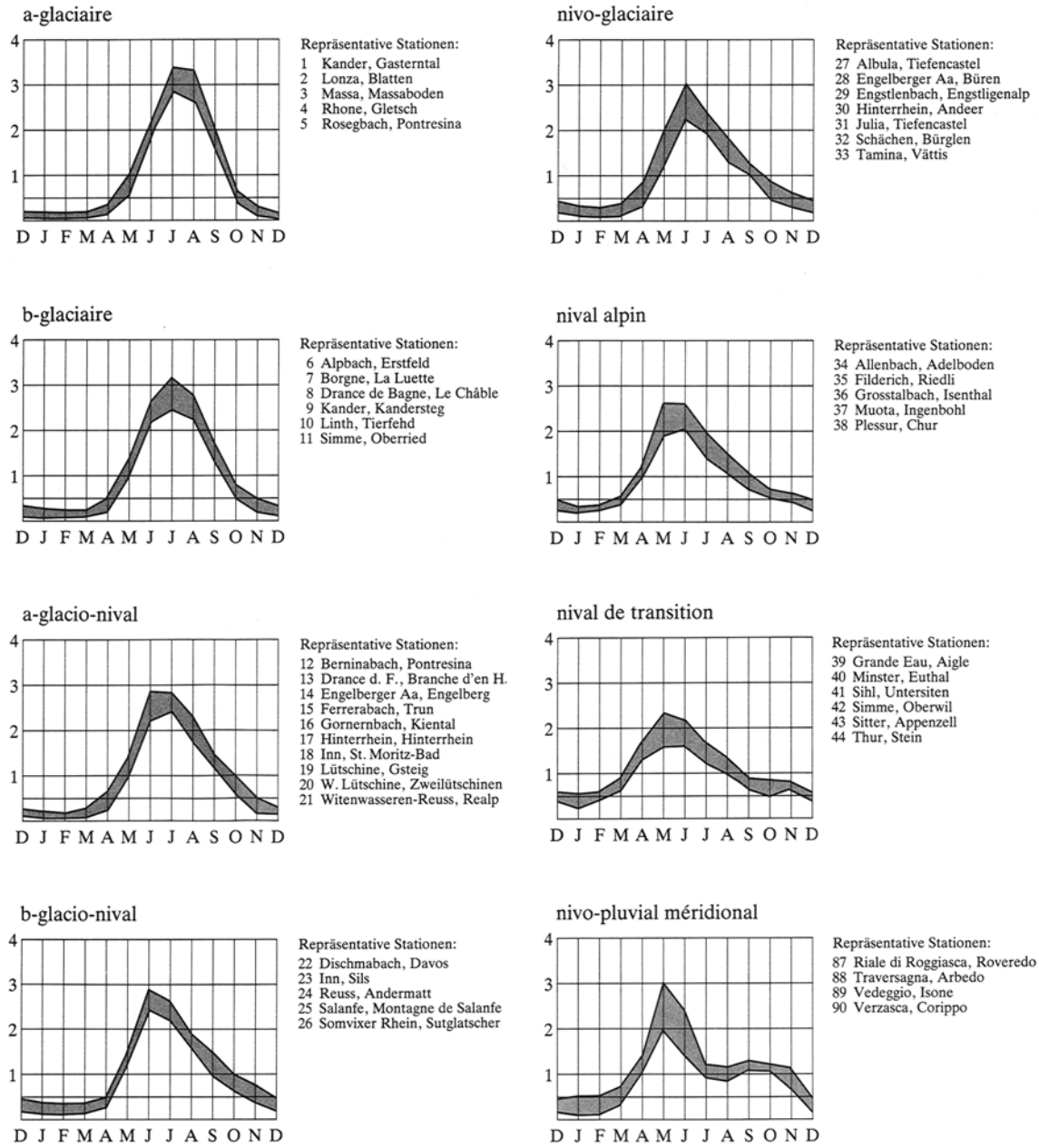

Figure 2: Illustration of the occurring discharge regimes (in Weingartner and Aschwanden, 1986). In ordinate are the Pardé coefficient values.

Table 1: Characteristics of the case study catchments, mean annual estimated precipitation and simulated runoff for the control period (see Table 2) and corresponding discharge regimes according to the regime definitions given by Aschwanden and Weingartner (1985) for the Swiss Alps.

Catchment	Area km^2	Glacier %	Mean altitude m a.s.l.	Altitude range m a.s.l.	Lapse rate °C/100m	Annual precipitation mm	Annual runoff mm	Hydrological regime
Drance de Bagnes	166.6	39.0	2940	1960 - 4310	-0.50	1620	1561	a-glaciaire
Saaser Vispa	65.2	33.2	2840	1710 - 4190	-0.46	1627	1408	b-glaciaire
Lonza	77.8	32.8	2600	1520 - 3900	-0.57	2187	2016	a-glaciaire
Rhone at Gletsch	38.9	50.0	2710	1760 - 3610	-0.55	2262	2236	a-glaciaire
Weisse Lütschine	164.0	16.4	2150	650 - 4170	-0.60	1774	1492	a-glacio-nival
Minster	59.2	-	1340	880 - 2290	-0.54	2197	1694	nival de transition
Tamina	147.0	1.4	1810	550 - 3220	-0.61	1554	1291	nival alpin
Vorderrhein	158.0	2.8	2150	750 - 3310	-0.58	1748	1506	nivo-glaciaire
Dischmabach	43.3	2.6	2360	1670 - 3130	-0.56	1460	1233	b-glacio-nival
Rosegbach	66.5	27.2	2710	1760 - 4010	-0.43	1412	1243	a-glaciaire
Verzasca	185.2	-	1650	480 - 2880	-0.57	2175	1790	nivo-pluvial méridional

All selected catchments (except the Verzasca catchment) show typical discharge patterns characterized by a single-peak occurring between May and August (Figure 2). This peak is due to snowmelt-induced high flows. For catchments with glacier, it is sustained by usually significant ice-melt induced flows occurring later in the melt season. The amplitude of the monthly flows is high between the low flows during the winter season and the high flows in late spring or summer. The amplitude as well as the occurrence date of the discharge peak strongly depends on the elevation range covered by the catchment. The higher the mean elevation of the catchment is, the later the peak occurs and the higher the amplitude is (see the regimes simulated for the control period, Figure 7). The Verzasca river has a typical regime of the Southern Alps and shows therefore a quite different regime: A second discharge peak occurs in fall due to heavy precipitation events usually observed in this period.

2.2 System models

The simulation of the system behavior for the different time periods requires setting up an integrated simulation tool including a hydrological model for the precipitation – runoff transformation and a land cover evolution model. For the present study, the only land cover change that is included in the simulation approach is the modification of the ice-covered surface. Land use changes related to the vegetation, namely the forest cover, could presumably have significant impact on future hydrological regimes. Zierl and Bugmann (2005) found however for 5 Swiss Alpine catchments that land use changes related to afforestation and deforestation have only a small impact on discharges under future climate change scenarios comparable to the ones used here.

Hydrological model

The hydrological discharge simulation is carried out at a daily time step through a conceptual reservoir-based model called GSM-SOCONT (Schaefli et al., 2005). The model has two levels

of discretization. The ice-covered part of the catchment is first separated from the not ice-covered part. Next, both parts are subdivided into elevation bands. Each of the resulting spatial units is characterized by its surface and its hypsometric curve and is assumed to have a homogenous hydrological behavior.

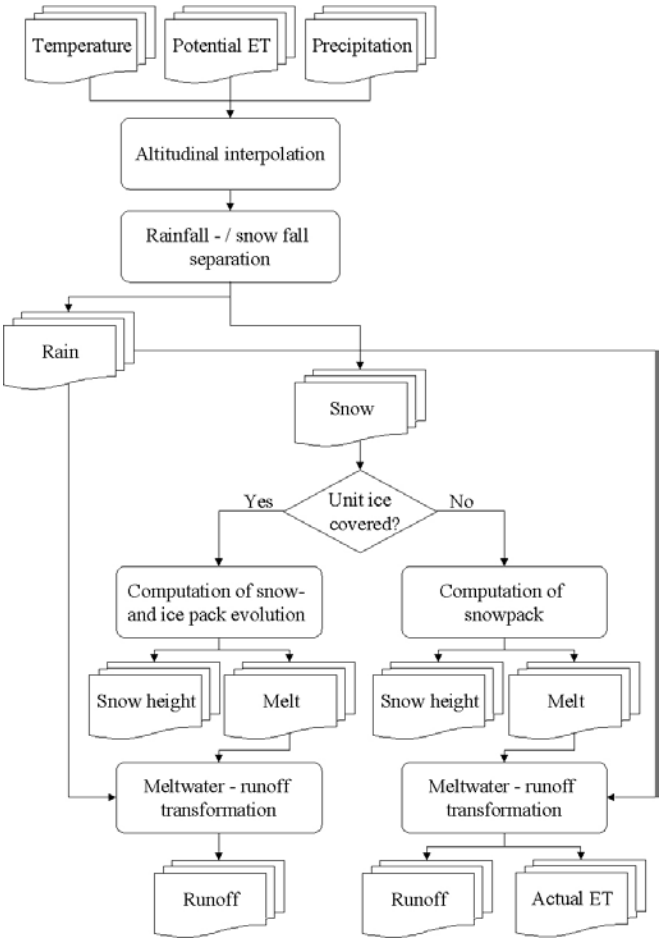

Figure 3: Hydrological model structure (for one spatial unit) showing the different submodels and the input and output time series (from Schaefli, 2005) (ET: evapotranspiration).

For each spatial unit, the meteorological data series are computed from data observed at neighboring meteorological stations. For temperature, regional altitudinal gradients are estimated based on the observed temperature series (see the estimated lapse rates in Table 1). Based on these gradients, the temperature time series for a given spatial unit is interpolated according to its mean elevation. Due to the considerable spatial variability of precipitation and to the scarcity of precipitation data at high altitudes, no reliable altitudinal gradient of precipitation can be identified based on the observations at raingauge stations within or close to the studied catchments. As all raingauges are located in the lowest parts of these catchments, an altitudinal correction of precipitation is however needed. To account for the enhancement of precipitation with altitude, a mesoscale precipitation gradient of 80 mm per 100 m and per year, estimated by

Kirchhofer and Sevruk (1991) for the entire Swiss Alpine region, is applied. The resulting area-average daily precipitation amounts are corrected by a constant multiplicative factor in order to respect the mean annual precipitation amounts estimated for each catchment by Schädler and Bigler (2002) based on a long term water balance analysis.

Based on the meteorological time series, the temporal evolution of the snowpack and of the glacier melt is computed. The aggregation state of precipitation (liquid, solid or mixed) is determined based on a fuzzy temperature threshold approach (e.g. Klok et al., 2001) : precipitation falls as snow (resp. as rain) when the temperature is below 0°C (resp. above 2°C) and is a mixture of both for temperatures in between (Hamdi et al. 2005). Snow and ice melt are simulated through a simple degree-day approach (see, e.g., Rango and Martinec, 1995). Ice melt is supposed to occur only when the glacier surface of the considered spatial unit is not covered by snow.

For each hydrological unit, a reservoir-based modeling approach is used to simulate the rainfall and melt water – runoff transformation. For ice-covered spatial units, this transformation is completed through two linear reservoirs, one for ice melt and one for the equivalent rainfall defined as the sum of snowmelt and rainfall. For not ice-covered spatial units, the equivalent rainfall is transformed into runoff through the conceptual model SOCONT (Consuegra and Vez, 1996). It is composed of two reservoirs, a linear reservoir for the slow contribution (accounting for soil infiltration processes) and a non-linear reservoir for direct or quick runoff.

The model has eight parameters to calibrate (five for catchments without glacier) (Table 3): the three degree-day factors necessary for the snow and ice melt computation (a_{ice} for ice, $a_{snow.high}$, $a_{snow.low}$ for snow respectively for the highest and lowest altitudes of the catchment), the four time constants of the linear reservoirs (k_{slow}, k_{quick}, k_{ice}, k_{snow}) and the maximum storage capacity of the slow reservoir (A). These parameters have no physical meaning.

Calibration and validation

The calibration procedure is based on the multicriteria calibration procedure presented by Schaefli et al. (2005). A special attention is paid to the reproduction of the observed mean annual and the mean monthly discharges. Time periods used for the calibration and the validation procedures are given in Table 2 and the final parameters sets are given in Table 3.

Table 2: Time periods used for the model calibration and validation and for the control period.

Catchment	Calibration	Validation	Control
Drance de Bagnes	1987 - 1993	1993 - 1999	1972 - 1995
Saaser Vispa	1953 - 1960	-	1961 - 1990
Lonza	1976 - 1983	1983 - 1990	1974 - 1998
Rhone at Gletsch	1973 - 1980	1983 - 1990	1961 - 1990
Weisse Lütschine	1973 - 1980	1963 - 1970	1961 - 1990
Minster	1973 - 1980	1963 - 1970	1961 - 1990
Tamina	1961 - 1967	1968 - 1974	1961 - 1990
Vorderrhein	1953 - 1960	1945 - 1950	1961 - 1990
Dischmabach	1973 - 1980	1983 - 1990	1961 - 1990
Rosegbach	1973 - 1980	1963 - 1970	1961 - 1990
Verzasca	1990 - 1996	1996 - 2000	1961 - 1990

Table 3: Calibrated parameters for the eleven case study catchments.

Catchment	a_{ice} mm/j°C	$a_{snow.high}$ mm/j°C	$a_{snow.low}$ mm/j°C	A mm	k_{slow} j	k_{quick} j	k_{ice} j	k_{snow} j
Drance de Bagnes	5.5	2.3	4.8	100	56	3.5	2.4	4.3
Saaser Vispa	3.3	2.3	3.0	550	56	1.1	1.8	3.4
Lonza	9.0	3.0	4.5	500	56	4.5	1.7	3.1
Rhone at Gletsch	3.5	3.0	5.5	400	56	4.5	1.6	2.9
Weisse Lütschine	5.5	6.5	8.5	150	56	4.5	2.1	3.9
Minster	-	2.8	3.6	50	56	2.0	-	-
Tamina	5.0	4.3	5.4	150	56	3.8	1.9	3.6
Vorderrhein	6.0	3.2	4.8	250	56	2.6	2.2	4.0
Dischmabach	6.0	3.0	6.0	250	56	4.5	1.4	2.6
Rosegbach	3.5	1.5	3.0	250	56	4.5	1.7	3.1
Verzasca	-	2.0	2.5	150	56	2.2	-	-

Table 4: Calibration and validation Nash criteria and bias for the eleven case study catchments.

Catchment	Calibration			Validation		
	Nash on daily series	Nash on monthly series	Bias	Nash on daily series	Nash on monthly series	Bias
Drance de Bagnes	92%	97%	0%	92%	98%	-4%
Saaser Vispa	86%	95%	4%	-	-	-
Lonza	90%	96%	-2%	91%	96%	-1%
Rhone glacier	89%	94%	1%	87%	93%	0%
Weisse Lütschine	87%	94%	1%	88%	95%	0%
Minster	74%	92%	1%	73%	94%	-3%
Tamina	86%	95%	3%	85%	94%	12%
Vorderrhein	85%	95%	2%	82%	94%	7%
Dischmabach	90%	96%	-7%	90%	96%	-1%
Rosegbach	86%	97%	2%	89%	96%	-1%
Verzasca	76%	93%	1%	74%	91%	-5%

The calibrated model performs well for all catchments. The Nash values (Nash and Sutcliffe, 1970) calculated on daily discharge series are higher than 0.8 for the calibration and the validation period except for the Minster and the Verzasca catchments, the two catchments without glacier (Table 4). This result is due to the fact, that these two catchments have a less strong annual discharge cycle and accordingly high Nash values are more difficult to achieve (see (Schaefli et al., 2005) for a further discussion of this problem). The Nash values calculated for the monthly discharges are all higher than 0.9 (Table 4). Though some biases were found for four catchments, these will be kept in selection knowing that the study focus is on relative changes in discharge regimes.

Visual comparisons of runoff regimes (calendar evolution of mean monthly discharges) yielded good results (Figure 4a,b) as well as semi-monthly flow series and annual amounts (Figure 4c). An illustration is given for the Rhone catchment (Figure 4). The same figures are given for all catchments in appendix.

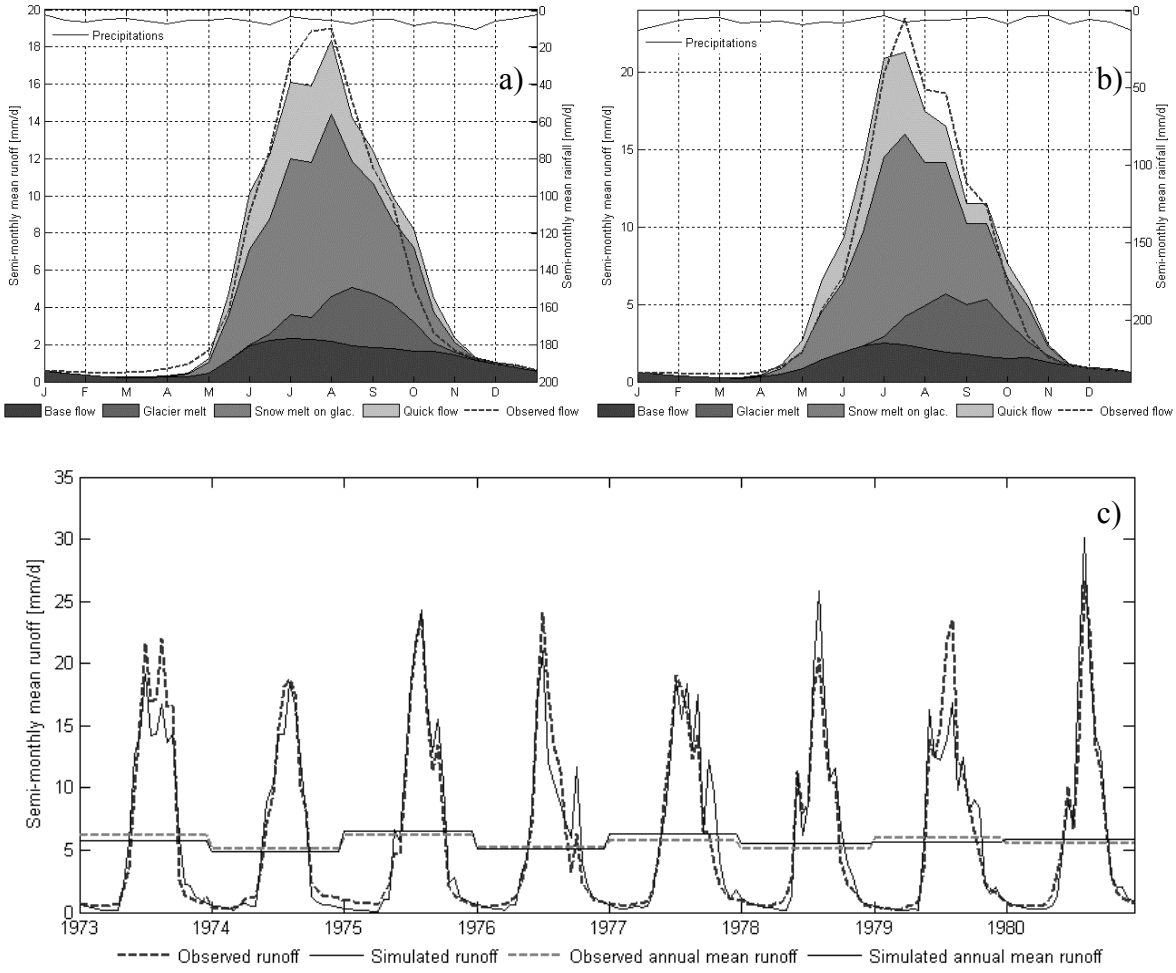

Figure 4: Calibration and validation results for the Rhone catchment at Gletsch. a) Calibration: observed and simulated semi-monthly cycle for 1973 to 1980 (the coloured zones correspond to the contributions of the different flow components to the total discharge), b) Validation: observed and simulated semi-monthly cycle for 1983 to 1990, c) Calibration: observed and simulated semi-monthly mean flow series for 1973 to 1980.

Glacier surface evolution model

In the hydrological model, the glacier surface is supposed to be constant for a given simulation period of several years. For the future scenario simulation, the ice-covered surface has to be updated. In the present study, this update is completed through the method presented by Schaefli (2005). This method is based on the so-called accumulation area ratio (AAR) (Anonymous, 1969) and assumes that the mean annual AAR value estimated over a long time period is characteristic for a given glacier system and that it remains constant for future climatic conditions.

The mean annual AAR value can be simulated for a given time period with known ice-covered area through the presented hydrological model: For a given hydrological year (starting on the 1st October), the AAR is computed from the sum of spatial units that experience snow accumulation. Simulating the mean annual AAR value AAR_m for the control climatic conditions

(for which the total ice-covered area is known) and the mean annual accumulation area A_{acc} [km^2] for the future climatic conditions, the future glacier surface A_{ice} [km^2] can be estimated according to Equation 2.

$$A_{ice} = \frac{A_{acc}}{AAR_m} \tag{2}$$

For a further discussion of the glacier surface evolution model, refer to Schaefli (2005).

2.3 Data

Data for the observed period

The glacio-hydrological model needs three input time series, namely daily precipitation, daily potential evapotranspiration and mean daily temperature. For all catchments, the precipitation and temperature data from nearby meteorological stations are obtained from the Swiss Meteorological Institute. The potential evapotranspiration (PET) data are derived from the monthly PET series estimated by New et al. (2000) for the control period according to the Penman-Monteith version given by Burman and Pochop (1994). The series of mean daily discharges for model calibration and validation are provided by the Swiss Federal Office for Water and Geology.

The spatial discretization of the catchment is completed based on a digital elevation model with a resolution of 25 m (SwissTopo, 1995) and on digital (vector-based) topographic maps with a scale of 1: 25000 (SwissTopo, 1997).

Future periods

The climate change data used in the present study result from a suite of regional climate model experiments conducted in the framework of the PRUDENCE EU project (Christensen et al., 2002). Each RCM experiment consists of a simulation for the period 1961-1990 (control run) and a simulation for the period 2070-2099 (future run). For each RCM experiment, the boundary conditions were obtained from one of the three AOGCMs used in PRUDENCE: ARPEGE/OPA (Royer et al., 2002), HadCM3 (Gordon et al., 2000; Pope et al., 2000) and ECHAM4/OPYC3 (Roeckner et al., 1999). In the case of HadCM3, a global model of the atmosphere alone (HadAM3H) was used between the global coupled model and the RCMs. The use of this intermediate model resulted in a much better simulation of the present-day climate (Hulme et al., 2002). The AOGCM experiments were completed for the two SRES emission scenarios A2 and B2 (Nakicenovic and Swart, 2000).

In the present study, 9 RCMs are included (see Table 5 for the list of models and institutions). Note that one of these models, ARPEGE, is not a regional but a global atmospheric model with variable horizontal resolution, from 50 km in the center of the Mediterranean Sea to 450 km in the southern Pacific Ocean (Gibelin and Déqué, 2003). In PRUDENCE, the low boundary conditions (sea surface temperatures, sea ice) were obtained from ARPEGE/OPA and HadCM3 (Déqué, personal communication). For the 11 catchments analyzed in the present study, the horizontal resolution is comparable to the other RCMs. Note that in the following, ARPEGE is considered as a RCM. Some RCMs were run successively using the boundary conditions of different AOGCMs. All RCMs were run at least for scenario A2 with one AOGCM. Some

RCMs were also run for scenario B2. 19 experiments are available in total, 12 for the scenario A2 and 7 for B2. A synthesis of these experiments is given in Table 6.

Table 5: a) The 3 AOGCMs and b) the 9 RCMs used in the PRUDENCE project (Christensen et al., 2002) and the corresponding institutions.

a) AOGCMs

Acronym	Institution	AOGCM	Reference
CNRM	Centre National de Recherches Météorologiques, Toulouse, F	ARPEGE/OPA	(Royer et al., 2002)
HC	Hadley Centre for Climate Prediction and Research, Bracknell, UK	HadCM3	(Gordon et al., 2000) (Pope et al., 2000)
MPI	Max-Planck-Institut für Meteorologie, Hamburg, D	ECHAM4/OPYC3	(Roeckner et al., 1999)

b) RCMs

Acronym	Institution	RCM	Reference
CNRM	Centre National de Recherches Météorologiques, Toulouse, France	ARPEGE	(Gibelin and Déqué, 2003)
DMI	Danish Meteorological Institute, Copenhagen, Denmark	HIRHAM	(Christensen et al., 2001)
ETHZ	Institute for Atmospheric and Climate Science, Zurich, Switzerland	CHRM	(Vidale et al., 2003)
GKSS	Institute for Coastal Research, Geesthacht, Germany	CLM	(Doms and Schättler, 1999)
HC	Hadley Centre for Climate Prediction and Research, United Kingdom	HadRM3H	(Hulme et al., 2002)
ICTP	International Centre for Theoretical Physics, Trieste, Italy	RegCM	(Giorgi et al., 1993a), (Giorgi et al., 1993b)
MPI	Max-Planck-Institut für Meteorologie, Hamburg, Germany	REMO	(Jacob, 2001)
SMHI	Swedish Meteorological and Hydrological Institute, Norrköping, Sweden	RCAO	(Räisänen et al., 2004)
UCM	Universidad Complutense de Madrid, Toledo, Spain	PROMES	(Arribas et al., 2003)

Table 6: RCM experiments according to driving AOGCM and to emission scenarios (all RCMs experiments were conducted in the framework of PRUDENCE).

Scenario Name	AOGCM Name	N°	RCM Name	N°
A2	HADCM3-HADAM3H	1	CHRM	1
	HADCM3-HADAM3H		CLM	2
	HADCM3-HADAM3H		HadRM3H	3
	HADCM3-HADAM3H		HIRHAM	4
	HADCM3-HADAM3H		PROMES	5
	HADCM3-HADAM3H		RCAO(H)	6
	HADCM3-HADAM3H		RegCM	7
	HADCM3-HADAM3H		REMO	8
	HADCM3-ARPEGE		ARPEGE	9
	ARPEGE/OPA	2	ARPEGE	10
	ECHAM4/OPYC3	3	HIRHAM	11
	ECHAM4/OPYC3		RCAO(E)	12
B2	HADCM3-/HADAM3H	4	HadRM3H	13
	HADCM3-/HADAM3H		PROMES	14
	HADCM3-HADAM3H		RCAO(H)	15
	HADCM3-ARPEGE		ARPEGE	16
	ARPEGE/OPA	5	ARPEGE	17
	ECHAM4/OPYC3	6	HIRHAM	18
	ECHAM4/OPYC3		RCAO(E)	19

The RCMs are reported to reproduce well the regional features of meteorological surface variables such as precipitation and temperature (e.g. Frei et al., 2003). Their reliability is however not the same for each individual grid box, in particular in mountainous regions. As a result, instead of considering only the grid box containing a given case study, several grid boxes should be taken into account for hydrological applications (Frei, personal communication). In the present study, for each analyzed catchment, the regional changes predicted by a given RCM are averaged over 9 grid boxes encompassing the catchment of interest. The spatial resolution of these area-averaged regional changes is too coarse for a direct use of the model outputs, namely precipitation and temperature, as an input for hydrological models. Different methodologies exist for the production of local scale climate change scenarios, using for example downscaling models that connect the local meteorological variables directly to synoptic scale variables (see, e.g., Xu, 1999 ; Wilby and Wigley, 1997 for a review). The development of reliable downscaling relationships for the daily precipitation in Alpine areas should consider several explanatory variables (such as atmospheric humidity, pressure fields at different geopotential heights) that are not always available for the used RCM experiments. Jasper et al. (2004) have applied a downscaling model to Alpine catchments that is based only on the generally available large-scale mean sea-level pressure. But they come to the conclusion that this downscaling model has only a modest performance for the reproduction of observed precipitations in the studied area.

The local scale meteorological time series are also frequently generated by perturbing the observed times series for a control period based on the regional climate changes of the considered mean variable as predicted by the climate models (see, e.g., Shabalova et al., 2003). As the present study focuses on the impacts of climate changes on hydrological regimes and mean annual or seasonal discharges, such a simple perturbation methodology is used for the generation of daily temperature and precipitation time series.

The method used for temperature perturbation is the one presented by Shabalova et al., (2003). It preserves the mean and variability given by the climate change scenario for each season. For a

given RCM experiment, the climate change scenario is defined in terms of the absolute changes of the mean temperature (XMT_s) between the control and the future run and in terms of the relative changes of the standard deviation of daily temperature ($XSDT_s$) where s refers to the season (s = 1: DJF, s = 2: MAM, s = 3: JJA, s = 4: SON). The future scenario temperature T_{scen} is calculated according to Equation 3.

$$T_{scen,s}(t) = [T_{obs,s}(t) - MT_{obs,s}] * (XSDT_s + 1) + MT_{obs,s} + XMT_s \quad (3)$$

where $T_{scen,s}(t)$ [°C] is the local scale scenario temperature on a day t in the season s, $T_{obs,s}(t)$ is the local temperature on day t observed during the control period and $MT_{obs,s}$ the corresponding mean daily temperature. The standard deviations of daily temperatures are not available for the PRUDENCE RCM experiments that produced grids of 90-days temperature variances for each season. In the present study, the standard deviations of daily temperatures are estimated based on the observed linear relationships between the 90-days and the daily variances according to the method presented by Hingray et al. (2005b, submitted manuscript[2]).

The future local scale precipitation time series are estimated based on a simple proportional relationship (Equation 4).

$$P_{scen,s}(t) = P_{obs,s}(t) \cdot \frac{MP_{fut,s}}{MP_{cont,s}} \quad (4)$$

where $P_{scen,s}(t)$ [°C] is the local scale scenario precipitation on day t of the season s (s = 1, 2, 3, 4), $P_{obs,s}(t)$ is the precipitation observed on day t during the control period, and $MP_{fut,s} / MP_{cont,s}$ is the ratio between the mean seasonal precipitation amounts obtained for the future and the control run for a given RCM experiment.

Note that for the future scenarios, the potential evapotranspiration is estimated as a function of the perturbed temperature based on the observed linear relationship for the control period, assuming that this relationship remains constant in the future. In fact, Ekström et al. (submitted manuscript[3]) have shown for the regional climate model HadRM3H that the calculated PET values are unrealistically high for the future period.

As described above, the different available RCM experiments were run in PRUDENCE for the period 2070-2099. In this study we are also interested in an intermediate scenario corresponding to a +1°C global warming scenario. For the three AOGCM's considered in this study, this global warming is expected to be obtained for the period 2020-2049 under both A2 and B2 emissions scenarios. The response pattern scaling approach introduced by Santer et al. (1990) and developed by Hingray et al. (submitted a) was applied to generate intermediate climate change scenarios for this global warming projection. The technique is currently widely used in climate

---

[2] Hingray, B., Mouhous, N., Mezghani, A., Bogner, K., Schaefli, B. and Musy, A.: Accounting for global warming and scaling uncertainties in climate change impact studies: application to a regulated lakes system. Submitted to Hydrology and Earth System Sciences.

[3] Ekström, M., Jones, P. D., Fowler, H.J., Lenderink, G., Buishand, A., Conway, D., 2005. Regional climate model data used within the SWURVE project 1: projected changes in seasonal patterns and estimation of PET. Submitted to Hydrology and Earth System Sciences.

scenarios studies (e.g. New and Hulme, 2000; Jones, 2000; Hulme et al. 2002, Hingray et al. submitted). It is based on the assumption that there is a linear relationship between the annual global-mean warming (the so-called scaler) and the response pattern of regional climate changes obtained from any global or regional climate model. In the work of Jones (2000) and of New and Hulme (2000), the response pattern is expressed for each variable as a simple scaling ratio, i.e. a constant regional temperature or precipitation change per degree of global warming. The response pattern used by Mitchell (2003) is the spatial climate change pattern of a GCM. This problem can be overcome by the technique of pattern scaling that combines SCMs and RCMs (or GCMs) outputs to produce a number of climate change scenarios (Mitchell, 2003). In our work, future climate scenarios for the period 2020-2049 - in terms of seasonal changes of the mean value and of the variability of temperature and precipitation - are obtained for the period 2070-2099 by scaling the meteorological response pattern from a RCM by the global warming projection under consideration ($\Delta T_I = +1°C$). The uncertainty inherent in the regional climate response is taken into account through the use of the 19 different meteorological response patterns derived from the 19 RCM experiments available trough the PRUDENCE project (Christensen et al., 2002).

Given a RCM called *r* that has been run for the control period (1961-1990) and the future period (2070-2099), the response pattern is defined as the following vector (Equation 5)

$$\mathbf{Y}_r = [Y_{v,s,r}]_{v:1..3,\, s:1..4} \tag{5}$$

where $Y_{v,s,r}$ is the scaling ratio for one of the four key statistics used ($Y_{1,s} = YMT_s$, $X_{2,s} = YSDT_s$, $X_{3,s} = YMP_s$) for season *s* and RCM experiment *r*. For each variable, the scaling ratio is defined as its regional change (absolute or relative) per degree of global-mean warming. For a given RCM experiment, the scaling ratios can thus be estimated by the variable anomaly normalized with respect to the scaler:

$$Y_{v,s,r} = X_{v,s,r} / \Delta T_r \tag{6}$$

where $X_{v,s,r}$ is the change in variable *V* for season *s* predicted by RCM experiment *r* between control and future periods and ΔT_r is the global-mean warming value obtained for the AOGCM used to drive RCM experiment *r*.

The pattern scaling technique is based on the critical assumption that there is a linear relationship between the scaler (annual global-mean warming) and the response pattern of regional climate changes obtained from the RCM. Mitchell et al. (1999) and Mitchell (2003) have examined this assumption for spatial changes in mean temperature and precipitation from different GCM scenarios. They found that that pattern scaling may be applicable to a wide range of variables. For the present case study, this assumption seems to be reasonable (see Figure 5 for *XMT* and *XMP*), even if some studies reported in the literature suggest that the response pattern may not be linearly correlated with the global warming (e.g. Schneider and Thompson, 1981, Mitchell, 2003).

3 Results

3.1 Climate changes

The three AOGCMs ARPEGE/OPA, HadCM3/HadAM3H and ECHAM4/OPYC3 predict for scenario B2 (2070-2099) a global-mean warming of +2.4 °C, +2.4°C respectively +2.8 °C and for the scenario A2 (2070-2099) the predicted values are +3.0 °C, +3.3 °C and +3.6 °C (Roeckner et al., 1999; Gordon et al., 2000; Gibelin and Déqué, 2003). The regional mean annual temperature increase predicted by the 19 PRUDENCE RCM experiments is higher than the corresponding predicted global-mean warming (Table 7). The mean temperature increase is around 3.0°C for the B2 scenario and 4.0°C for the A2 scenario for the different catchments. This enhanced regional warming has already been observed in the Swiss Alps over the 20th century (see, e.g., Beniston et al., 1994; Weber et al., 1997). Note also that according to our scaling approach the mean regional temperature increase is +1.2°C for the +1°C scenario.

Table 7: Minimum, median and maximum regional climate changes (annual changes of mean temperature and precipitation and seasonal changes of mean precipitation amounts for winter (DJF) and summer (JJA)) predicted by PRUDENCE RCM experiments: a) for the +1°C scenario (2020-2049, 19 experiments), b) for the B2 scenario (2070-2099, 7 experiments), c) for the A2 scenario (2070-2099, 12 experiments).

a) Climate changes for the +1°C scenario (2020-2049)

Catchment	Annual temperature (°C)			Annual precipitation (%)			Seasonal precipitation (%)					
							DJF			JJA		
	Min	Med	Max	Min	Med	Max	Min	Med	Max	Min	Med	Max
Drance de Bagnes	1.1	1.3	1.7	-6	-3	0	0	4	8	-19	-8	-1
Saaser Vispa	1.0	1.2	1.7	-6	-3	0	0	5	9	-18	-8	-1
Lonza	1.0	1.2	1.7	-6	-2	1	0	5	9	-18	-8	-1
Rhone at Gletsch	1.0	1.2	1.7	-6	-2	1	-2	5	8	-16	-8	0
Weisse Lütschine	1.0	1.2	1.8	-7	-2	0	-2	5	8	-16	-8	-1
Minster	1.0	1.2	1.8	-7	-2	0	-1	6	9	-15	-7	0
Tamina	1.0	1.2	1.7	-7	-2	0	0	6	8	-16	-7	1
Vorderrhein	1.0	1.2	1.7	-6	-2	0	-1	6	8	-17	-7	0
Dischmabach	1.0	1.2	1.7	-7	-3	1	0	6	9	-15	-7	1
Rosegbach	1.0	1.2	1.7	-7	-3	1	3	8	11	-18	-7	0
Verzasca	1.0	1.2	1.7	-7	-3	1	1	7	10	-19	-8	0
Median	1.0	1.2	1.7	-7	-2	0	0	6	9	-17	-8	0

Table 7 (continue)

b) Climate changes for the B2 scenario (2070-2099)

Catchment	Annual temperature (°C)			Annual precipitation (%)			Seasonal precipitation (%) DJF			JJA		
	Min	Med	Max	Min	Med	Max	Min	Med	Max	Min	Med	Max
Drance de Bagnes	2.5	3.0	4.7	-11	-6	0	7	10	23	-46	-23	-3
Saaser Vispa	2.5	3.0	4.6	-12	-6	0	3	12	23	-43	-26	-2
Lonza	2.5	3.0	4.6	-9	-5	1	3	12	23	-43	-26	-2
Rhone at Gletsch	2.4	3.0	4.6	-10	-4	0	-1	15	20	-39	-32	-1
Weisse Lütschine	2.5	3.1	4.7	-13	-6	-1	1	15	18	-39	-31	-2
Minster	2.4	3.1	4.7	-13	-5	0	0	16	22	-37	-28	0
Tamina	2.4	3.0	4.6	-13	-8	1	2	15	20	-39	-31	1
Vorderrhein	2.4	3.0	4.6	-12	-5	0	0	15	21	-40	-32	0
Dischmabach	2.4	2.9	4.7	-13	-9	2	3	15	21	-37	-26	3
Rosegbach	2.4	3.0	4.6	-15	-8	2	8	17	24	-42	-30	0
Verzasca	2.4	3.1	4.5	-16	-8	1	3	13	29	-46	-34	-1
Median	2.4	3.0	4.6	-13	-6	0	3	15	22	-40	-30	-1

c) Climate changes for the A2 scenario (2070-2099)

Catchment	Annual temperature (°C)			Annual precipitation (%)			Seasonal precipitation (%) DJF			JJA		
	Min	Med	Max	Min	Med	Max	Min	Med	Max	Min	Med	Max
Drance de Bagnes	3.3	4.2	6.1	-21	-8	0	0	14	28	-52	-27	-10
Saaser Vispa	3.3	4.0	6.1	-22	-8	-1	-1	15	28	-48	-27	-9
Lonza	3.3	4.0	6.1	-19	-6	2	-1	15	28	-48	-27	-9
Rhone at Gletsch	3.2	3.9	6.2	-20	-6	2	-6	16	28	-51	-25	-9
Weisse Lütschine	3.2	3.9	6.2	-25	-7	-3	-5	14	26	-49	-27	-12
Minster	3.2	3.8	6.3	-25	-5	-2	-4	14	24	-55	-22	-8
Tamina	3.2	3.9	6.2	-24	-7	-1	-1	21	27	-50	-22	-6
Vorderrhein	3.2	3.9	6.1	-22	-6	0	-4	19	28	-52	-23	-7
Dischmabach	3.2	4.0	6.2	-24	-7	0	1	22	29	-45	-21	-3
Rosegbach	3.2	4.0	6.1	-26	-11	-2	11	27	37	-50	-23	-5
Verzasca	3.2	4.0	6.1	-26	-11	-2	6	24	30	-54	-26	-6
Median	3.2	4.0	6.1	-24	-7	-1	-1	16	28	-50	-25	-8

Note that the estimated regional temperature changes are quite similar for all catchments (Table 7). There is a clear gradation of the projected regional warming between the +1°C , the B2 and the A2 scenario: Every percentile of the temperature distribution estimated based on the RCM experiments for +1°C has a lower value than the one estimated for B2, which has lower value than the one estimated for A2. The spread of regional changes obtained from the different RCM experiments for a given emission scenario is however considerable (Table 7 and Figure 5), ranging for example for the Rhone catchment between +3.2 °C and +6.2 °C for the A2 scenario (the same data are given for all catchments in appendix). As a result, the prediction ranges obtained for A2 and B2 are overlapping. The median regional temperature warming predictions obtained for A2 are even smaller than the highest predictions obtained for B2. Note that the predicted regional warming for the summer is higher and has a larger variability range than the predicted regional warming for the other seasons (see an example in Figure 5 and Figure 6). For

the Rhone catchment, the maximum summer warming predicted for A2 is as large as +8.1 °C (only around +5.2 °C to +6 °C for the other seasons). The same figures are given for all catchments in appendix.

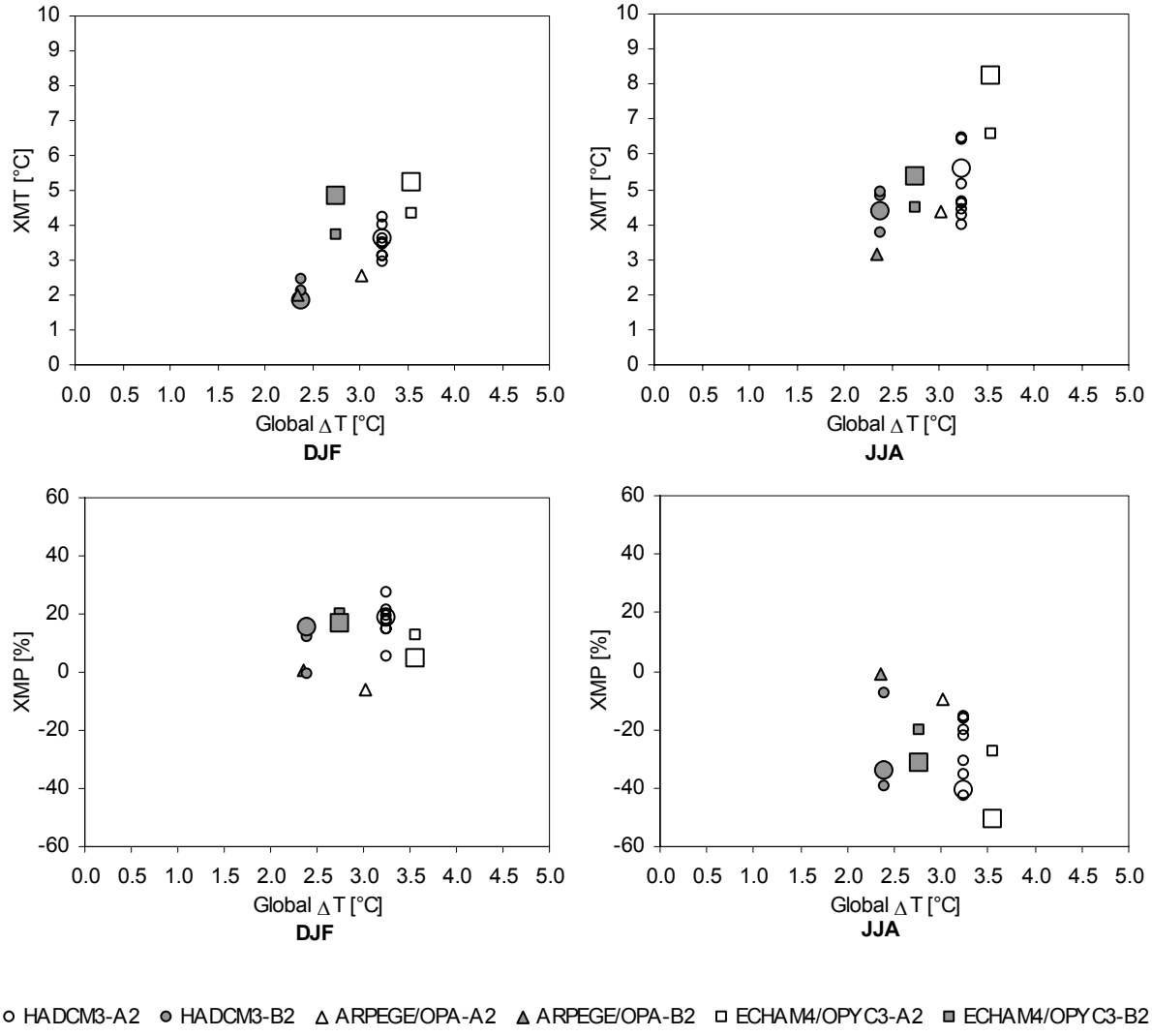

Figure 5: Regional seasonal changes of precipitation and temperature as a function of the annual global mean warming as predicted by the PRUDENCE RCM experiments for the Rhone catchment at Gletsch for the period 2070-2099; top: regional temperature changes; bottom: regional precipitation changes; the bigger symbols identify the RCAO experiments.

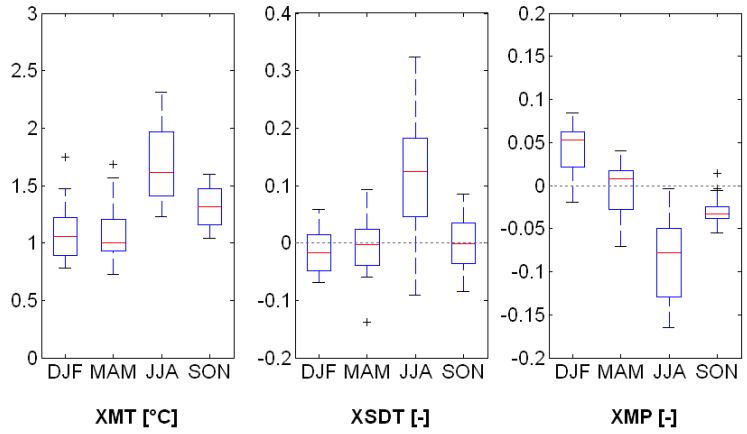

Figure 6: Box plots of regional changes in seasonal temperature (mean XMT and standard deviation XSDT) and precipitation (mean XMP) for the scenario +1°C global mean warming (2020-2049) (scaled from A2 and B2 PRUDENCE experiments). Rhone catchment at Gletsch.

Except for a few experiments and catchments, a decrease of the annual precipitation is predicted (Table 7). For the different catchments, the median relative change of annual precipitation under the emission scenario A2 ranges between –11 % and –5 %. For B2, the median predicted decrease is between –9 % and – 4 %. Finally, for the +1°C scenario it ranges between -3 % and -2 %. Note that there is no clear gradation in the projected changes of the annual precipitation between B2 and A2: The predicted median changes are similar for both scenarios.

During the winter, the precipitation is predicted to increase for all catchments and most RCMs (Table 7, Figure 6 and Figure 5) whereas most RCMs predict a decrease during summer for both scenarios. The relative change in winter and summer precipitation is globally smaller for the B2 than for the A2 scenario. For spring, the predictions of the different RCMs do not have a clear tendency towards an increase or a decrease (for all catchments and both scenarios). Whereas the relative change in fall precipitation is always predicted to decrease for the A2 scenario, the direction of the change is uncertain for B2.

3.2 Glacier surface decrease

The predicted decrease of glacier surfaces is considerable (Table 8), even for the +1°C scenario (2020-2049), where ice-covered areas shrank to approximately half of their present coverage. For that period, the Dischmabach catchment seems even to loose all ice-covered surfaces.

For the A2 and B2 scenarios (2070-2099), there are almost no ice-covered areas left. For the highest catchment, the Drance catchment, the median future predictions correspond to 2 % of glacier cover for the B2 scenario and to around 1 % for the A2 scenario. This result is due to the important annual temperature increase and especially to the strong increase during the summer. The resulting enhanced melting of snow and ice is not compensated by additional precipitation during the accumulation season. For the Drance catchment, the predicted median increase of mean temperature of +4.2 °C corresponds to an upward shift of around 850 m of the 0 °C isotherm. This shift cannot be directly translated into a reduction of the glacier surface as there is

no linear relationship between the glacier surface and the 0°C isotherm. Consider nevertheless that the mean altitude of the glacierized area for the control period is around 3150 m a.s.l. and the highest point of the glacier is 4305 m a.s.l., only about 1150 m higher. For a further discussion of the glacier surface simulation refer to Schaefli (2005).

Table 8: Predicted glaciation rate (%) for the +1°C scenario (2020-2049) and the B2 and A2 scenarios (2070-2099): the minimum, median and maximum values of the 7 respectively 12 PRUDENCE RCM experiments available for B2 respectively A2.

Catchment	Control	+1°C scenario			B2 scenario			A2 scenario		
		Min	Med	Max	Min	Med	Max	Min	Med	Max
Drance de Bagnes	39.0	12.1	18.1	22.8	0.9	1.8	6.6	0.0	1.0	1.7
Saaser Vispa	33.2	11.3	15.7	19.0	0.6	3.7	7.0	0.0	1.4	3.4
Lonza	32.8	9.3	16.9	20.9	1.0	2.5	5.1	0.0	1.6	2.3
Rhone at Gletsch	50.0	11.6	21.3	26.9	0.0	0.2	6.7	0.0	0.0	0.0
Weisse Lütschine	16.4	7.0	9.1	11.1	0.5	2.2	6.2	0.0	0.9	2.6
Tamina	1.4	0.2	0.4	0.6	0.0	0.0	0.1	0.0	0.0	0.0
Vorderrhein	2.8	0.0	0.1	0.2	0.0	0.0	0.0	0.0	0.0	0.0
Dischmabach	2.6	0.0	0.0	0.0	0.0	0.0	0.0	0.0	0.0	0.0
Rosegbach	27.2	5.2	11.1	15.6	0.0	1.3	2.3	0.0	0.3	1.3

3.3 Hydrological regime modifications

All simulations under the future regional climate scenarios for 2070-2099 show the same significant changes of the hydrological regimes and the same trends of these changes: Summer discharge is significantly reduced, winter discharge increases, the snowmelt induced peak is shifted to earlier periods in the year and decreases for most case studies (Figure 7). Due to the important reduction of the glacierized areas, pure glacial discharge regimes tend to disappear.

The results are however highly variable for the different RCM experiments. A gradation of changes is observed between the B2 and the A2 scenario: The changes predicted for B2 tend to be enhanced for A2. The median shift of the maximum monthly or semi-monthly discharge is for example around half a month for B2 and an entire month for A2. The changes are very similar for catchments having the same present regime, independently of their geographical situation. Figure 7 illustrates the simulated regime modifications for the Rhone catchment (a-glacial regime), the Weisse Lütschine (a-glacio-nival regime), the Verzasca (nivo-pluvial meridional regime) and the Minster catchment (nival of transition regime). The same figures are given in colors for all catchments in appendixes.

For the +1°C scenario (2020-2049), changes show the same trend, but are smaller. Summer discharge is still significantly reduced for most catchments but winter discharge increase is not more significant (Figure 8). The resulting shift of the snowmelt induced peak is around half a month earlier in the year. The same figures are given in colors for all catchments in appendix.

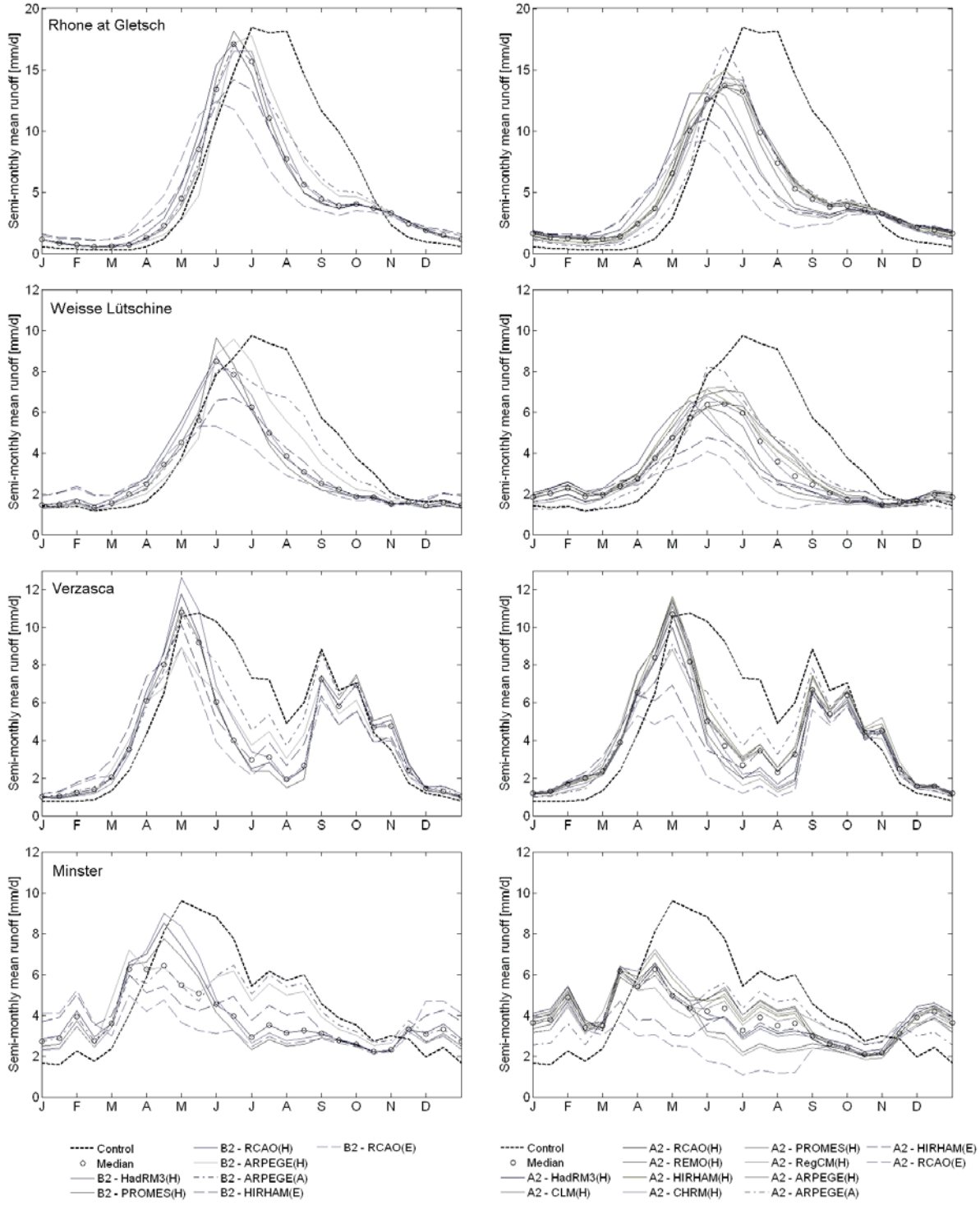

Figure 7: Changes of the hydrological regimes obtained by the 19 PRUDENCE RCM experiments for the period 2070-2099; left panel: B2 scenario (7 experiments); right panel: A2 scenario (12 experiments); regime simulated for the control period (1961-1990) in bold dashed line.

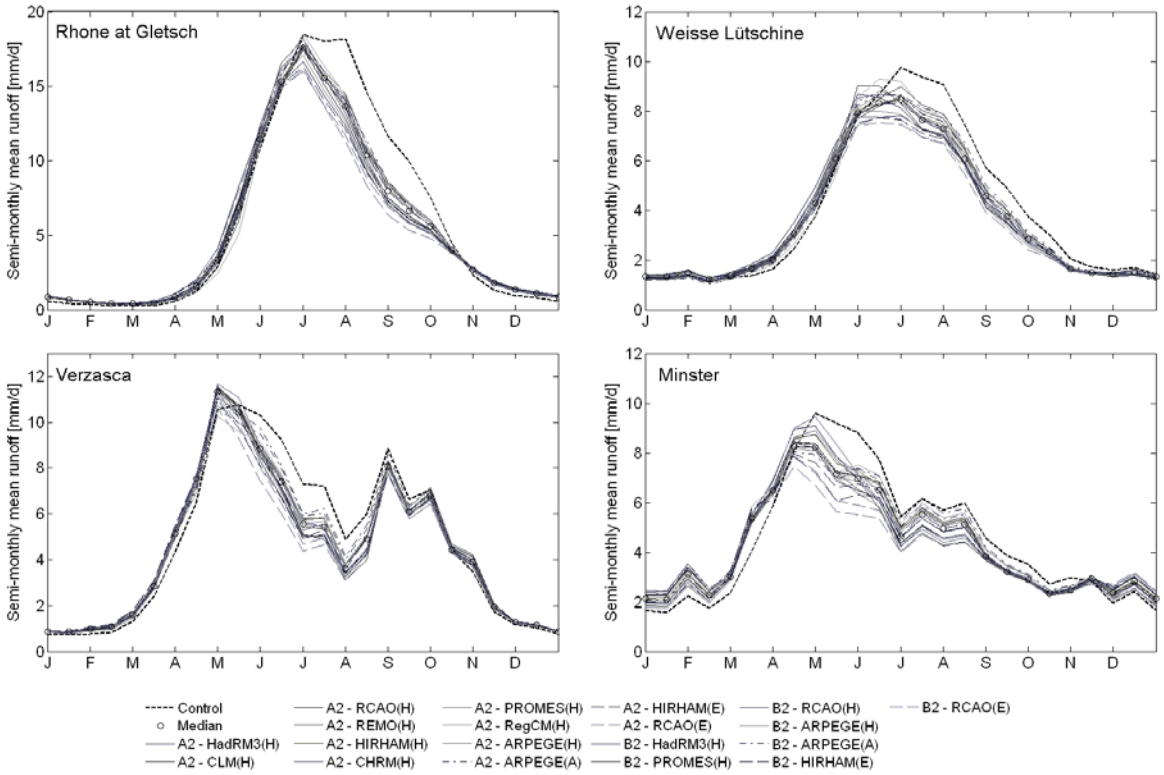

Figure 8: Changes of the hydrological regimes obtained by the 19 PRUDENCE RCM experiments for the +1°C scenario (2020-2049); regime simulated for the control period (1961-1990) in bold dashed line.

For both A2 and B2 scenarios, the Rhone catchment and the Weisse Lütschine catchment tend to have a future regime essentially driven by spring snowmelt. The variability of the results obtained for the different climate models is however high and the corresponding regimes can be quite different (Figure 7). The snowmelt-induced peak occurs for example between late May and July. The attenuation of this maximum monthly discharge is also highly variable from one scenario to the other (Figure 7). The changes obtained for the Verzasca catchment are slightly less variable. The shift of snowmelt is about half a month for all experiments. The rainfall response peak in fall does not shift, but varies in amount. This catchment is thus still expected to exhibit the same nivo-pluvial meridional regime as for the present. For the Minster catchment, the peak observed for the control run in May-June is shifted to April-May under B2 and to even earlier periods for A2. The seasonality of discharges is still significant but much less pronounced than for the control period; for A2, it tends to disappear. For both emission scenarios, the predicted changes vary significantly between the RCM experiments. For the two extreme climate experiments (RCMs driven by ECHAM4/OPYC3), the Minster regime even becomes exclusively driven by rainfall.

We tried to classify the new discharge regimes on the basis of the official Swiss classification (Aschwanden and Weingartner, 1985). Median changes in key Pardé coefficients used for hydrological regime identification are given in Table 9. If there is no significant change on maximum Pardé coefficients, the significant increase of minimum Pardé coefficients leads to much lower amplitudes between months. The smallest median amplitude changes occur for the

Verzasca for the +1°C scenario (-10%) and for the Weisse Lütschine for B2 and A2 scenarios (-20 % reduction under B2 and -44 % under A2). The largest median amplitude decrease is obtained for the Drance de Bagnes for the +1°C scenario (48 % reduction) and for the Rosegbach for B2 and A2 (-69 % reduction under B2 down to -84 % for A2)

Despite these changes, the identification of the new regimes is somehow difficult: the future regimes actually differ to some extent from the presently occurring regimes. As the meteorological conditions of the present hydro-climatic regions will change, the characteristics of the typical regimes are not preserved. For many catchments, the main difference compared to the present regime types is the appearance of a small secondary peak in fall that does not exist in present intra-Alpine regimes, but only in South-Alpine regimes.

Table 9: key Pardé coefficients (maximal and minimal Pardé coefficients, amplitude) for the control period, for the +1°C (2020-2049) and for B2 and A2 scenarios (2070-2099) (Mean values).

Catchment	Control			+1°C			B2			A2		
	Min	Max	Ampl	Min	Max	Ampl	Min	Max	Ampl	Min	Max	Ampl
Drance de Bagnes	0.04	3.49	91	0.07	3.49	48	0.10	3.74	37	0.29	3.21	11
Saaser Vispa	0.06	2.86	46	0.10	2.66	26	0.15	2.69	17	0.29	2.41	8
Lonza	0.07	2.93	40	0.11	2.81	25	0.17	2.78	16	0.32	2.65	8
Rhone at Gletsch	0.05	2.97	58	0.09	3.00	35	0.13	2.92	22	0.27	2.68	10
Weisse Lütschine	0.32	2.33	7	0.35	2.18	6	0.44	2.47	6	0.51	2.06	4
Minster	0.34	2.00	6	0.46	1.70	4	0.64	1.45	2	0.58	1.46	2
Tamina	0.27	2.30	9	0.34	2.18	6	0.43	2.07	5	0.61	2.03	3
Vorderrhein	0.17	2.55	15	0.25	2.63	11	0.32	2.61	8	0.47	2.47	5
Dischmabach	0.09	2.78	32	0.12	2.87	24	0.16	2.76	17	0.35	2.32	7
Rosegbach	0.04	3.06	75	0.07	2.84	39	0.12	2.92	23	0.23	2.51	11
Verzasca	0.16	2.14	14	0.19	2.30	12	0.24	2.09	9	0.29	2.22	8

3.4 Contribution of seasonal runoff to annual discharge

Seasonal discharge distribution is of high importance for hydropower production strategies. Table 10 gives this distribution for the control period and for the three considered scenarios. The same tendencies as previously depicted can be seen in this table.

As a consequence of an earlier snowmelt, winter and spring relative contributions to annual discharge generally increase (Table 10). This increase is enhanced by the increase of winter precipitation. The largest winter contribution increase, given in terms of ratio between the median future winter contribution and the present one, occurs for the Rhone under the B2 scenario (2.5) and for the Drance de Bagnes under the A2 scenario (4.8) and under the +1°C scenario (1.7). The smallest winter contribution increase occurs for the Weisse Lütschine under the A2, B2 and +1°C scenarios (the ratio between future and control contribution is respectively 1.9, 1.3 and 1.0). For the three scenarios and most case studies, the increase of the spring contribution to annual discharge is usually smaller than the increase in winter contribution. The largest increase in spring contribution is always obtained for the Drance de Bagnes catchment (4.2 for A2, 2.8 for B2 and 1.7 for scenario +1°C). In summer, smaller snow and ice-melt

amounts leads to reduced discharges usually enhanced by fewer summer precipitation. The largest decrease in summer contribution to annual discharges occurs for the Verzasca for the A2, B2 and +1°C scenarios, (the ratio between future and control contribution is respectively 0.5, 0.6 and 0.8). Fall is also usually characterized by a decrease of its contribution for most catchments, but in a slighter way.

Table 10: Seasonal discharge distribution (in % of mean annual discharge) for the control period, the +1°C scenario (2020-2049) and the B2 and A2 scenarios (2070-2099). Each value is the 50th percentile of the results obtained from the different runs.

Catchment	Control				+1°C scenario				B2 scenario				A2 scenario			
	DJF	MAM	JJA	SON	DJF	MAM	JJA	SON	DJF	MAM	JJA	SON	DJF	MAM	JJA	SON
Drance de Bagnes	2	6	72	21	3	10	70	16	4	16	65	13	9	24	54	14
Saaser Vispa	4	9	64	23	5	11	60	23	7	16	56	22	9	23	46	22
Lonza	3	10	66	21	5	13	62	20	7	17	58	18	10	22	51	18
Rhone at Gletsch	2	8	65	25	4	11	64	21	6	16	61	18	8	22	52	18
Weisse Lütschine	9	17	53	21	9	21	51	19	11	27	46	15	16	31	40	15
Minster	11	35	36	18	14	36	32	17	20	34	22	18	25	32	26	17
Tamina	7	27	47	19	9	31	41	19	11	37	32	19	16	38	29	19
Vorderrhein	6	22	52	20	7	29	46	18	9	36	38	18	13	40	32	18
Dischmabach	4	16	60	20	5	22	54	20	6	29	46	20	10	33	40	20
Rosegbach	2	8	68	22	4	11	63	23	6	16	56	23	7	21	49	24
Verzasca	5	31	38	27	6	35	32	28	7	40	22	30	9	40	20	30

3.5 Annual discharge

The simulated annual discharges show a significant decrease compared to the control period, for all catchments and for all climate experiments (Table 11). The median decrease ranges between -15 % (Drance de Bagnes) and -5 % (Saaser Vispa, Minster and Tamina) under the +1°C scenario (2020-2049), between – 26 % (Drance de Bagnes) and – 12 % (Vorderrhein) under the B2 scenario (2070-2099), and between – 30 % (Drance de Bagnes) and – 14 % (Vorderrhein) under scenario A2 (2070-2099).

Table 11: Predicted change of the annual runoff for the +1°C, the B2 and the A2 scenarios: the minimum, median and maximum values of the 7 respectively 12 PRUDENCE RCM experiments available for B2 respectively A2.

Catchment	+1°C scenario			B2 scenario			A2 scenario		
	Min	Med	Max	Min	Med	Max	Min	Med	Max
Drance de Bagnes	-22	-15	-11	-36	-26	-19	-49	-30	-24
Saaser Vispa	-10	-5	-2	-21	-13	-5	-34	-17	-9
Lonza	-13	-8	-4	-19	-14	-7	-32	-16	-8
Rhone at Gletsch	-19	-12	-9	-28	-20	-15	-40	-23	-16
Weisse Lütschine	-16	-9	-6	-33	-23	-12	-47	-25	-20
Minster	-13	-5	-3	-26	-14	-6	-42	-16	-11
Tamina	-12	-5	-2	-24	-16	-5	-39	-16	-10
Vorderrhein	-12	-6	-3	-22	-12	-6	-35	-14	-8
Dischmabach	-12	-7	-3	-24	-17	-4	-39	-16	-10
Rosegbach	-16	-10	-4	-28	-18	-6	-41	-22	-13
Verzasca	-12	-6	-2	-27	-16	-3	-40	-19	-10
Min	-22	-15	-11	-36	-26	-19	-49	-30	-24
Med	-13	-7	-3	-26	-16	-6	-40	-17	-10
Max	-10	-5	-2	-19	-12	-3	-32	-14	-8

The considerable decrease of the mean annual discharges has several reasons: The most evident is the mean annual precipitation decrease. For the currently glacierized catchments, the important decrease of the glacier surface (Table 8) also contributes to the discharge reduction. The long-term reduction of discharge as a result of glacier surface decrease is discussed by several authors (see, e.g., Braun et al., 2000; Chen and Ohmura, 1990). Note however that this discharge reduction is not exclusively due to a reduction of the ice melt contribution (for the studied catchments, the present ice melt contribution resulting from the currently observed negative glacier mass balances is small compared to the total precipitation). A significant part of the discharge reduction is also due to the increase of evapotranspiration. This latter is partly a consequence of the glacier retreat involving the increase of the catchment area where evapotranspiration is subtracted from precipitation. Note that for ice-covered catchment parts, the loss of annual precipitation through evaporation is not simulated in the hydrological model. As occurring sublimation processes at the glacier surface only influence the long-term glacier mass balance, the amount of evapotranspiration on the ice-covered part has actually no direct influence on the discharge.

Additionally, the substantial temperature increase throughout the seasons enforces the total evapotranspiration on ice-free areas and accordingly, all catchments show a strong increase of total evapotranspiration (Table 12). The increase is less important for the dry summers than for the winters. For both seasons potential evapotranspiration is higher but summer precipitation is expected to decrease conversely to winter precipitation. Actual evapotranspiration does not necessary increase in summer conversely to winter.

Table 12: Simulated actual evapotranspiration for control and future period (median value) for the B2 and A2 scenarios; the values are specific values only for the ice-free part.

Catchment	Relative to the ice-free part (mm)			
	Control	+1°C	B2 sc.	A2 sc.
Drance de Bagnes	296	333	377	416
Saaser Vispa	243	272	305	328
Lonza	269	300	338	371
Rhone at Gletsch	294	337	373	414
Weisse Lütschine	391	452	502	533
Minster	507	555	610	646
Tamina	274	305	341	376
Vorderrhein	274	295	333	363
Dischmabach	255	277	313	341
Rosegbach	229	250	276	298
Verzasca	380	420	462	494
Median increase	-	31	69	102

The maximum predicted discharge decrease for the A2 scenario is significantly higher than for the B2 scenario (for all catchments) but the ranges of predicted decreases are overlapping and the median and minimum decreases are quite similar. This means that the variability of the results due to the different RCM experiments is as large as the difference of the results obtained for different emission scenarios.

Note that for the +1°C scenario (2020-2049), the mean interannual discharge decrease estimated from our simulations may be overestimated as a result of the highly simplified simulation of the glacier retreat. The way the glacier surface is updated for a future climate scenario, is based on the assumption that the glacier has reached a stationary state for the considered future climate situation. This will probably not be exactly the case due to the non-negligible reaction time of the considered glaciers (from several years to a few decades depending on the glacier configuration). The real glacier state for a given future climate scenario will thus correspond to a time period preceding the future time period under consideration. The amount of glacier available for ice melt during this future period will thus be larger than the one simulated with our model. The simplification on the glacier evolution simulation will not have the same impact for the A2 and B2 scenarios. The glacier retreat for these scenarios is expected to be as large that the contribution of glacier melt to the future hydrological regime will be negligible. Even a 50% error on the future glacier surface can be expected to have only little influence on the estimated glacier contribution.

4 Discussion

The large range of climate change impacts predicted by the 19 RCM experiments is worth of further analysis. First, we would like to highlight how this variability acts on the discharge regime prediction. The regime modifications of catchments with high elevations are highly conditioned by the changes of the seasonal temperatures. The simulated maximum monthly discharge is for example highly correlated to the change in mean spring temperature (Figure 10). The main reason is that the higher the mean spring temperature is, the higher the volume of snow melt during this period is and as a consequence, the lower the volume of the remaining snowpack at the beginning of the summer period is. Accordingly, the high variability of the regional temperature prediction has a strong influence on the range of predicted future regimes (Figure 9). For catchments at lower altitudes the influence of precipitation modification is more pronounced and the variability of the predicted climate change impact is mainly due to the large range of predicted regional precipitation changes (Figure 9). This general mechanism of discharge regime modification induced by climate change has already been highlighted by Braun et al. (2000) for comparable discharge regimes and for a doubling CO_2 climate change scenario.

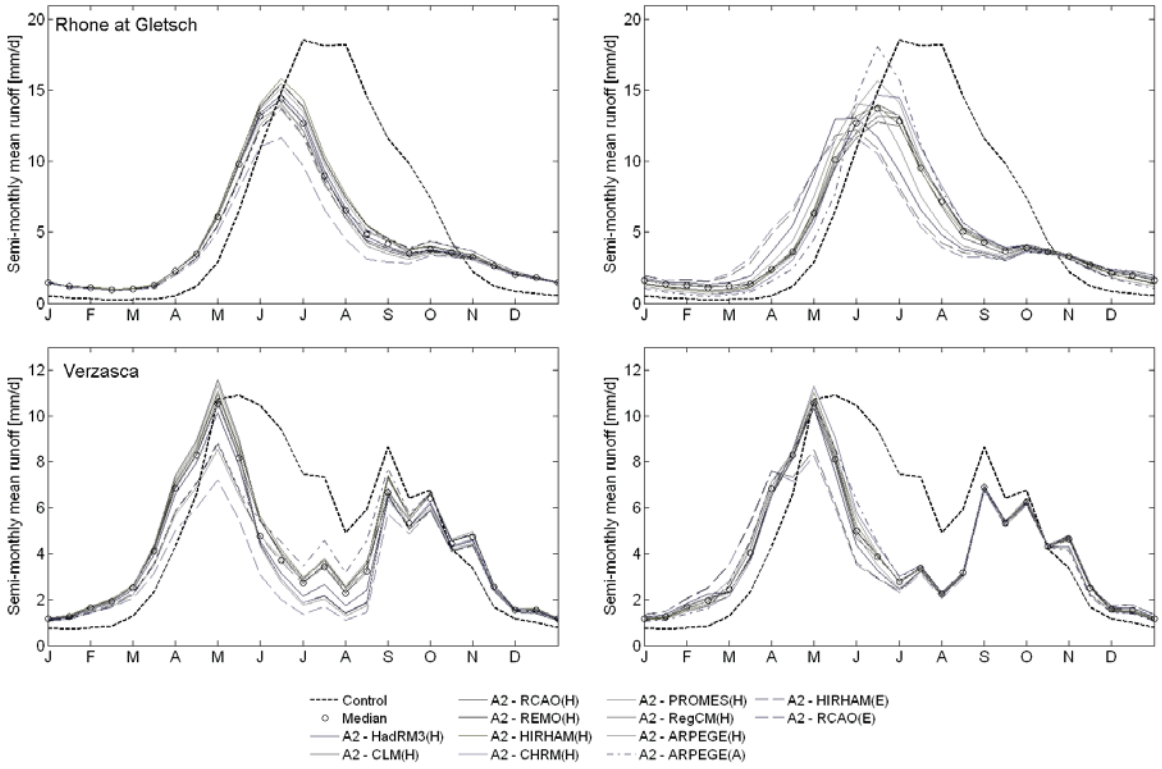

Figure 9: Sensitivity of the hydrological regimes to temperature and precipitation variability of the PRUDENCE RCM experiments (for the Rhone and the Verzasca catchment, scenario A2, period 2070-2099); left panel: regime variability induced by the precipitation variability under median predicted seasonal temperature increase, right panel: regime variability induced by temperature variability under median predicted precipitation change.

The main question we would finally like to answer is whether this variability is induced by the driving AOGCMs or whether the different RCM contribute substantially to this variability. A plot of the regional temperature and precipitation changes predicted by the RCMs as a function of the global-mean warming predicted by the driving AOGCMs highlights the two different sources of prediction variability: i) Considering a given RCM (for example the RCAO in Figure 5), the driving AOGCM induces a so large variability that the predicted regional warming for the scenario A2 and B2 can be overlapping. ii) Considering a given AOGCM, the inter-RCM variability represents an important additional source of prediction uncertainty (see an example for winter and summer changes for the Rhone catchment in Figure 5). While for each AOGCM the predicted global-mean warming is clearly distinct for the B2 and A2 scenarios, the ranges of regional changes predicted by the different RCMs for each of them are overlapping. As illustrated in Figure 5, these two levels of prediction variability are also observed for the regional precipitation changes.

In terms of impact on the hydrological regime, this substantial contribution of the inter-RCM variability to the total prediction variability can also be pointed out. We use the relationship between a characteristic regime modification and a characteristic regional climate change as an indicator.

The regime modification considered here is the maximum monthly discharge. As mentioned before, for the high mountainous catchments, it is highly correlated to the change in mean spring temperature (Figure 10). For a rainfall driven regime (the Verzasca catchment in Figure 10), the relationship between the maximum monthly discharge and the increase of spring temperature is still significant but much weaker. The changes of spring precipitation become conversely a more relevant explanatory variable (Figure 10). The plots of these relationships highlight clearly the two levels of prediction variability that have been identified for the regional climate change prediction and that propagate to the impact prediction. The results suggest that the driving AOGCM may induce more impact prediction variability than the inter-RCM variability for a given AOGCM. For the RCAO model, the maximum monthly discharge predicted for the Verzasca catchment for A2 with HadCM3/HadAM3H as a driving model is around twice as high as with ECHAM4/OPYC3 as a driving model. Nevertheless, the results show that the inter-RCM variability is far from being negligible as for example illustrated in Figure 10 by the spread of the predicted maximum monthly discharges for HadCM3/HadAM3H under scenario A2. Note that a quantitative evaluation of the uncertainty induced by each of the two climate modeling levels would require more RCM experiments.

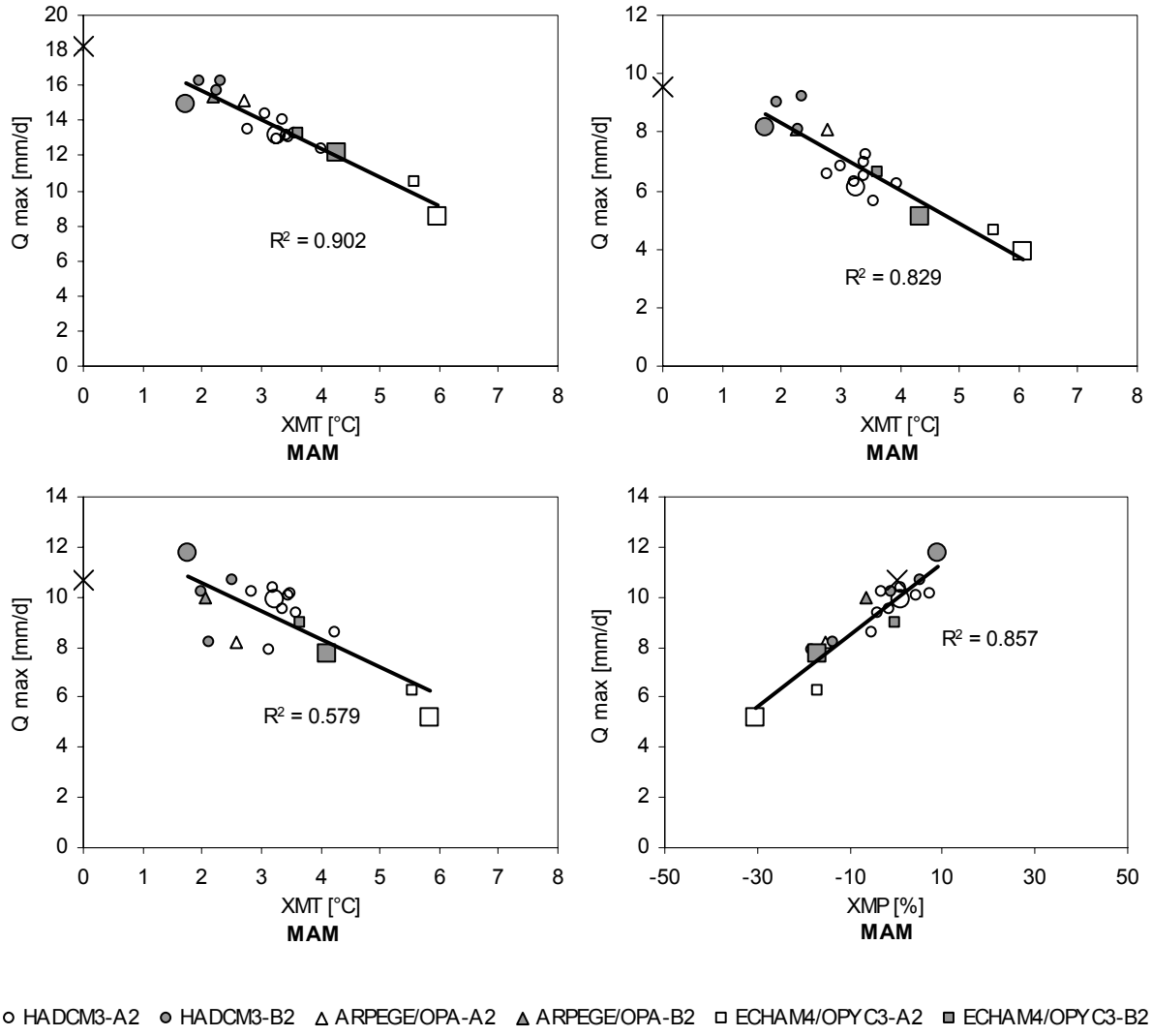

Figure 10: Maximum mean monthly discharge (Qmax) as a function of regional changes of either mean spring temperature or mean spring precipitation; top left: Rhone at Gletsch, top right: Weisse Lütchine, bottom, left: Verzasca, bottom, right: Verzasca (the bigger symbols identify the RCAO experiments, the cross indicates the value for the control period, R^2 is the coefficient of determination of the linear regression).

5 Conclusion

The presented study focuses on the impacts of climate change on mountainous discharge regimes. Impacts were analysed for the 2070-2099 future period under the two SRES A2 and B2 emission scenarios and for a +1°C global warming scenario corresponding in first approximation to the 2020-2049 future period. The studied catchments are representative of the different hydro-climatic regions of the Swiss Alps and accordingly some general conclusions can be drawn for the studied Alpine area. The analysis is based on a classical simulation approach using the outputs of 19 climate model experiments to drive a hydrological model and a land cover evolution model. The underlying modeling framework has been developed for a fully probabilistic analysis of climate change impacts on Alpine catchments (see Schaefli, 2005).,The present study highlights the climate change prediction uncertainty induced by the use of different climate models. For this purpose, a suite of 19 climate experiments done within the PRUDENCE EU project was used. They were obtained under emission scenario A2 and B2 from 9 different regional climate models respectively driven by one of the three coupled atmosphere-ocean general circulation models applied within PRUDENCE. 19 additional scenarios were obtained from a classical pattern scaling approach for the +1°C global warming scenario.

Considering the various hydrological regimes and the predictions given by the different climate models, there is a general trend in the simulated climate change impact for the three considered scenarios: The predicted climate change results in a significant decrease of the total annual discharge and in a shift of the monthly maximum discharge to earlier periods of the year due to the temperature increase and the resulting impact on the snow melting processes. As illustrated in Figure 11, two main impacts on hydroelectricity production in the Swiss Alps are next expected. They are:

- **Reduction of the mean annual hydroelectricity potential** (for hydropower production systems such as those existing today) due to a significant decrease of mean annual discharges. Note that for the +1°C scenario (2020-2049), the mean interannual discharge decrease estimated from our simulations may be overestimated as a result of the highly simplified simulation of the glacier retreat.

- **Reduction of the amplitude between summer and winter discharges.** Larger amounts of water are expected in winter and spring, slightly lower discharges are expected in summer. These changes are not really significant for the +1°C scenario (2020-2049) but may take place later. This more regular contribution of discharges over the year is expected to make the management of water storage easier. Note that this change in seasonality is expected to have another consequence. The future hydrological regimes are actually expected to be less driven by snow-melt and glacier melt processes but more by the regimes of precipitation. As a result, the interannual variability of mean annual discharges is expected to increase. These future variations of the year-to-year hydroelectricity potential are worth of further investigations.

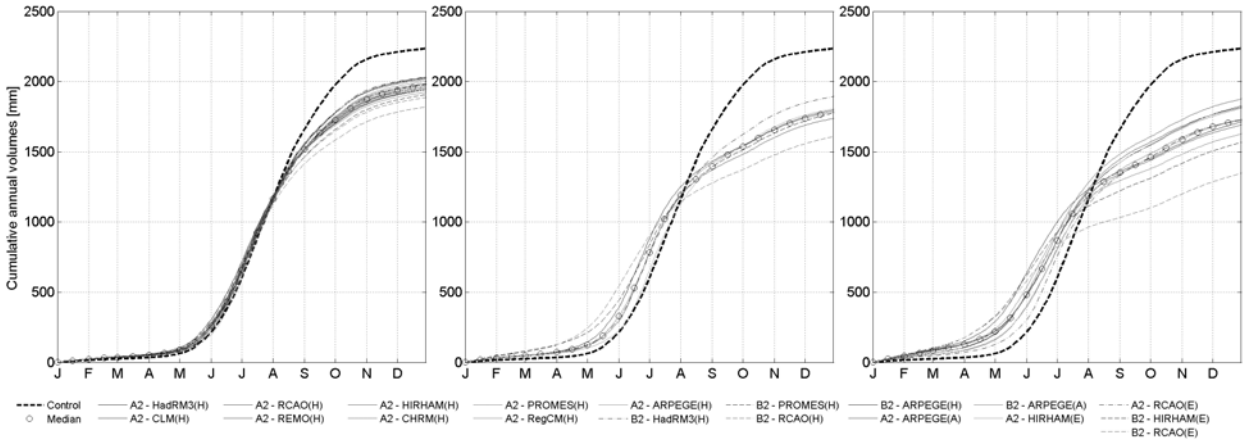

Figure 11: Changes of the cumulative discharge obtained by the 19 PRUDENCE RCM experiments for the Rhone catchment at Gletsch; left panel: +1°C scenario (2020-2049) (19 experiments); central panel: B2 scenario (2070-2099) (7 experiments); right panel: A2 scenario (2070-2099) (12 experiments); regime simulated for the control period (1961-1990) in bold dashed line.

Note that all scenarios and all models predict changes of same trend; only amplitude and timing of these changes differ. As a clear gradation exists between the three considered scenarios, one can consider the corresponding potential impacts in a chronological manner: assuming that climate models are reasonable representations of the real climate system, impacts simulated for the +1°C global warming scenario are very likely to occur in a nearby period, impacts simulated for the B2 (2070-2099) scenario are expected to be observed later but eventually before the 2070-2099 period if the real time evolution of emissions is close to that defined for the A2 emission scenario (2070-2099). If impacts simulated for these scenarios are likely to occur, the uncertainty on emission scenario may be transferred to the uncertainty on the occurrence time of these changes.

For each climate change scenario analyzed in this work, the modifications of annual discharges and hydrological regimes simulated for the different RCM runs are significantly variable. For a given RCM experiment, the hydrological regimes associated with each of the two A2 and B2 emission scenarios are clearly distinct but considering all RCM experiments, the resulting ranges of hydrological regimes for both emission scenarios are overlapping and accordingly an unambiguous prediction of the climate change impacts associated with a given green house gas emission scenario is not possible. The large prediction variability induced by the 19 RCM experiments considered here is partly induced by the underlying driving AOGCMs. This source of climate change impact uncertainty as already been highlighted by Zierl and Bugmann (2005) for Alpine catchments. The results presented in this study show however clearly that the differences between different RCM experiments with the same driving AOGCM can result in comparably high impact differences as the use of different AOGCMs to drive a given RCM. This result suggests that the inter-RCM variability should always be considered in climate change impact studies.

The presented results are conditioned on the different models, data and assumptions used in this study. The reliability of climate change data is first conditioned by the different hypotheses and

simplifications used for climate models elaboration (AOGCM's and RCM's). The possibility that AOGCM's and RCM's share the same errors in their response to emission scenarios cannot be excluded. The possibility of a climatic surprise is not accounted for either. The perturbation methodology applied in this paper for the generation of local-scale temperature and precipitation time series has the advantage of simplicity but has also some drawbacks that are important to point out. Climate changes in weather frequency or persistence are not accounted for (see Mearns et al. 1996 for an illustration of possible related impacts). This is especially critical when extreme events are analysed (floods, droughts). Even on a seasonal time step, the risk of extreme events in a future climate is not negligible (Palmer and Räisänen, 2002; Schaer et al., 2004). Possible long-term droughts such as the year 2003 drought experienced over whole Europe or possible n-days extreme rainfall events can however not be simulated with a simple scaling approach whatever the number of generated scenarios is. The improvement of downscaling methodologies is thus essential to give more reliable estimates of climate change impacts.

The present study does not consider the modeling uncertainties associated with the hydrological model. Schaefli (2005) showed that the uncertainty induced by the parameter uncertainty and the total modeling error for a given model structure is far less important than the uncertainty due to the climate predictions. However, as for the climate models, it is not possible to design a unique best hydrological model for a given catchment. The one that has been retained for this study represents just one possible model structure. The analysis of several equivalent hydrological models would complete the current results. The multi-model approach presented by Schaefli (2005) suggests that different hydrological models could increase considerably the uncertainty of the future discharge predictions. An important additional source of uncertainty is namely the estimation of the potential evapotranspiration and the simulation of the corresponding actual evapotranspiration through the hydrological model. Further research in this area is crucial for a detailed analysis of the climate change impact uncertainty inherent in the system response modeling.

Acknowledgements

Part of this work has been funded by the Swiss Federal Office for Energy. We also wish to thank the Forces Motrices de Mauvoisin and the Swiss Federal Office for Water and Geology for providing the discharge data and the national weather service MeteoSwiss for providing the meteorological time series. Useful comments and suggestions from B. Schaedler, M. Maisch and M. Zappa are also gratefully acknowledged.

References

Anonymous, 1969. Mass-balance terms. *Journal of Glaciology*, **8**(52): 3-7.

Arnell, N. W. and Hulme, M., 2000. *Implications of Climate Changes for large dams and their management. Thematic Review II.2 prepared as an imput to the World Commission on Dams*, Cape Town.

Arribas, A., Gallardo, C., M.A., G. and Castro, M., 2003. Sensitivity of the Iberian Peninsula climate to a land degradation. *Climate Dynamics*, **20**: 477-489.

Aschwanden, H. and Weingartner, R., 1985. *Die Abflussregimes der Schweiz*. 65, Bern.

Beniston, M., Rebetez, M., Giorgi, F. and Marinucci, M. R., 1994. An analysis of regional climate-change in Switzerland. *Theoretical and Applied Climatology*, **49**(3): 135-159.

Braun, L. N., 1999. The diminution of high alpine glaciation and its impact on water resources. In *Geosciences in High Asia - Proceedings of a symposium held in Dushanbe (10/11 October 1998) on occasion of the 70th anniversary of the German-Soviet Alai-Pamir expedition in 1928*. Z. W. (eds)Bayreuther Bodenkundliche Berichte, Bayreuth, 79-96.

Braun, L. N., Weber, M. and Schulz, M., 2000. Consequences of climate change for runoff from Alpine regions. *Annals of Glaciology*, **31**: 19-25.

Burlando, P., Pellicciotti, F. and Strasser, U., 2002. Modelling mountainous water systems between learning and speculating looking for challenges. *Nordic Hydrology*, **33**(1): 47-74.

Burman, R. and Pochop, L. O., 1994. *Evaporation, evapotranspiration and climatic data*. Elsevier, Amsterdam, 278.

Chen, J. and Ohmura, A., 1990. On the influence of Alpine glaciers on runoff. In *Hydrology in Mountainous Regions I: Hydrological Measurements; the Water Cycle*. H. Lang and A. Musy (Editors). IAHS Publ. No. 193, Wallingford, Oxfordshire UK, 117-125.

Christensen, J. H., Carter, T. R. and Giorgi, F., 2002. PRUDENCE employs new methods to assess European Climate Change. *EOS Transactions, AGU*, **83**: 147.

Christensen, J. H., Räisänen, J., Iversen, T., Bjørge, D., Christensen, O. B. and Rummukainen, M., 2001. A synthesis of regional climate change simulations - A Scandinavian perspective. *Geophysical Research Letters*, **28**: 1003-1006.

Consuegra, D. and Vez, E., 1996. *AMIE: Analyse et Modélisation Intégrées du cheminement des Eaux en zones habitées, modélisation hydrologique, Application au bassin versant de la Haute Broye*, IATE/HYDRAM, Ecole Polytechnique Fédérale de Lausanne, Lausanne, Switzerland.

Doms, G. and Schättler, U., 1999. *The Nonhydrostatic Limited-Area Model LM (Lokal-Modell) of DWD, Part I: Scientific Documentation*, Deutscher Wetterdienst, Meteorologische Analyse und Modellierung, Offenbach, Germany.

Etchevers, P., Golaz, C., Habets, F. and Noilhan, J., 2002. Impact of a climate change on the Rhone river catchment hydrology. *Journal of Geophysical Research - Atmospheres*, **107**(D16), doi: 10.1029/2001JD000490.

Frei, C., Christensen, J. H., Deque, M., Jacob, D., Jones, R. G. and Vidale, P. L., 2003. Daily precipitation statistics in regional climate models: Evaluation and intercomparison for the European Alps. *Journal of Geophysical Research - Atmospheres*, **108**(D3), doi: 10.1029/2002JD002287.

Gibelin, A. L. and Déqué, M., 2003. Anthropogenic climate change over the Mediterranean region simulated by a global variable resolution model. *Clim. Dynam.*, **20**(4): 327-339.

Giorgi, F., Marinucci, M. R. and Bates, G. T., 1993a. Development of a second generation regional climate model (REGCM2). Part I: Boundary layer and radiative transfer processes. *Monthly Weather Review*, **121**: 2794-2813.

Giorgi, F., Marinucci, M. R., Bates, G. T. and DeCanio, G., 1993b. Development of a second generation regional climate model (REGCM2). Part II: Cumulus cloud and assimilation of lateral boundary conditions. *Monthly Weather Review*, **121**: 2814-2832.

Gordon, C., Cooper, C., Senior, C. A., Banks, H., Gregory, J. M., Johns, T. C., Mitchell, J. F. B. and Wood, R. A., 2000. The simulation of SST, sea ice extents and ocean heat transports in a version of the Hadley Centre coupled model without flux adjustments. *Climate Dynamics*, **16**(2-3): 147-168.

Hulme, M., Jenkins, G., Lu, X., Turnpenny, J.R., Mitchell, T.D., Jones, R.G., Lowe, J., Murphy, J.M., Hassell, D., Boorman, P., McDonald, R. and Hill, S., 2002. *Climate Change Scenarios for the United Kingdom: The UKCIP02 Scientific Report*. Tyndall Centre for Climate Change Research, School of Environmental Sciences, University of East Anglia, Norwich, U.K.

Jacob, D., 2001. A note to the simulation of the annual and inter-annual variability of the water budget over the Baltic Sea drainage basin. *Meteorology and Atmospheric Physics*, **77**(1-4): 61-73.

Jasper, K., Calanca, P., Gyalistras, D. and Fuhrer, J., 2004. Differential impacts of climate change on the hydrology of two alpine river basins. *Climate Research*, **26**(2): 113-129.

Jenkins, G. and Lowe, J., 2003. *Handling uncertainties in the UKCIP02 scenarios of climate change*, Hadley Centre, Technical note 44, Exeter, UK.

Jones, R.N., 2000. Analysing the risk of climate change using an irrigation demand model, *Clim. Res.*, **14**: 89-100.

Kirchhofer, W. and Sevruk, B., 1991. *Mean annual corrected precipitation depths 1951-1980, Atlas hydrologique de la Suisse.* Service Hydrologique et Géologique National, Bern.

Klok, E. J., Jasper, K., Roelofsma, K. P., Gurtz, J. and Badoux, A., 2001. Distributed hydrological modelling of a heavily glaciated Alpine river basin. *Hydrological Sciences Journal*, **46**(4): 553-570.

Laternser, M. and Schneebeli, M., 2002. *Spatial Grouping of Snow Stations, Snow and Avalanche Climatology of Switzerland*. ETH Zürich.

Mearns, L.O., Rosenzweig, C. and Goldberg, R., 1996. The effect of changes in daily and interannual climatic variability on ceres-wheat: A sensitivity study. *Clim. Change* **32**(3): 257-292.

Mitchell, TD., 2003. Pattern scaling - An examination of the accuracy of the technique for describing future climates. *Clim. Change* **60**(3): 217-242.

Nakicenovic, N. and Swart, R. (Editors), 2000. *Special Report on Emissions Scenarios (Intergovernmental Panel on Climate Change)*. Cambridge University Press, Cambridge, UK, 570.

Nash, J. E. and Sutcliffe, J. V., 1970. River flow forecasting through conceptual models. Part I, a discussion of principles. *Journal of Hydrology*, **10**(3): 282-290.

New, M. and Hulme, M., 2000. Representing Uncertainty in Climate Change Scenarios: a Monte Carlo approach. *Integrated Assess*. **1**: 203-213.

New, M., Hulme, M. and Jones, P., 2000. Representing twentieth-century space-time climate variability. Part II: Development of 1901-96 monthly grids of terrestrial surface climate. *Journal of Climate*, **13**(13): 2217-2238.

Palmer, T.N. and Räisänen, J., 2002. Quantifying the risk of extreme seasonal precipitation events in a changing climate. *Nature*, **415**: 512-514.

Pardé, M., 1933. Le régime des cours d'eau de l'Europe orientale (en collaboration avec St.Kolupaila). *Revue Geographie Alpine*, **T.XXI**(IV): 651-748.

Pope, V. D., Gallani, M. L., Rowntree, P. R. and Stratton, R. A., 2000. The impact of new physical parametrizations in the Hadley Centre climate model - HadAM3. *Climate Dynamics*, **16**: 123-146.

Räisänen, J., 2001. CO2-induced climate change in CMIP2 experiments: Quantification of agreement and role of internal variability. *Journal of Climate*, **14**(9): 2088-2104.

Räisänen, J., 2002. CO2-induced changes in interannual temperature and precipitation variability in 19 CMIP2 experiments. *Journal of Climate*, **15**(17): 2395-2411.

Räisänen, J., Hansson, U., Ullerstig, A., Döscher, R., Graham, L. P., Jones, C., Meier, H. E. M., Samuelsson, P. and Willén, U., 2004. European climate in the late 21st century: regional simulations with two driving global models and two forcing scenarios. *Climate Dynamics*, **22**(1): 13-31.

Rango, A. and Martinec, J., 1995. Revisiting the degree-day method for snowmelt computations. *Water Resources Bulletin*, **31**(4): 657-669.

Roeckner, E., Bengtsson, L., Feichter, J., Lelieveld, J. and Rodhe, H., 1999. Transient climate change simulations with a coupled atmosphere-ocean GCM including the tropospheric sulfur cycle. *Journal of Climate*, **12**(10): 3004-3032.

Royer, J. F., et al., 2002. Simulation of climate changes during the 21st century including stratospheric ozone. *Comptes Rendus Geoscience*, **334**: 147-154.

Santer, B.D., Wigley, T.M.L., Schlesinger, M.E. and Mitchell, J.F.B. 1990. *Developing climate scenarios for equilibrium GCM results*. MPI report 47, Hamburg.

Schädler, B. and Bigler, R., 2002. *Components of the natural water balance 1961-1990, Atlas hydrologique de la Suisse*. Service Hydrologique et Géologique National, Bern.

Schaefli, B., 2005. *Quantification of modelling uncertainties in climate change impact studies on water resources : Application to a glacier-fed hydropower production system in the Swiss Alps*. Doctoral Thesis N° 3225, Ecole Polytechnique Fédérale de Lausanne, Lausanne, 209.

Schaefli, B., Hingray, B., Niggli, M. and Musy, A., 2005. A conceptual glacio-hydrological model for high mountainous catchments. *Hydrology and Earth System Sciences Discussions*, **2**: 73-117.

Schaer, C., Vidale, P.L., Luthi, D., Frei, C., Haberli, C., Liniger, M.A. and Appenzeller, C., 2004. The role of increasing temperature variability in European summer heatwaves. *Nature*, **427**(6972): 332-336.

Schneider, S.H. and Thompson, S.L., 1981. Atmospheric CO2 and climate – importance of the transient response. *J. Geophys. Res. Oc. Atm*. **86**: 3135-3147.

Shabalova, M. V., Van Deursen, W. P. A. and Buishand, T. A., 2003. Assessing future discharge of the river Rhine using regional climate model integrations and a hydrological model. *Climate Research*, **23**: 223-246.

SwissTopo, 1995. *Digital height model of Switzerland - DHM25*, Wabern, Switzerland.

SwissTopo, 1997. *Digital National Maps of Switzerland - PM25*, Wabern, Switzerland.

Vidale, P. L., Lüthi, D., Frei, C., Seneviratne, S. and Schär, C., 2003. Predictability and uncertainty in a Regional Climate Model. *Journal of Geophysical Research - Atmospheres*, **108**(D18): 4586, doi: 10.1029/2002JD002810.

Weber, R. O., Talkner, P., Auer, I., Bohm, R., GajicCapka, M., Zaninovic, K., Brazdil, R. and Fasko, P., 1997. 20th-century changes of temperature in the mountain regions of Central Europe. *Climatic Change*, **36**(3-4): 327-344.

Weingartner, R., Aschwanden, H., 1986. *Die Abflussregimes der Schweiz*. Geographisches Institut der Universität Bern, Bern.

Wilby, R. L. and Wigley, T. M. L., 1997. Downscaling general circulation model output: a review of methods and limitations. *Progress in Physical Geography*, **21**(4): 530-548.

Willis, I. and Bonvin, J.-M., 1995. Climate change in mountain environments: hydrological and water resource implications. *Geography*, **80**(3): 247-261.

Xu, C. Y., 1999. From GCMs to river flow: a review of downscaling methods and hydrologic modelling approaches. *Progress in Physical Geography*, **23**(2): 229-249.

Zierl, B. and Bugmann, H., 2005. Global change impacts on hydrological processes in Alpine catchments. *Water Resources Research*, **41**: W02028, doi: 10.1029/2004WR003447.

Appendices

Appendices contain detailed results for every catchment of the impacts predicted by the 27 EU PRUDENCE climate experiments. The Appendices list is given hereafter.

App. 1. Drance de Bagnes
App. 2. Saaser Vispa
App. 3. Lonza
App. 4. Rhone at Gletsch
App. 5. Weisse Lütschine
App. 6. Minster
App. 7. Tamina
App. 8. Vorderrhein
App. 9. Dischmabach
App. 10. Rosegbach
App. 11. Verzasca

Appendix 1 : The Dranse de Bagnes catchment

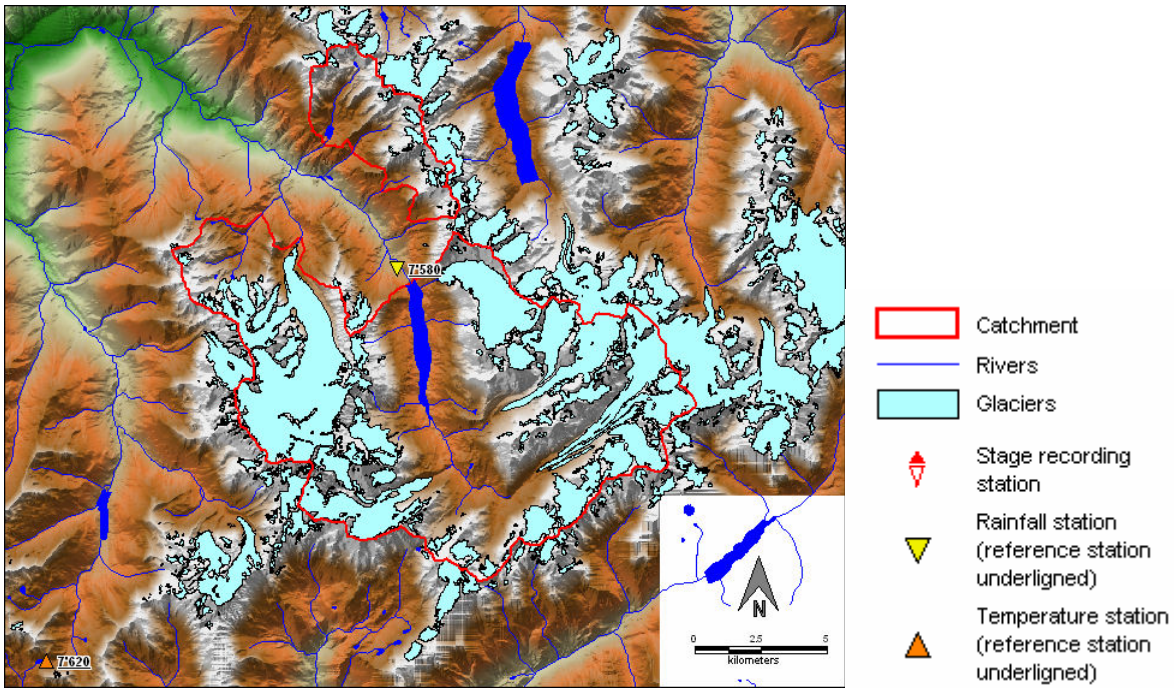

Fig. AI.1: Catchment situation

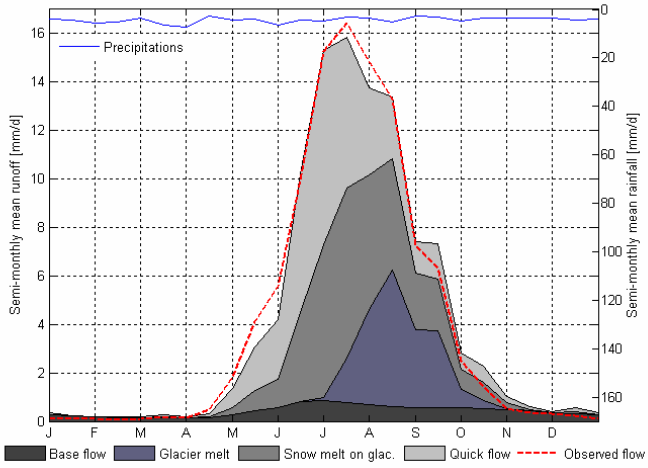

Fig. AI.2: Calibration – Semi-monthly cycle for 1987-1993

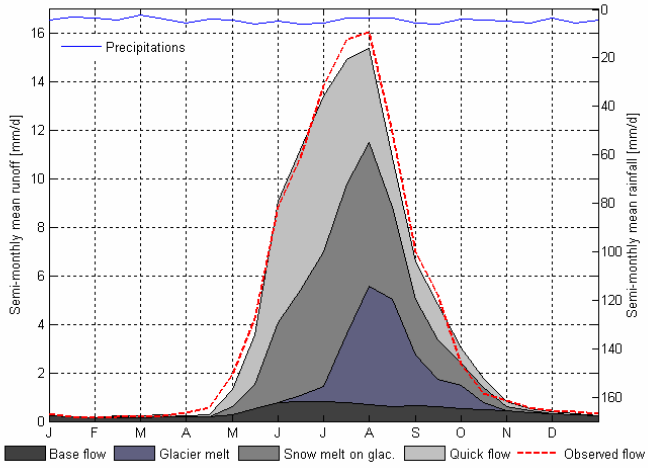

Fig. AI.3: Validation – Semi-monthly cycle for 1993-1999

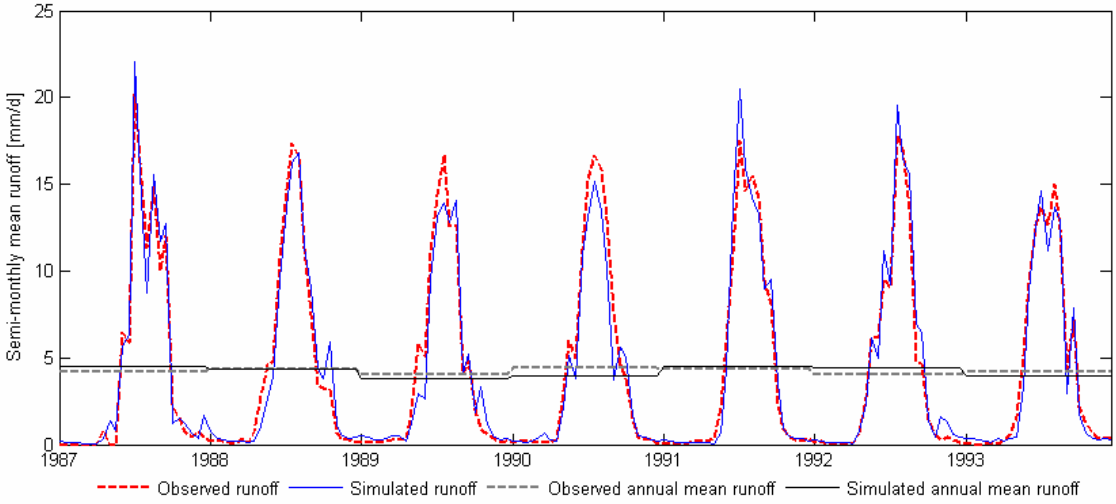

Fig. AI.4: Calibration – Semi-monthly mean flow for 1987-1993

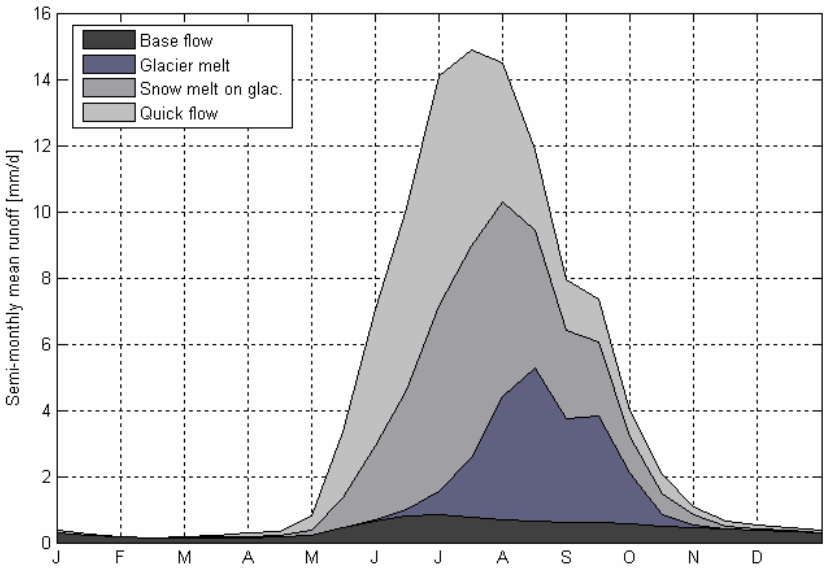

Fig. AI.5: Hydrograph components for the control period (1972-1995)

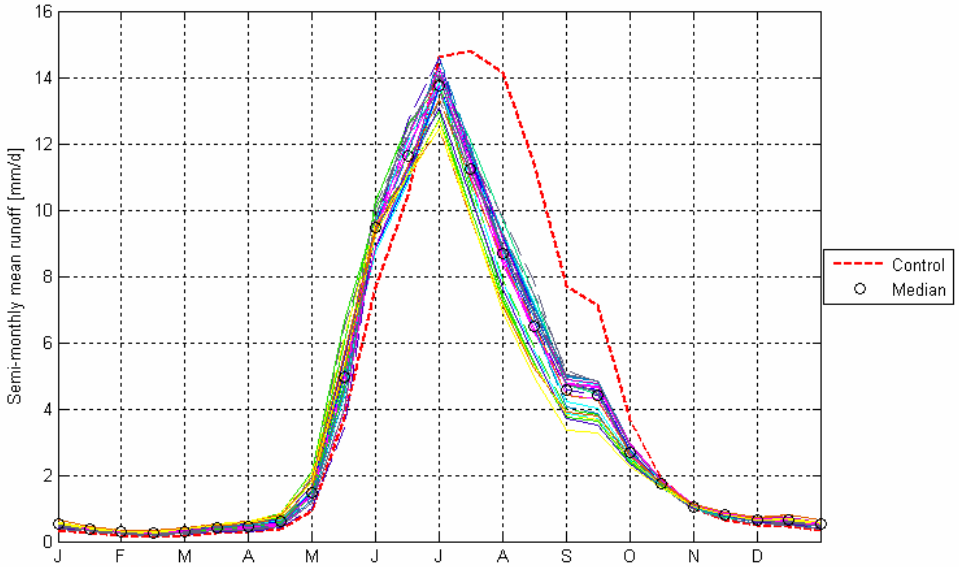

Fig. AI.6: Changes in hydrological regime for 1 °C global mean warming (scaled from A2 and B2 PRUDENCE experiments)

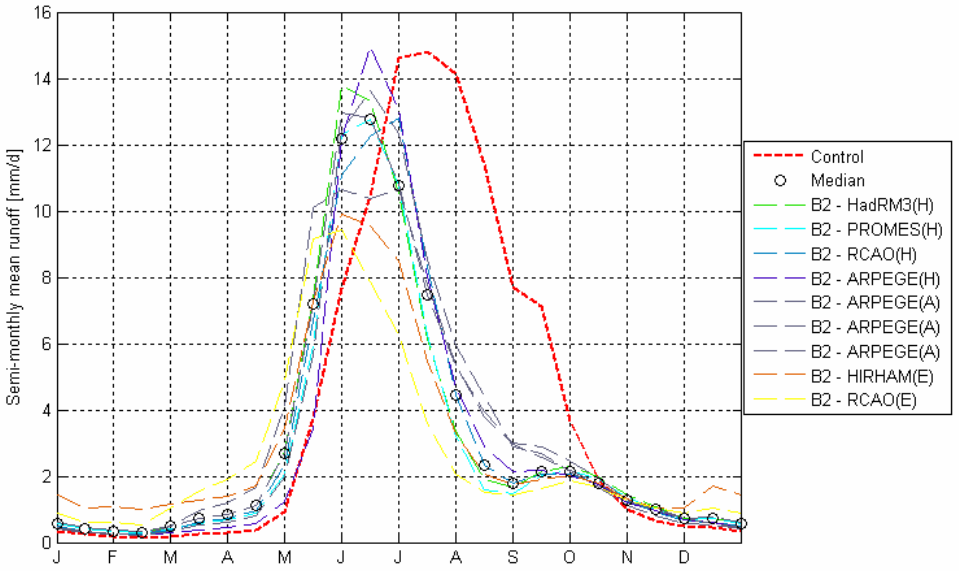

Fig. AI.7: Changes in hydrological regime for 2070-2099 – B2 scenario

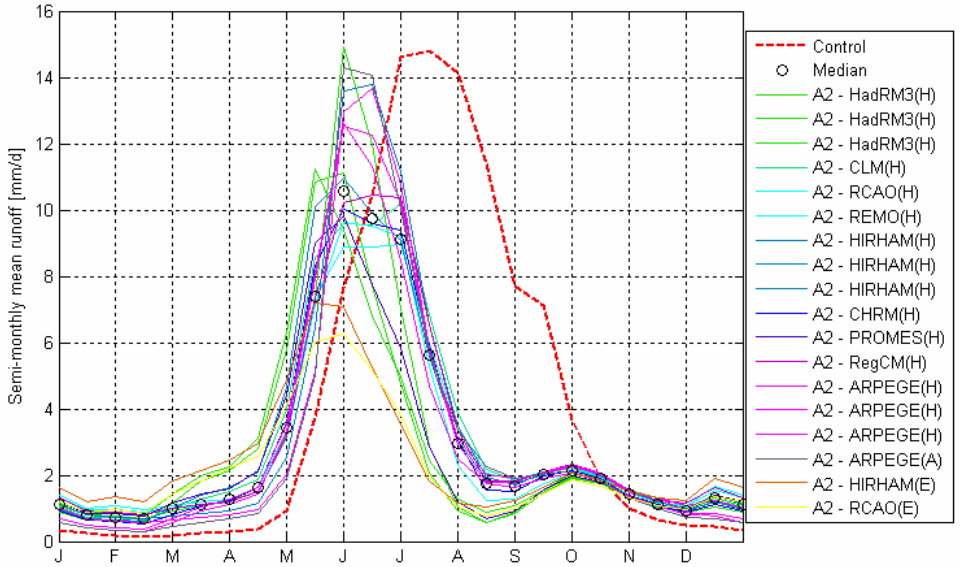

Fig. AI.8: Changes in hydrological regime for 2070-2099 – A2 scenario

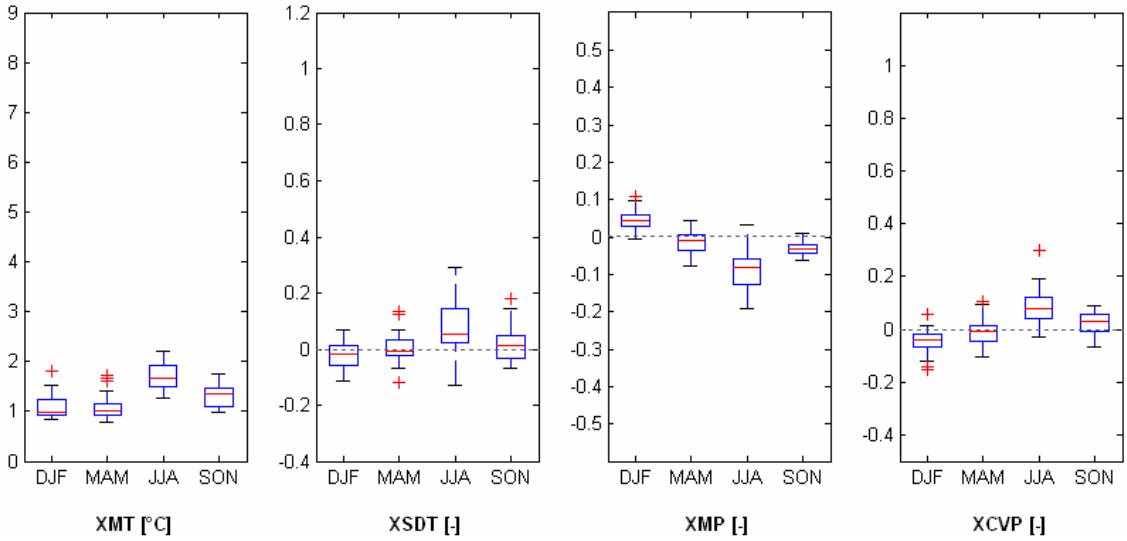

Fig. AI.9: Box plots of regional seasonal changes for 1°C global mean warming (2020-2049) (scaled from A2 and B2 PRUDENCE experiments)

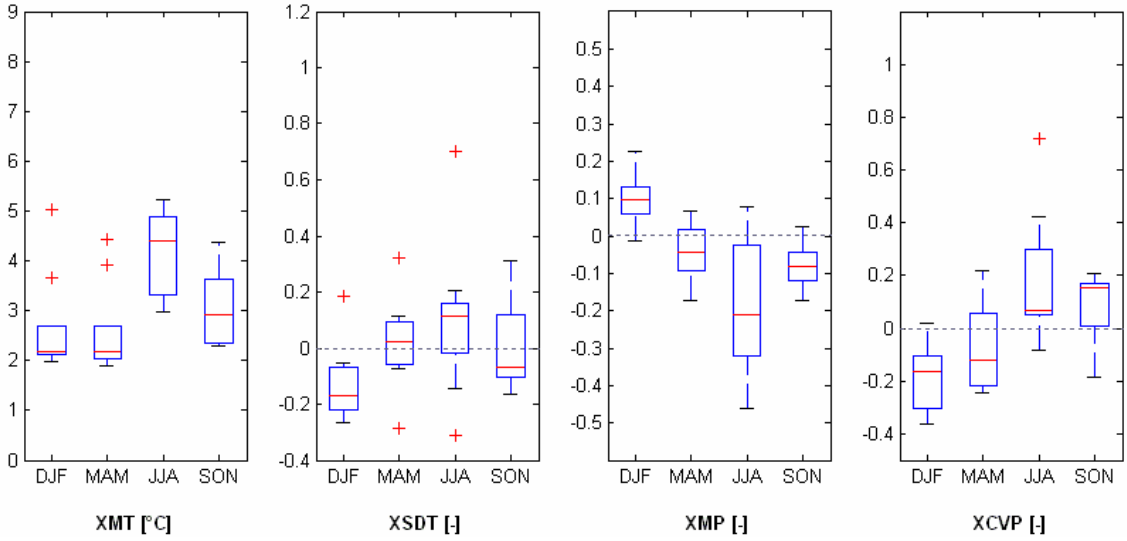

Fig. AI.10: Box plots of regional seasonal changes predicted by PRUDENCE RCM experiments for 2070-2099 – B2 scenario

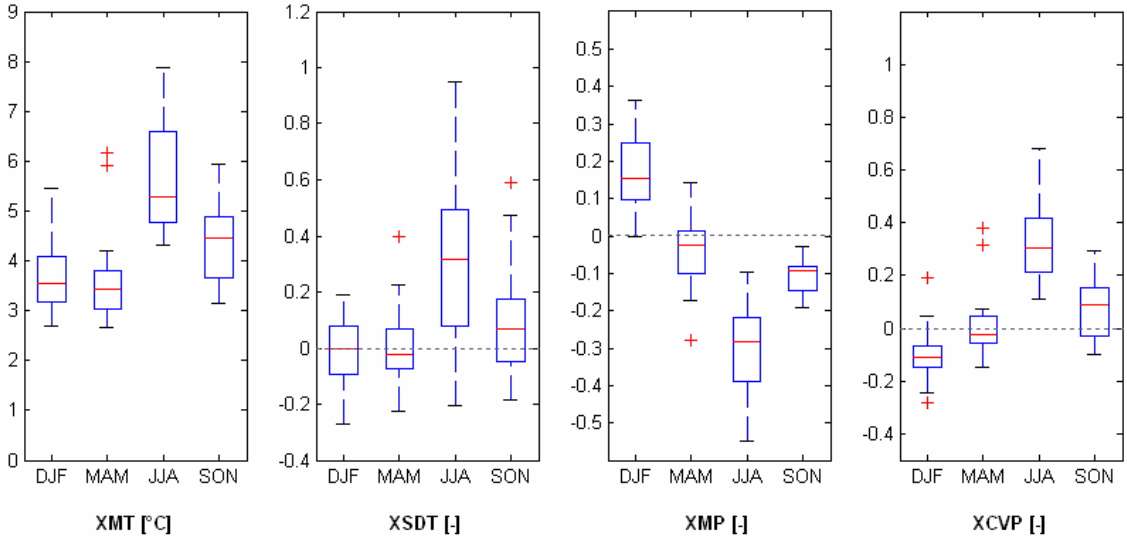

Fig. AI.11: Box plots of regional seasonal changes predicted by PRUDENCE RCM experiments for 2070-2099 – A2 scenario

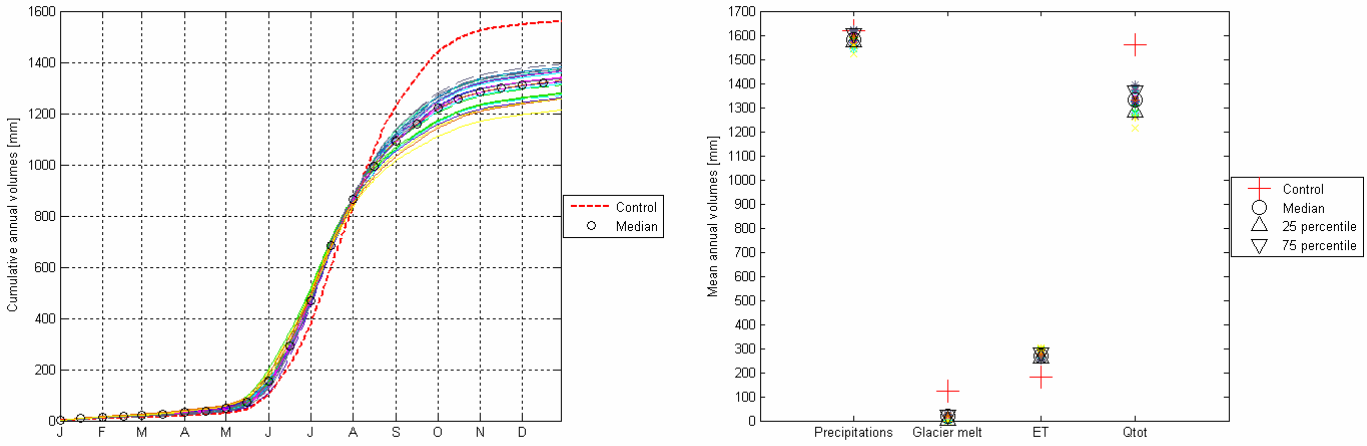

Fig. AI.12: Cumulative mean flow and water balance components for 1°C global mean warming (2020-2049) (see Fig. AI.13 and Fig. AI.14 for colors meaning)

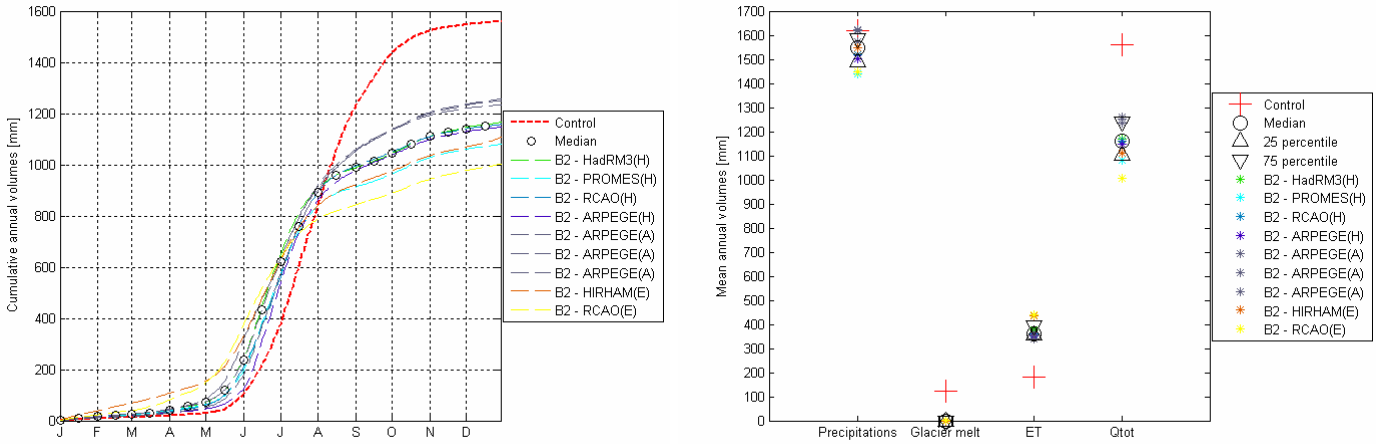

Fig. AI.13: Cumulative mean flow and water balance components for 2070-2099 – B2 scenario

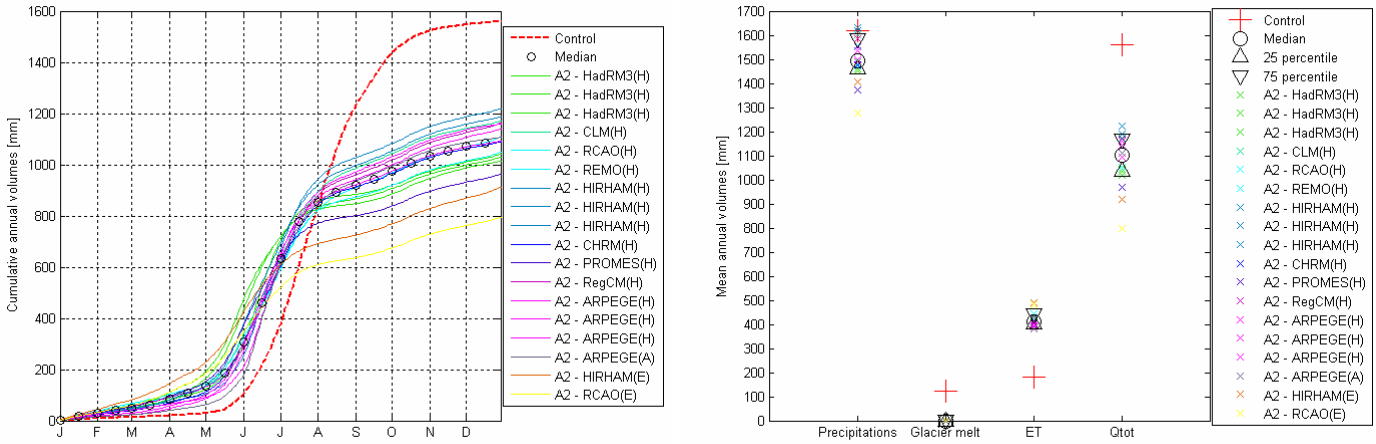

Fig. AI.14: Cumulative mean flow and water balance components for 2070-2099 – A2 scenario

Appendix 2 : The Saaser Vispa catchment

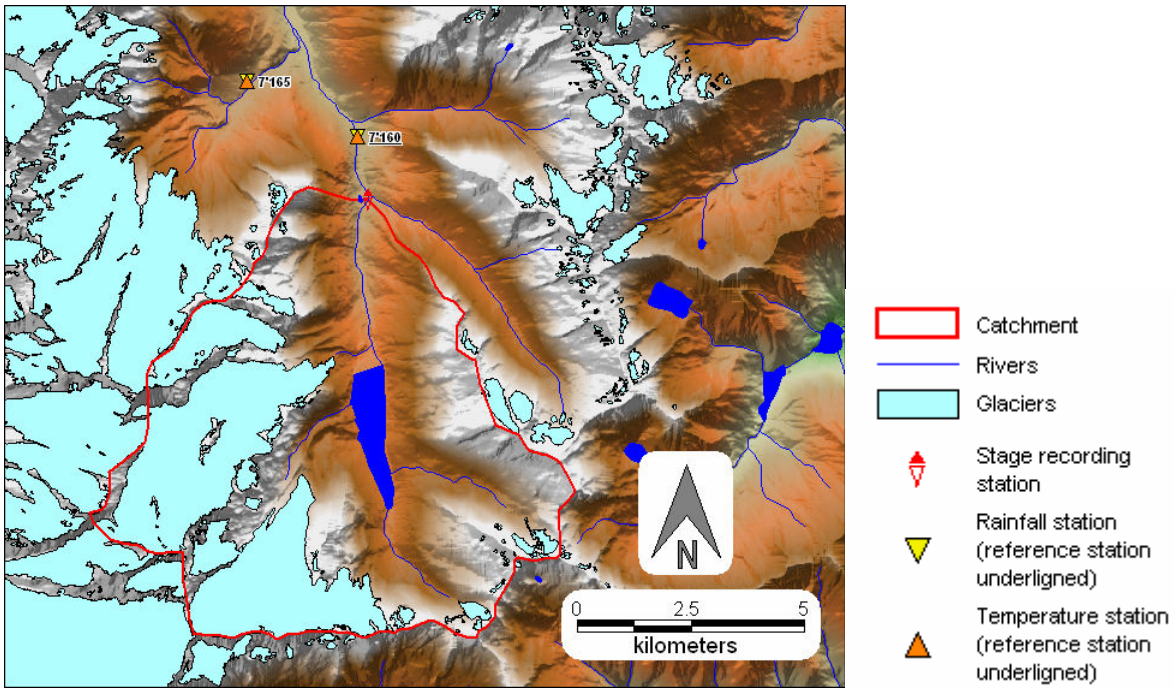

Fig. AII.1: Catchment situation

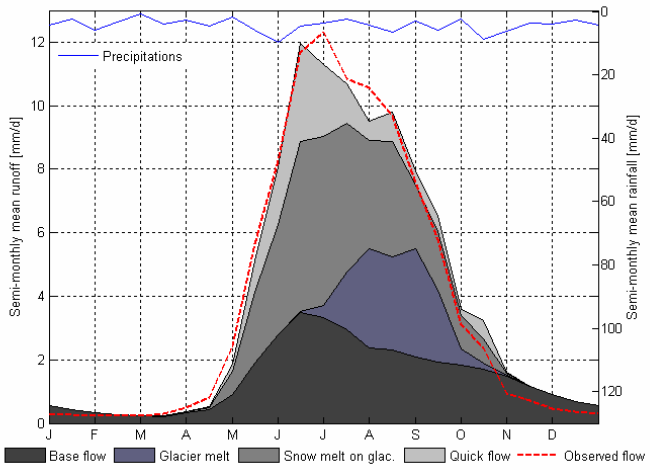

Fig. AII.2: Calibration – Semi-monthly cycle for 1953-1960

No available data for the validation period

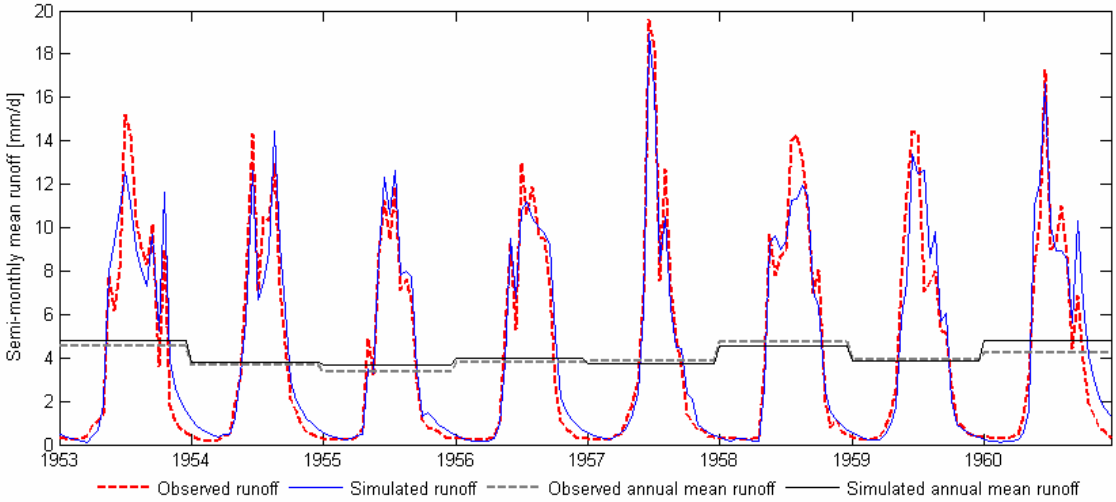

Fig. AII.4: Calibration – Semi-monthly mean flow for 1953-1960

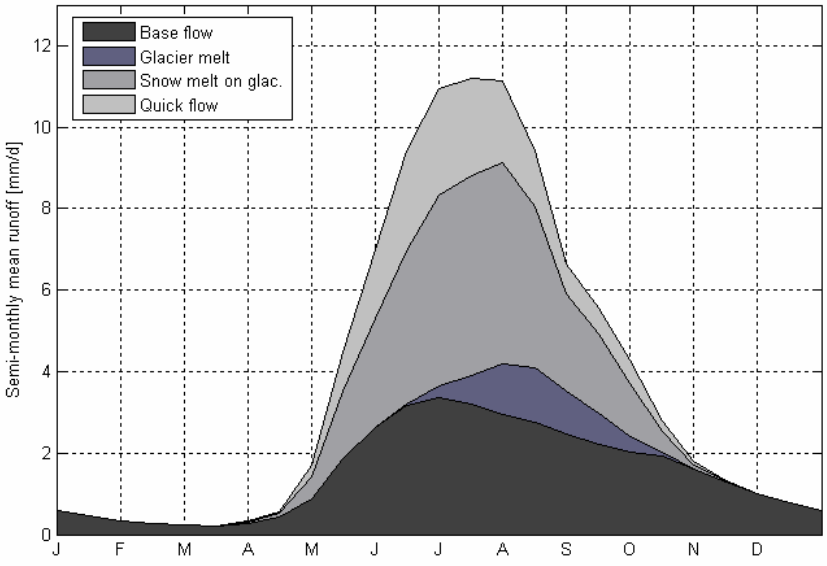

Fig. AII.5: Hydrograph components for the control period (1961-1990)

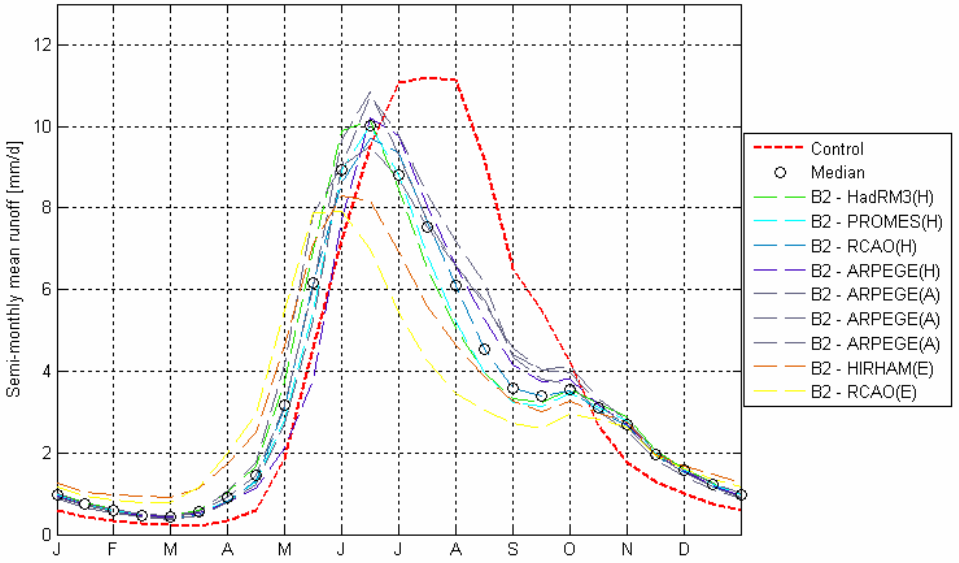

Fig. AII.7: Changes in hydrological regime for 2070-2099 – B2 scenario

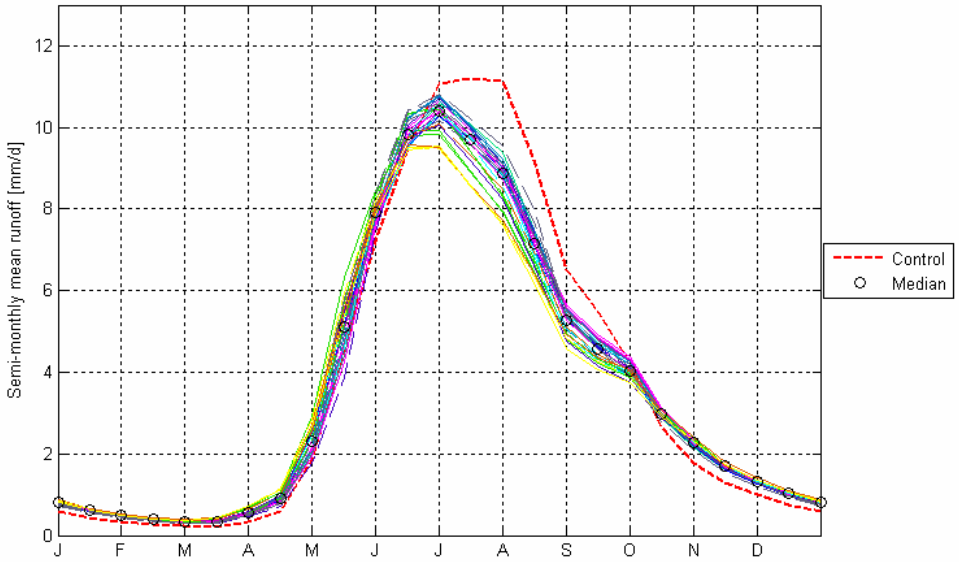

Fig. AII.6: Changes in hydrological regime for 1°C global mean warming (scaled from A2 and B2 PRUDENCE experiments)

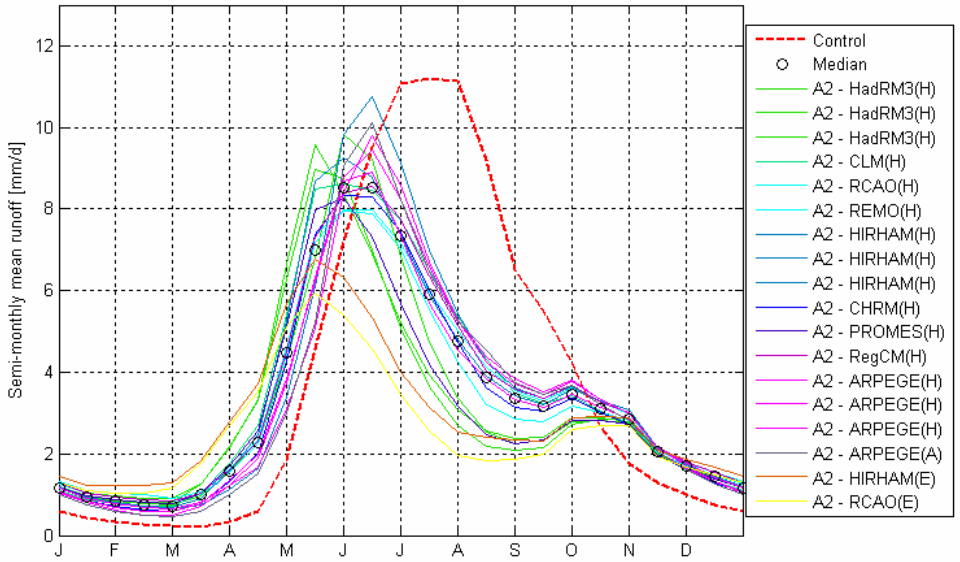

Fig. AII.8: Changes in hydrological regime for 2070-2099 – A2 scenario

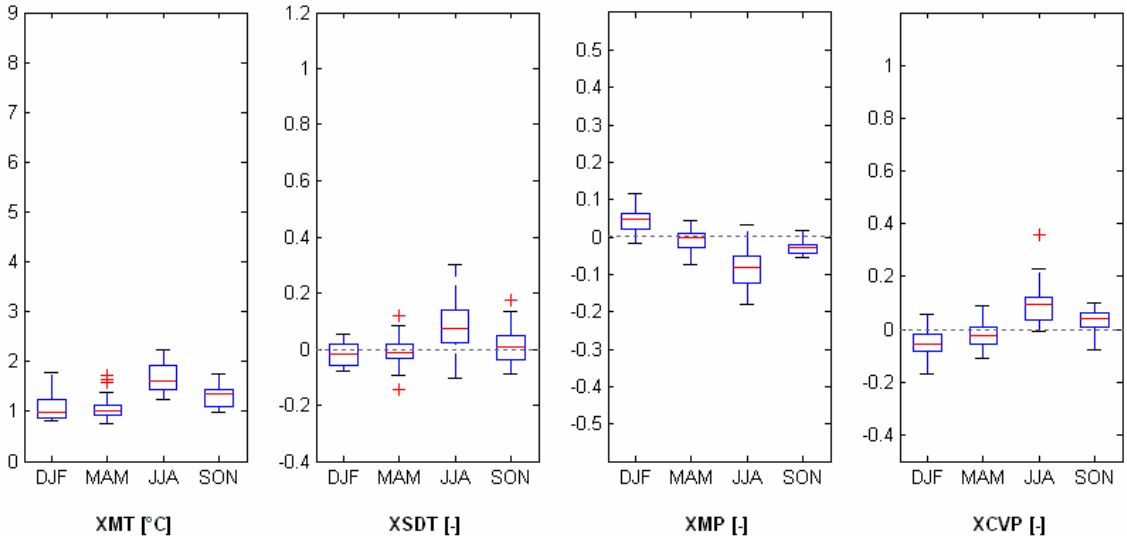

Fig. AII.9: Box plots of regional seasonal changes for 1 °C global mean warming (2020-2049) (scaled from A2 and B2 PRUDENCE experiments)

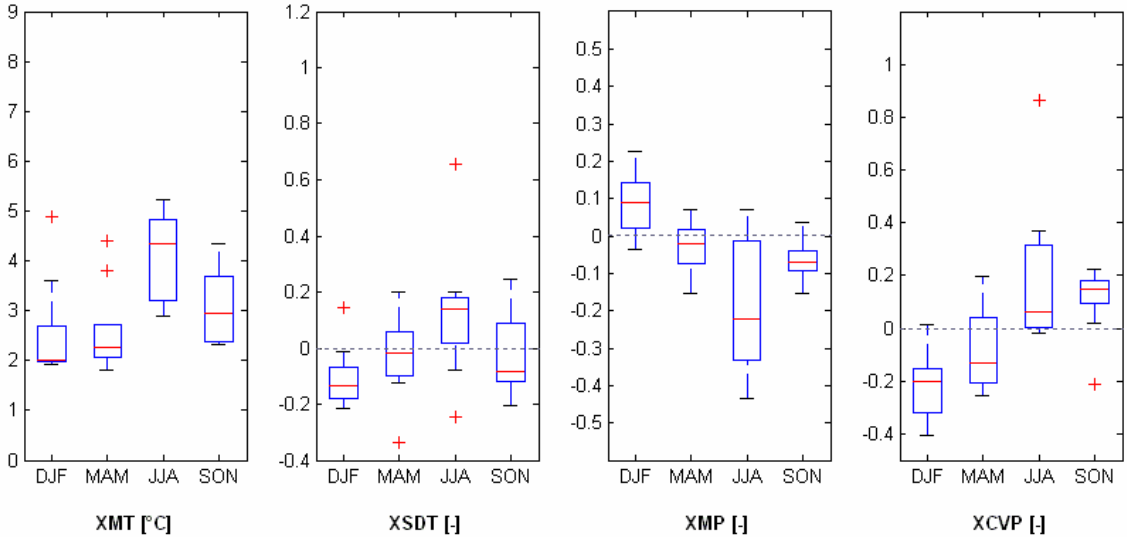

Fig. AII.10: Box plots of regional seasonal changes predicted by PRUDENCE RCM experiments for 2070-2099 – B2 scenario

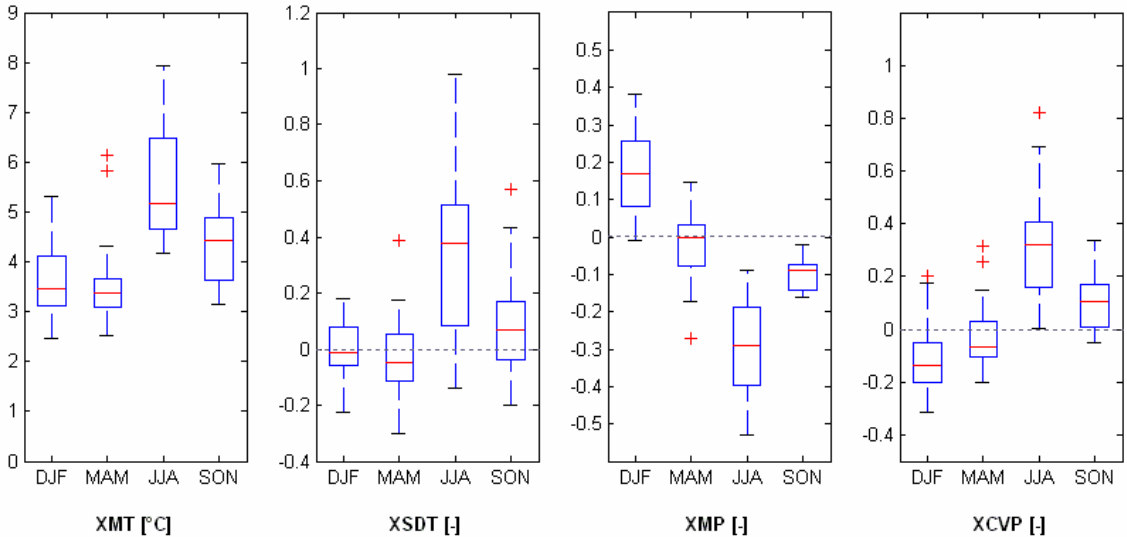

Fig. AII.11: Box plots of regional seasonal changes predicted by PRUDENCE RCM experiments for 2070-2099 – A2 scenario

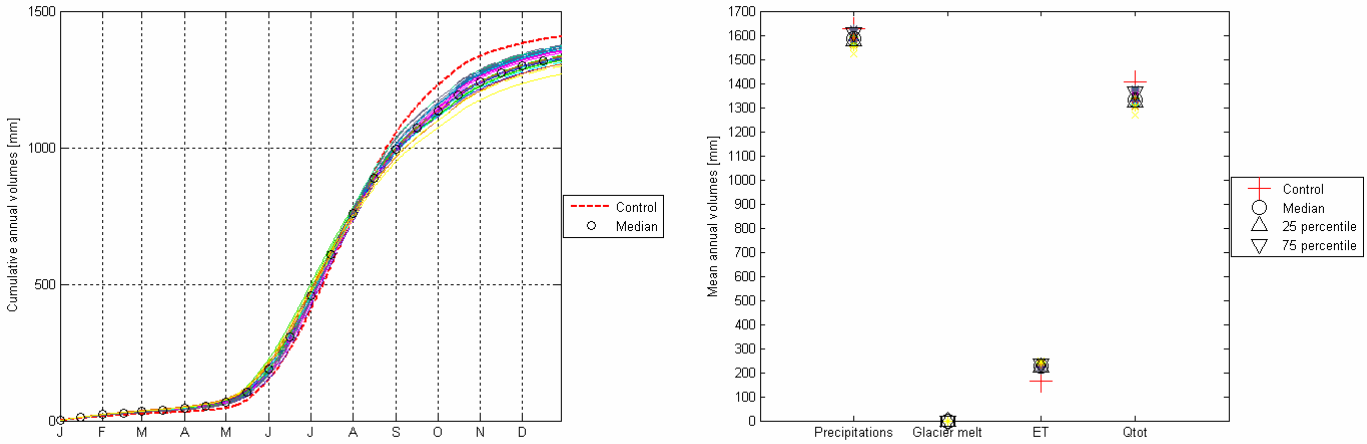

Fig. AII.12: Cumulative mean flow and water balance components for 1°C global mean warming (2020-2049) (see Fig. AII.13 and Fig. AII.14 for colors meaning)

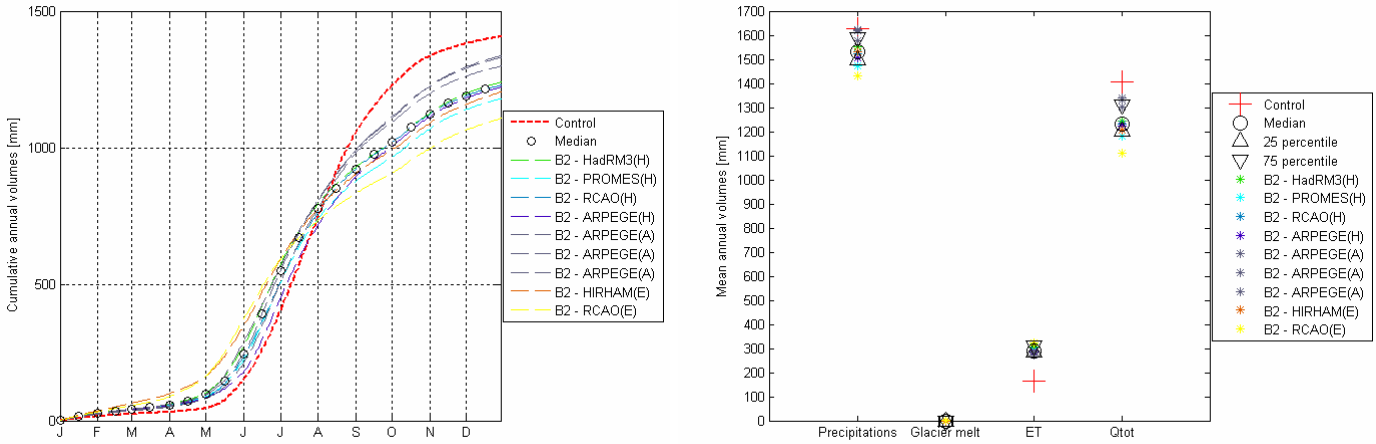

Fig. AII.13: Cumulative mean flow and water balance components for 2070-2099 – B2 scenario

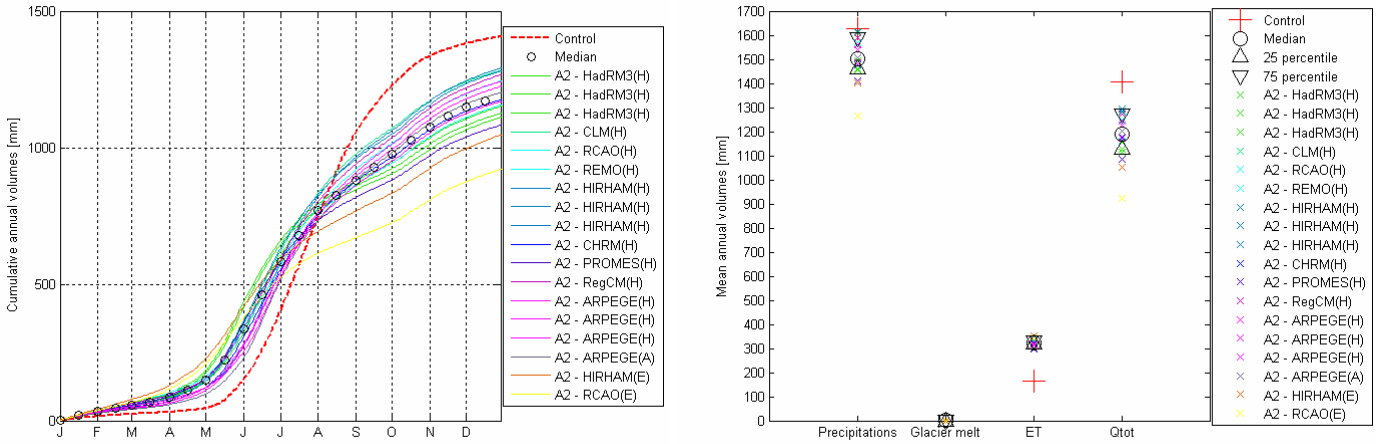

Fig. AII.14: Cumulative mean flow and water balance components for 2070-2099 – A2 scenario

Appendix 3 : The Lonza catchment

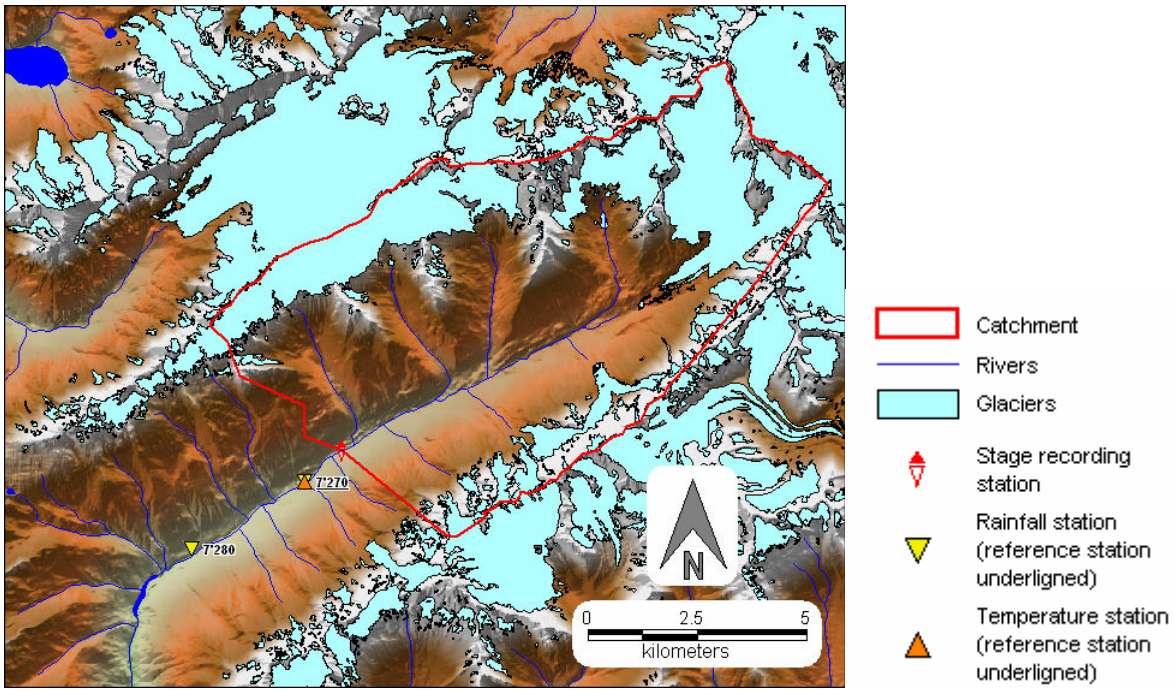

Fig. AIII.1: Catchment situation

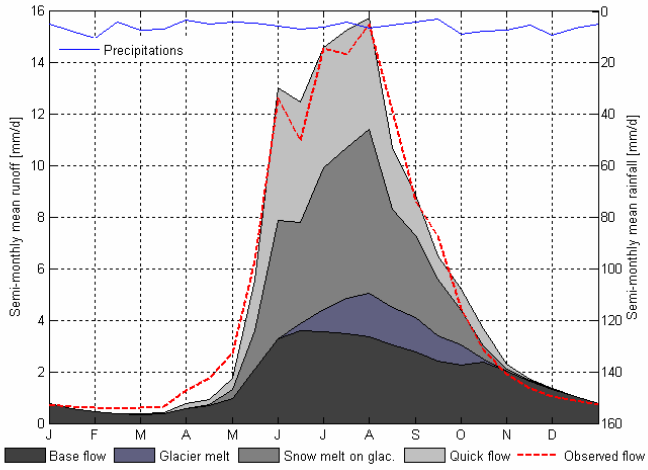

Fig. AIII.2: Calibration – Semi-monthly cycle for 1976-1983

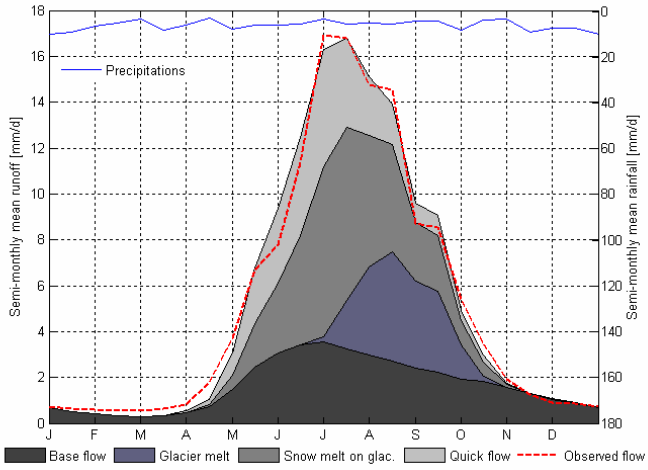

Fig. AIII.3: Validation – Semi-monthly cycle for 1983-1990

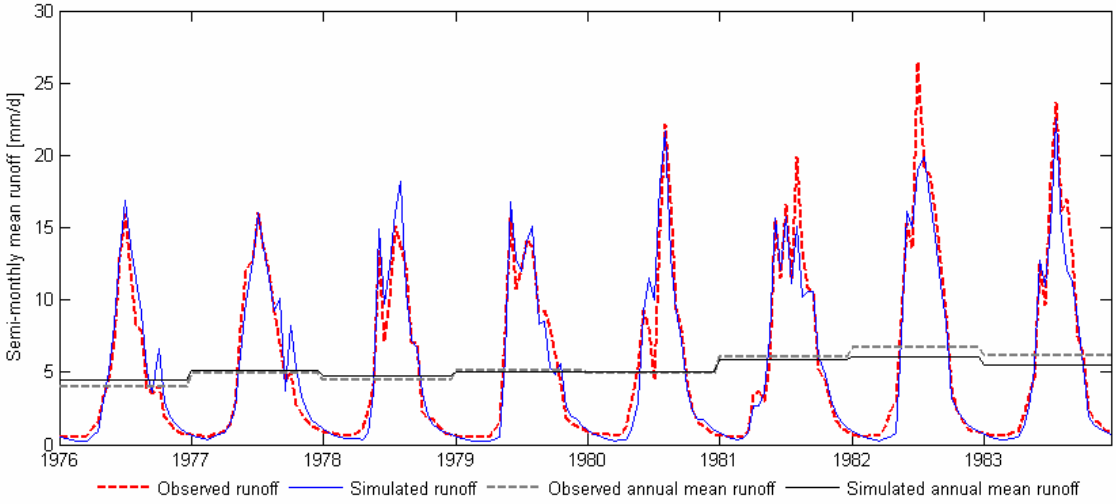

Fig. AIII.4: Calibration – Semi-monthly mean flow for 1976-1983

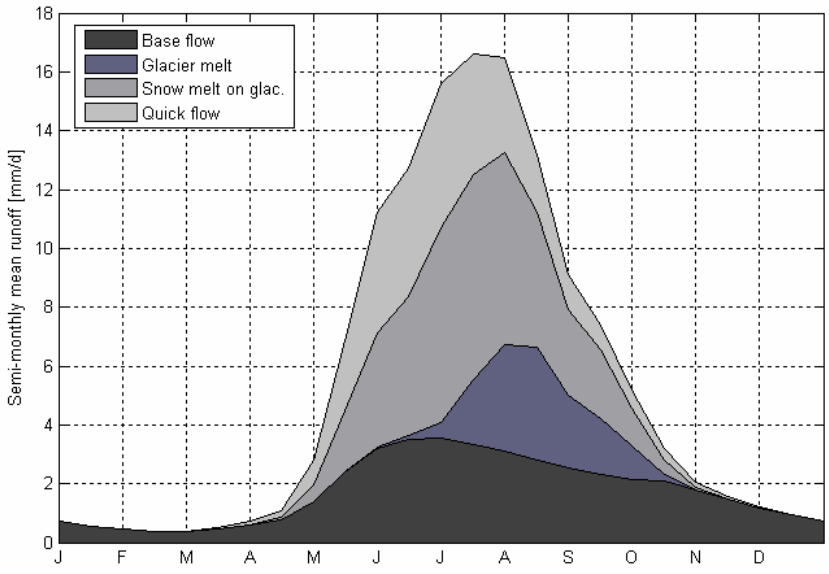

Fig. AIII.5: Hydrograph components for the control period (1974-1998)

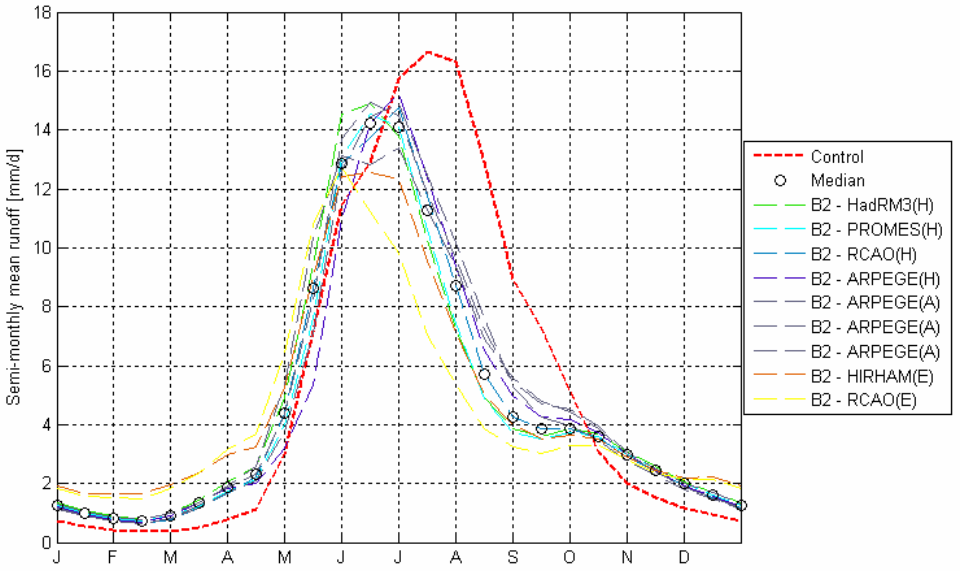

Fig. AIII.7: Changes in hydrological regime for 2070-2099 – B2 scenario

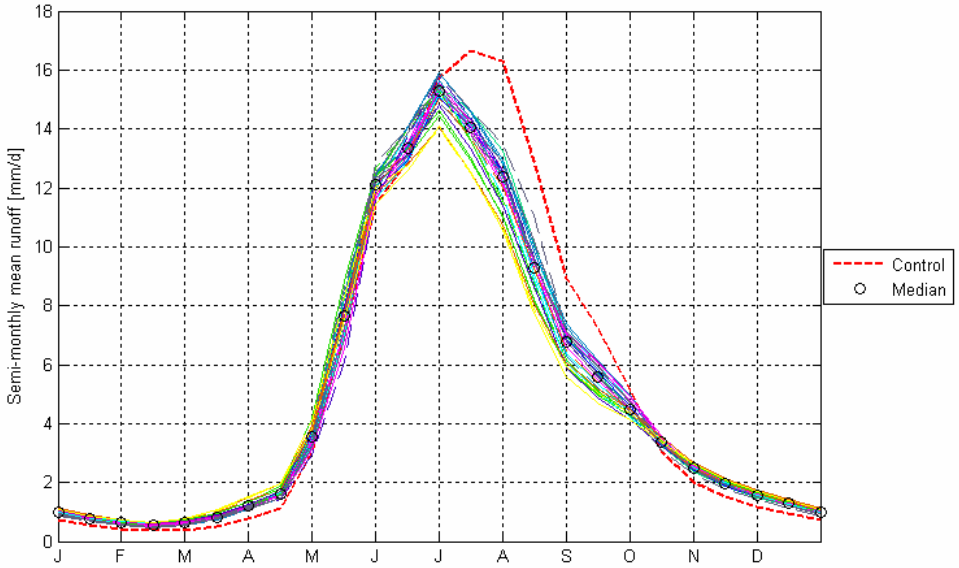

Fig. AIII.6: Changes in hydrological regime for 1°C global mean warming (scaled from A2 and B2 PRUDENCE experiments)

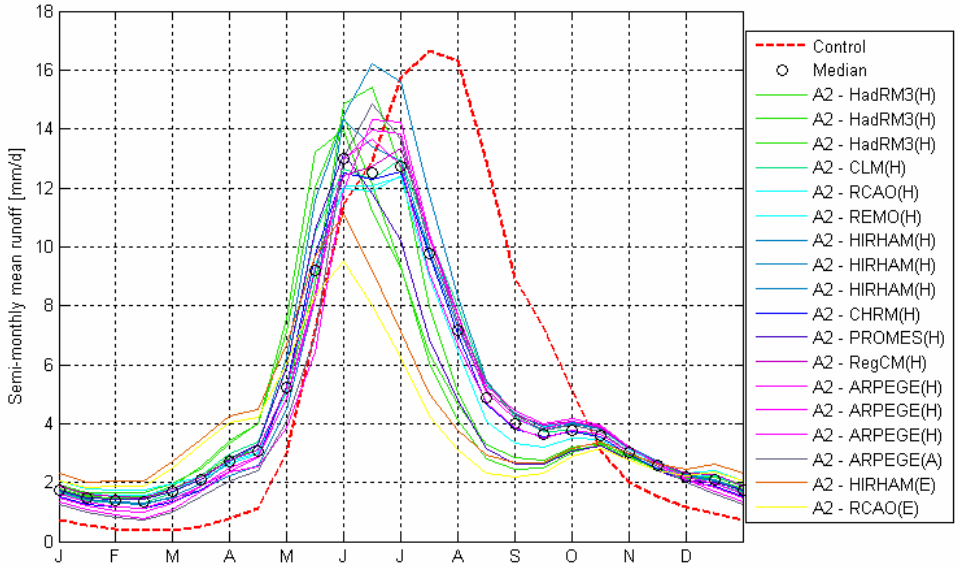

Fig. AIII.8: Changes in hydrological regime for 2070-2099 – A2 scenario

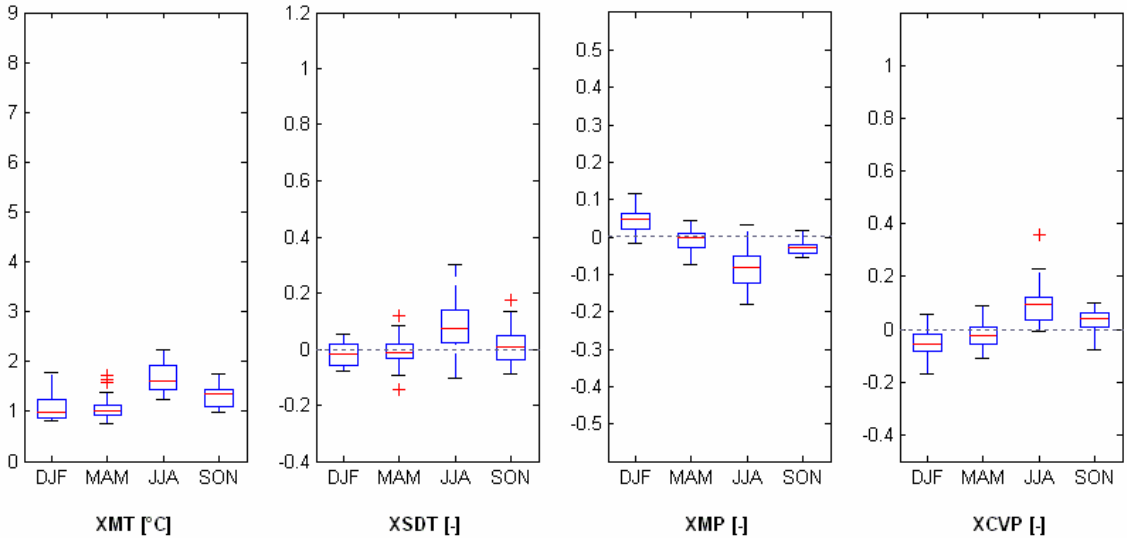

Fig. AIII.9: Box plots of regional seasonal changes for 1°C global mean warming (2020-2049) (scaled from A2 and B2 PRUDENCE experiments)

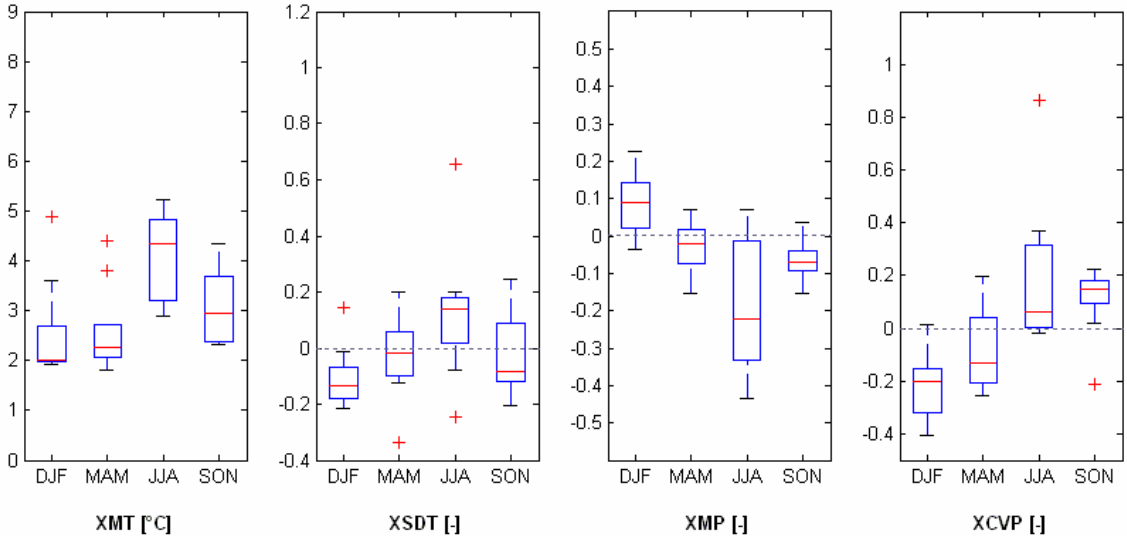

Fig. AIII.10: Box plots of regional seasonal changes predicted by PRUDENCE RCM experiments for 2070-2099 – B2 scenario

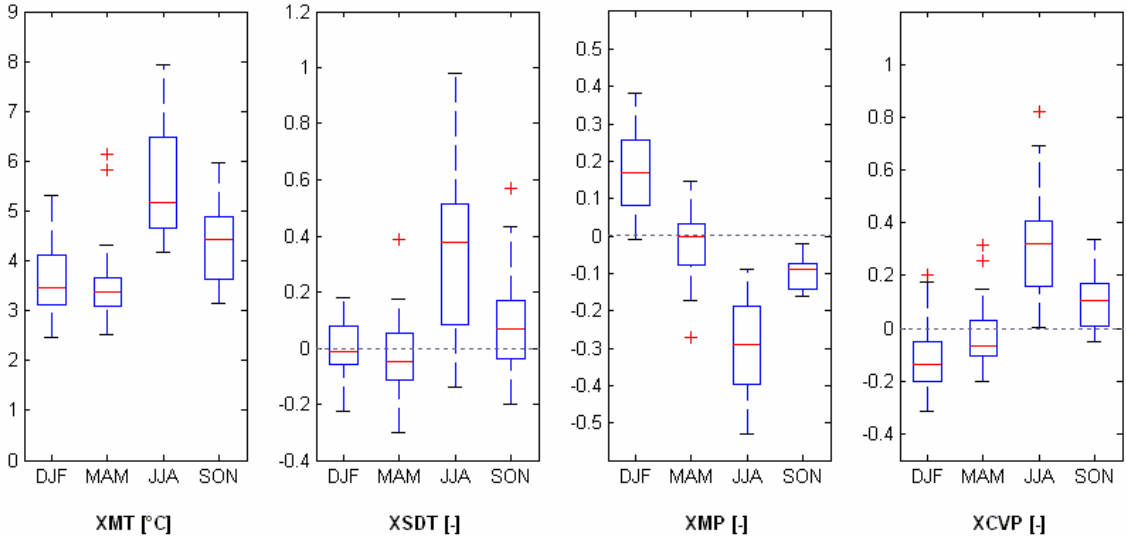

Fig. AIII.11: Box plots of regional seasonal changes predicted by PRUDENCE RCM experiments for 2070-2099 – A2 scenario

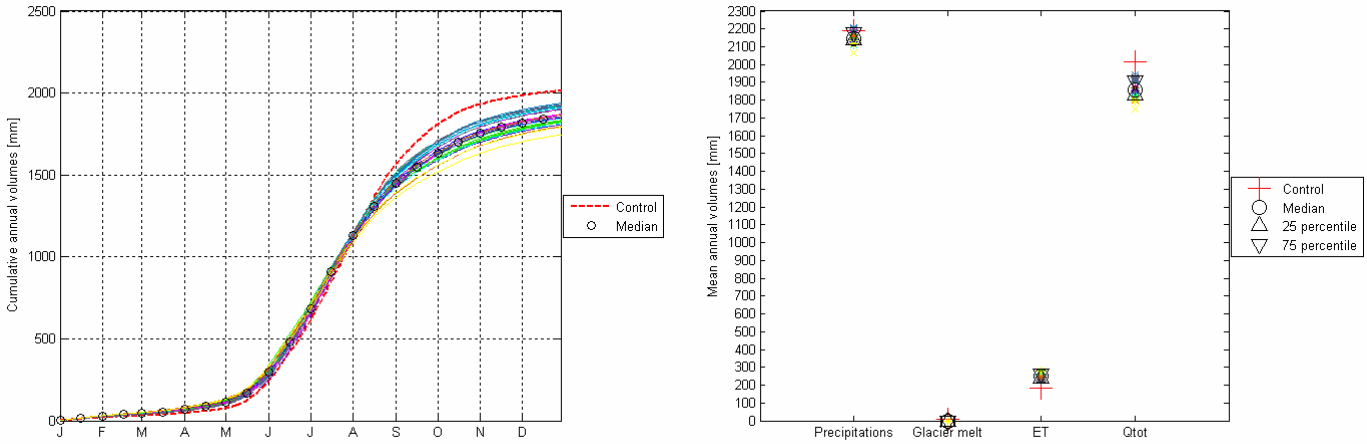

Fig. AIII.12: Cumulative mean flow and water balance components for 1°C global mean warming (2020-2049) (see Fig. AIII.13 and Fig. AIII.14 for colors meaning)

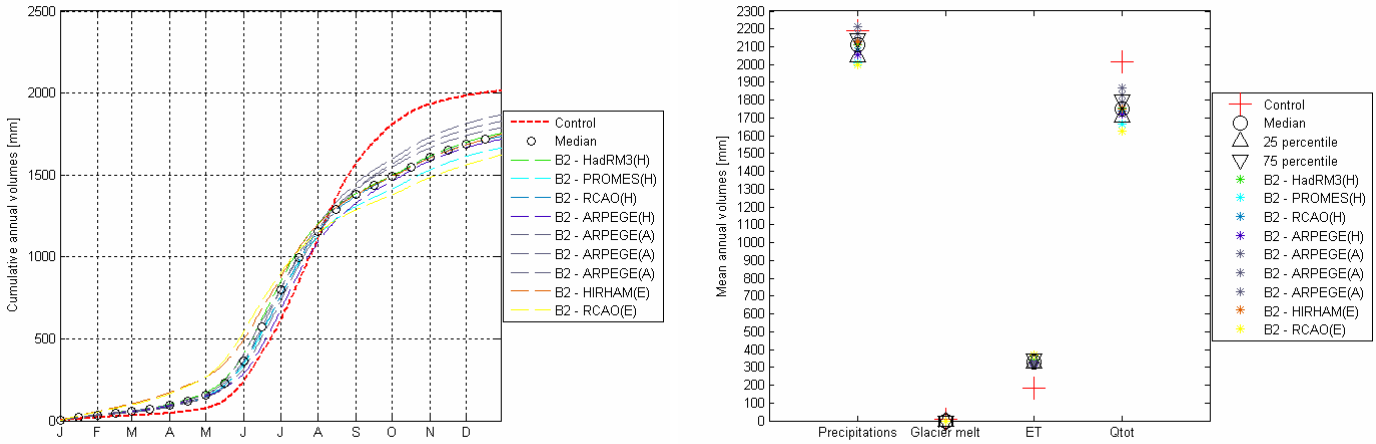

Fig. AIII.13: Cumulative mean flow and water balance components for 2070-2099 – B2 scenario

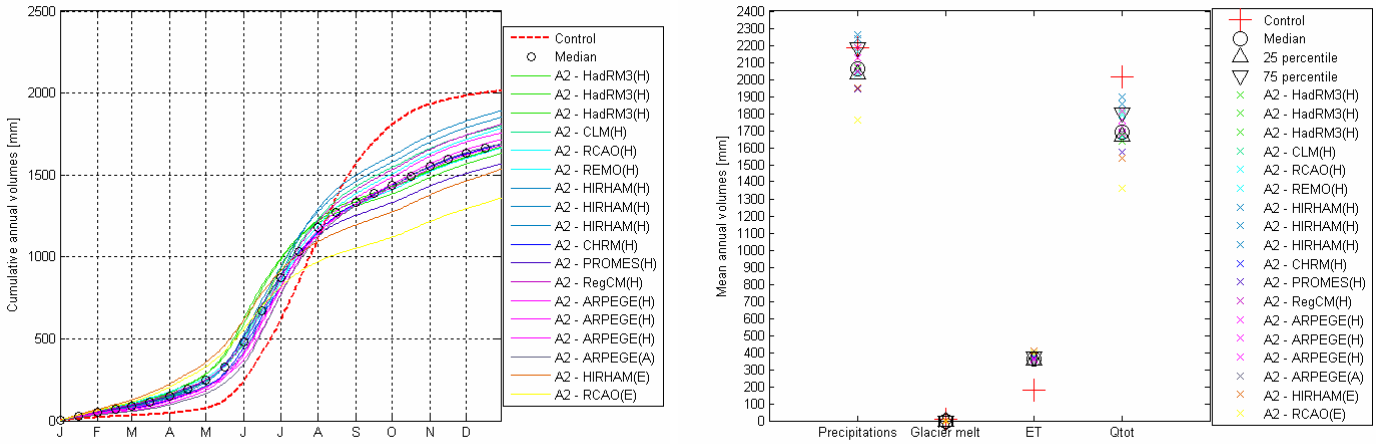

Fig. AIII.14: Cumulative mean flow and water balance components for 2070-2099 – A2 scenario

Appendix 4 : The Rhone catchment at Gletsch

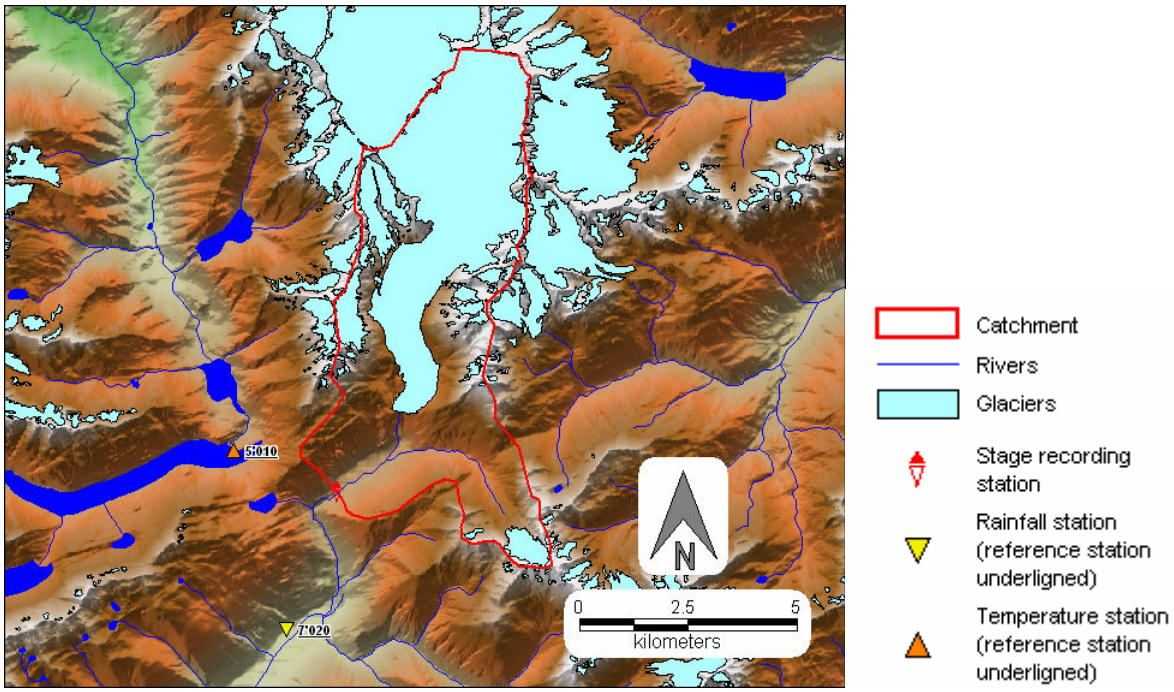

Fig. AIV.1: Catchment situation

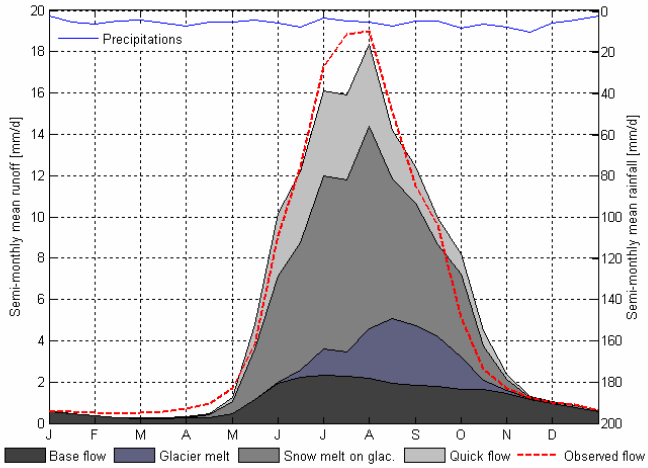

Fig. AIV.2: Calibration – Semi-monthly cycle for 1973-1980

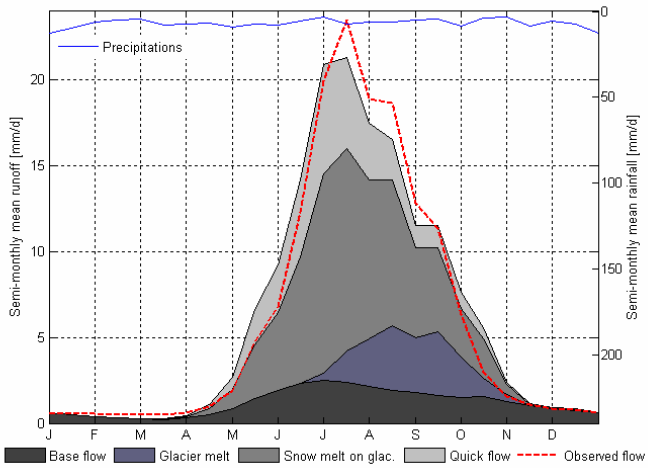

Fig. AIV.3: Validation – Semi-monthly cycle for 1983-1990

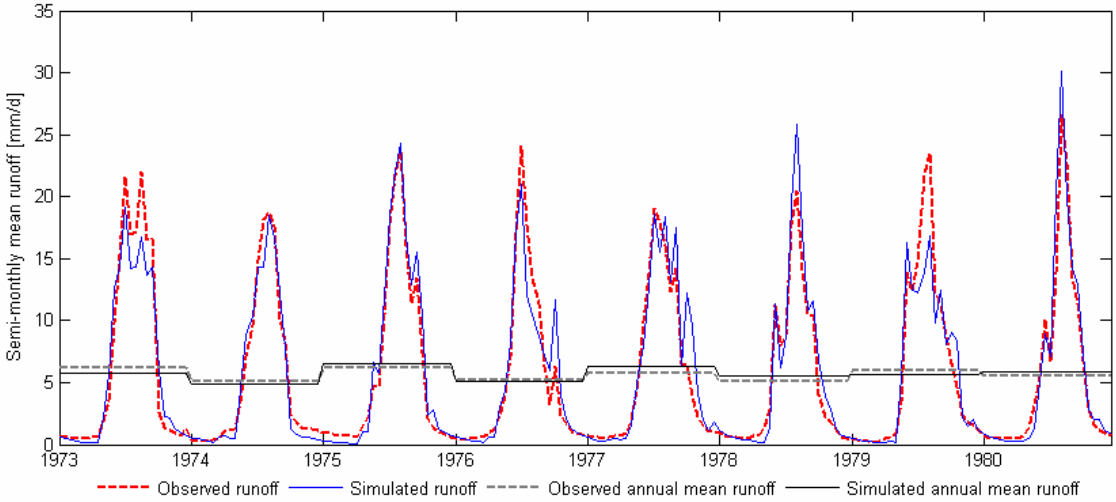

Fig. AIV.4: Calibration – Semi-monthly mean flow for 1973-1980

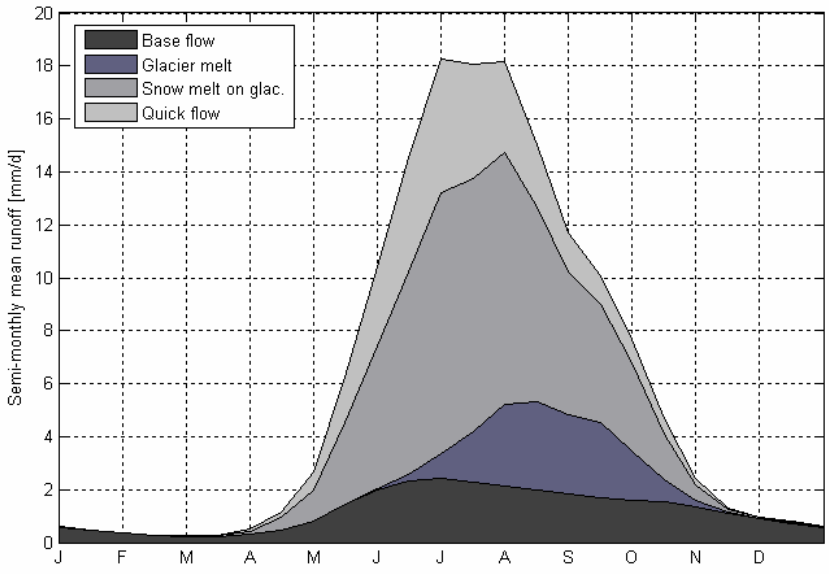

Fig. AIV.5: Hydrograph components for the control period (1961-1990)

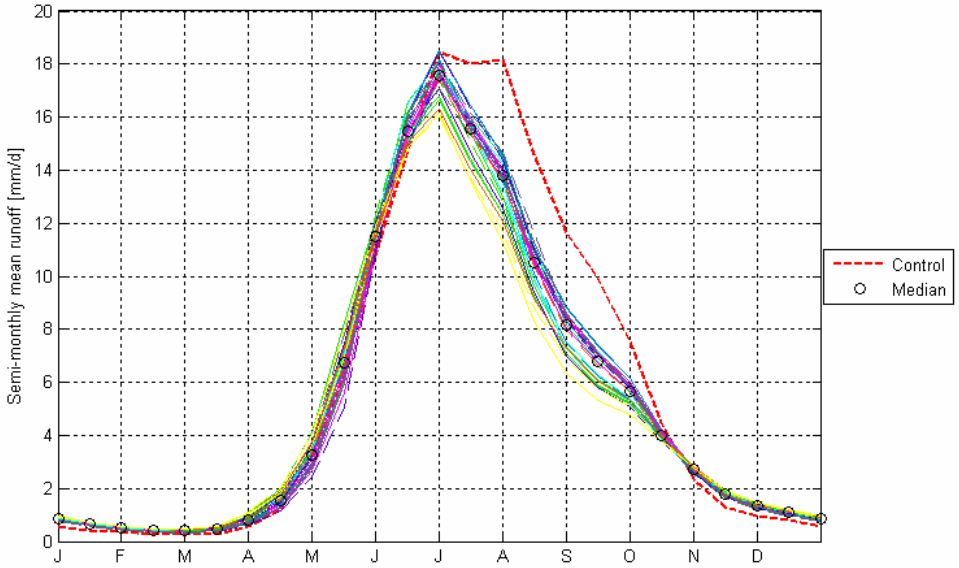

Fig. AIV.6: Changes in hydrological regime for 1°C global mean warming (scaled from A2 and B2 PRUDENCE experiments)

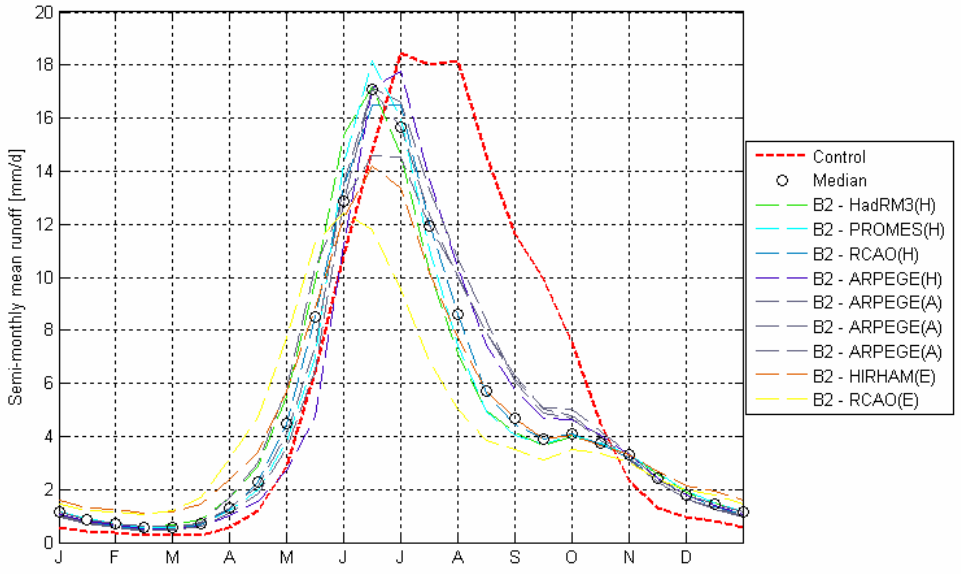

Fig. AIV.7: Changes in hydrological regime for 2070-2099 – B2 scenario

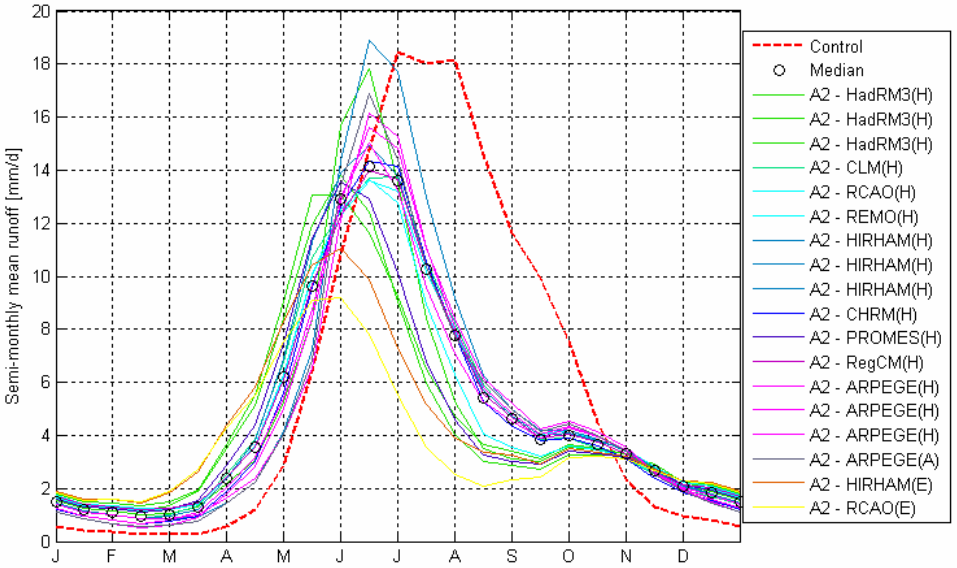

Fig. AIV.8: Changes in hydrological regime for 2070-2099 – A2 scenario

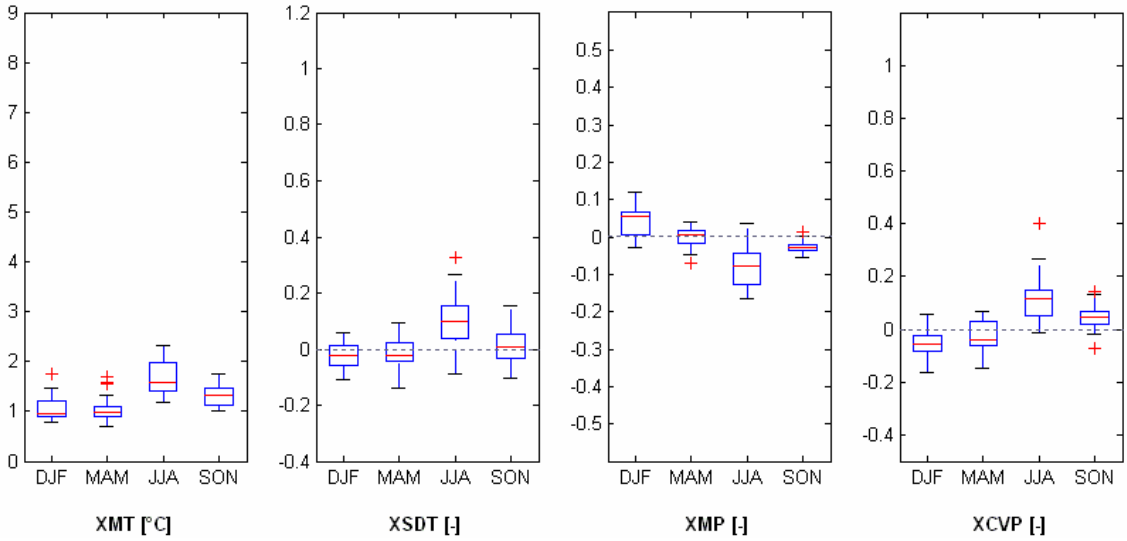

Fig. AIV.9: Box plots of regional seasonal changes for 1 °C global mean warming (2020-2049) (scaled from A2 and B2 PRUDENCE experiments)

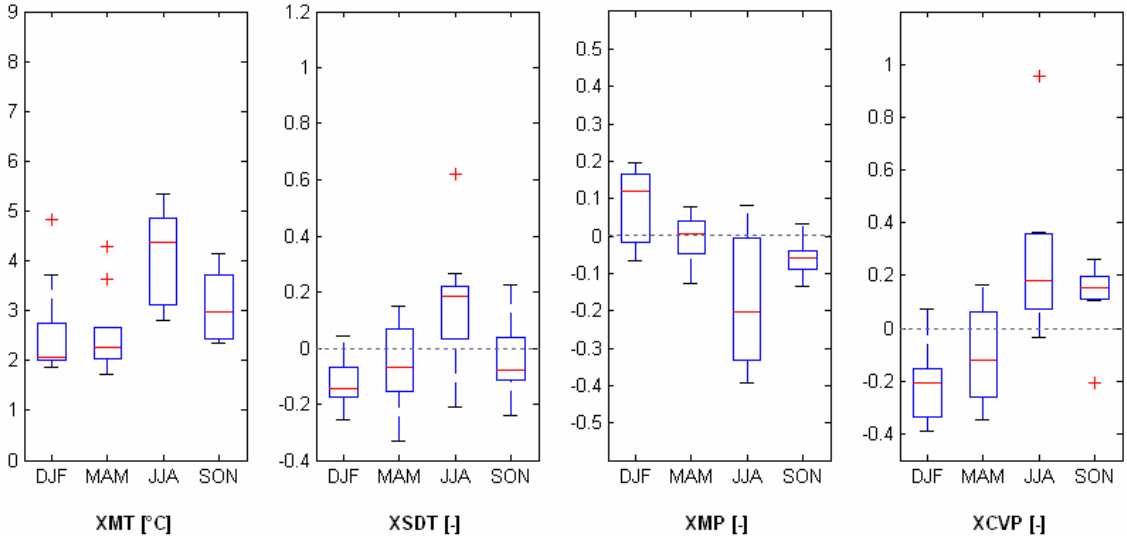

Fig. AIV.10: Box plots of regional seasonal changes predicted by PRUDENCE RCM experiments for 2070-2099 – B2 scenario

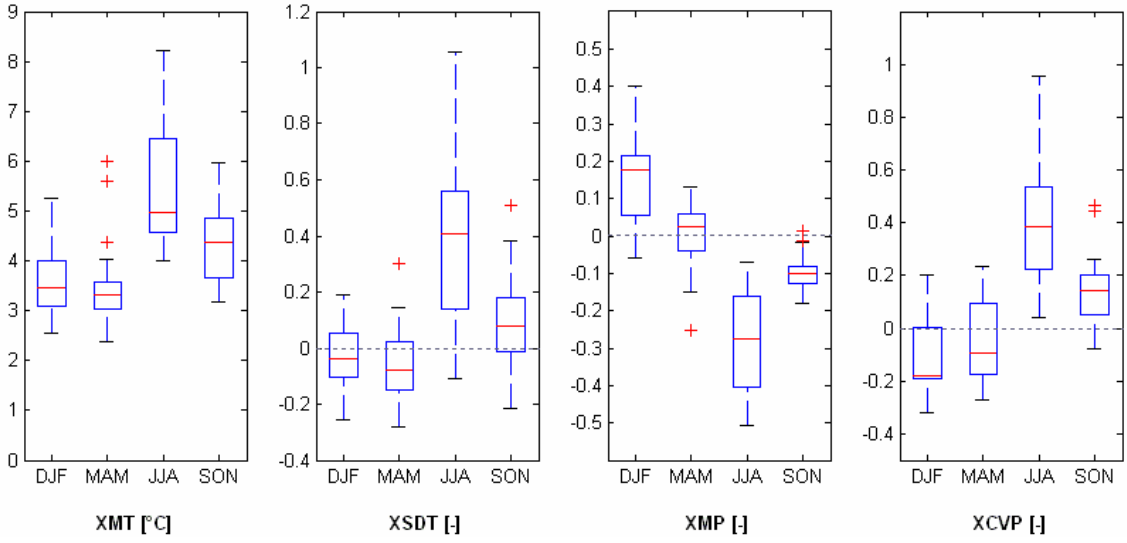

Fig. AIV.11: Box plots of regional seasonal changes predicted by PRUDENCE RCM experiments for 2070-2099 – A2 scenario

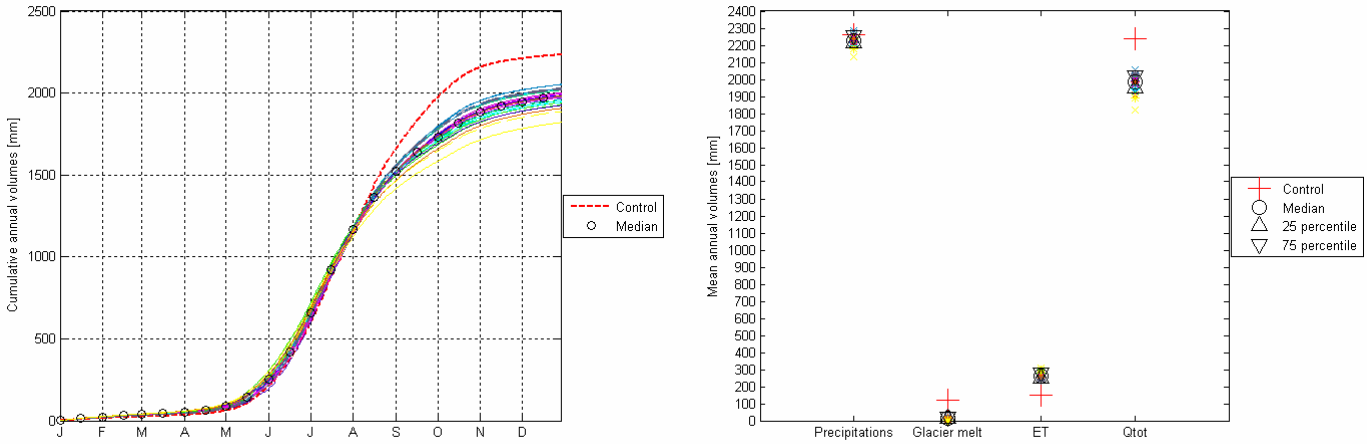

Fig. AIV.12: Cumulative mean flow and water balance components for 1°C global mean warming (2020-2049) (see Fig. AIV.13 and Fig. AIV.14 for colors meaning)

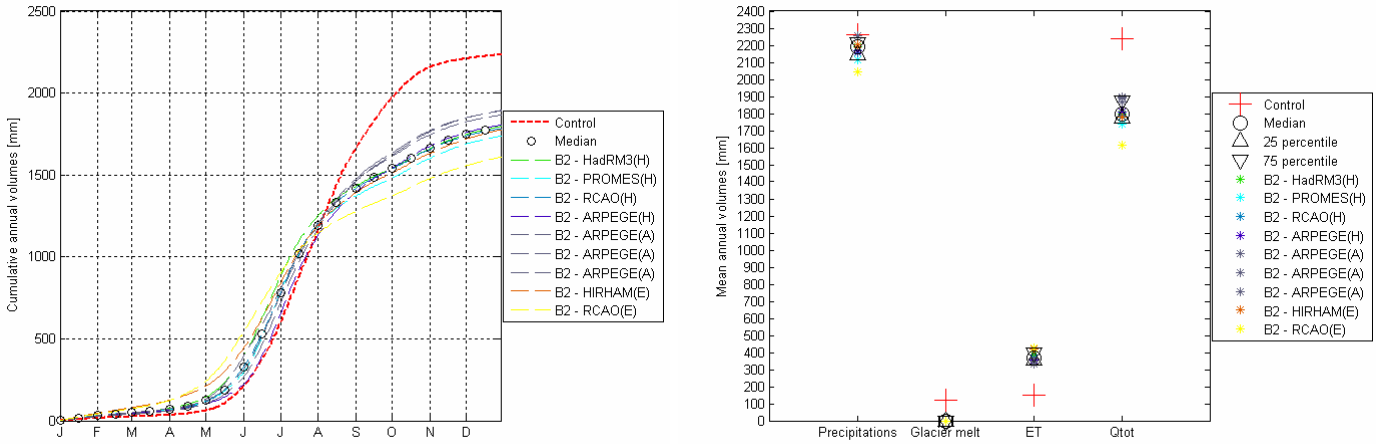

Fig. AIV.13: Cumulative mean flow and water balance components for 2070-2099 – B2 scenario

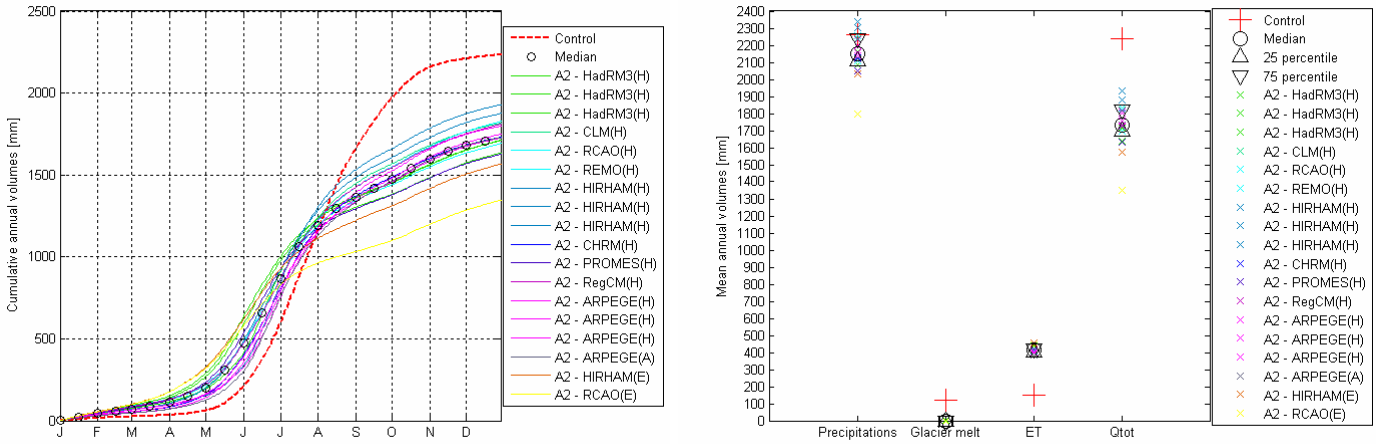

Fig. AIV.14: Cumulative mean flow and water balance components for 2070-2099 – A2 scenario

Appendix 5 : The Weisse Lütschine catchment

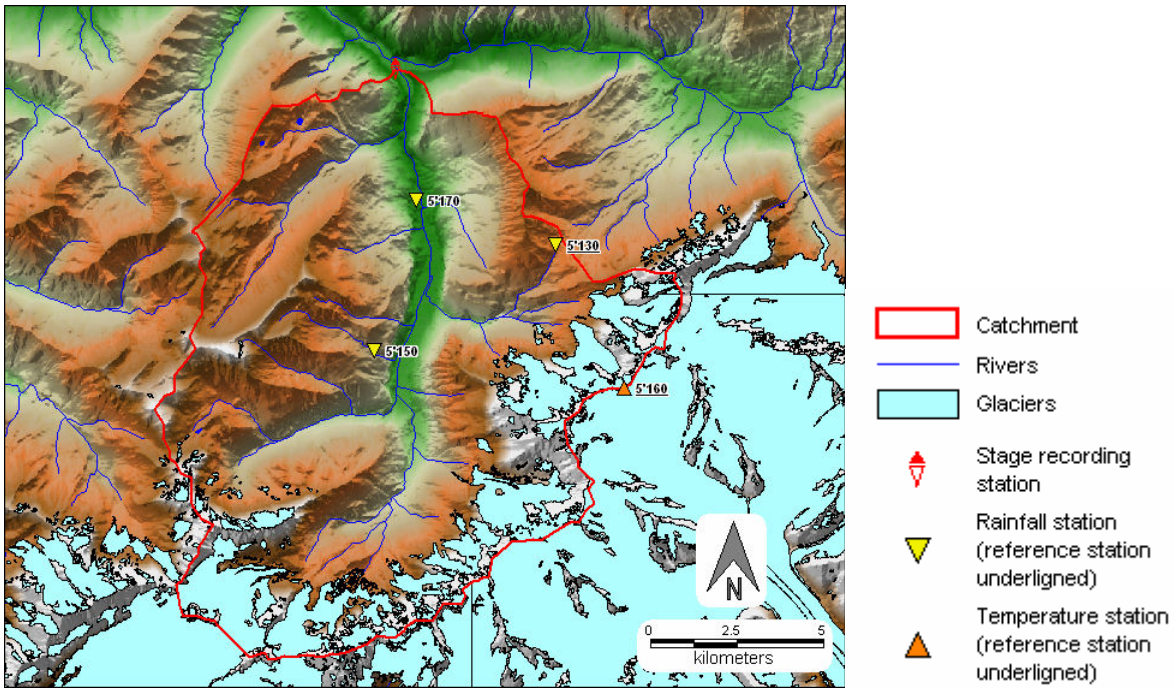

Fig. AV.1: Catchment situation

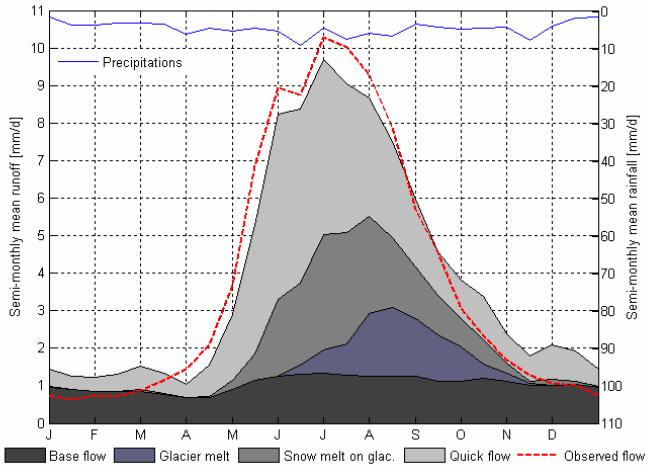

Fig. AV.2: Calibration – Semi-monthly cycle for 1973-1980

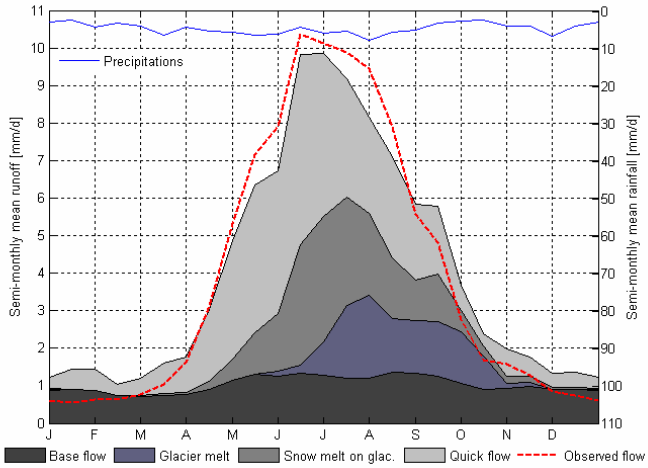

Fig. AV.3: Validation – Semi-monthly cycle for 1963-1970

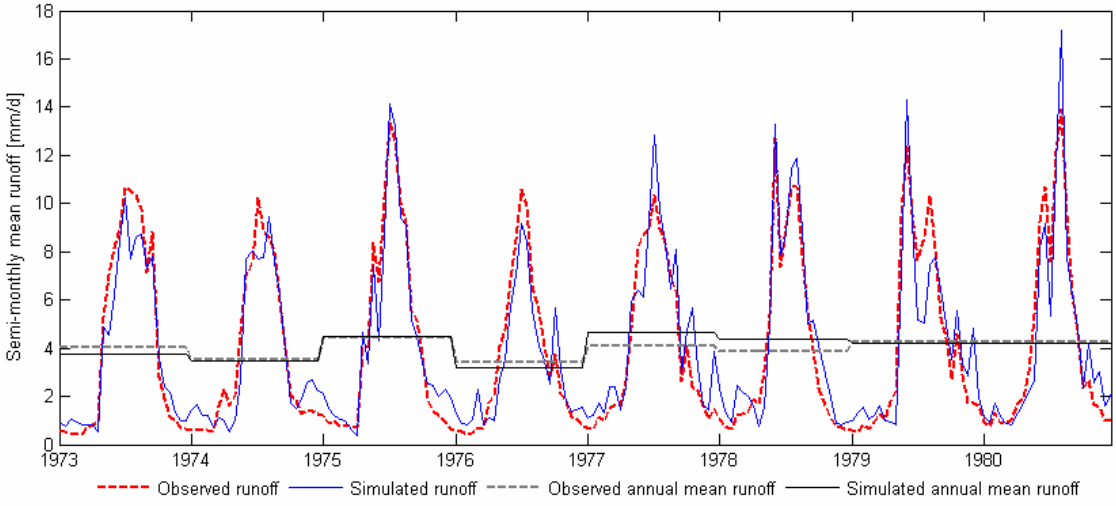

Fig. AV.4: Calibration – Semi-monthly mean flow for 1973-1980

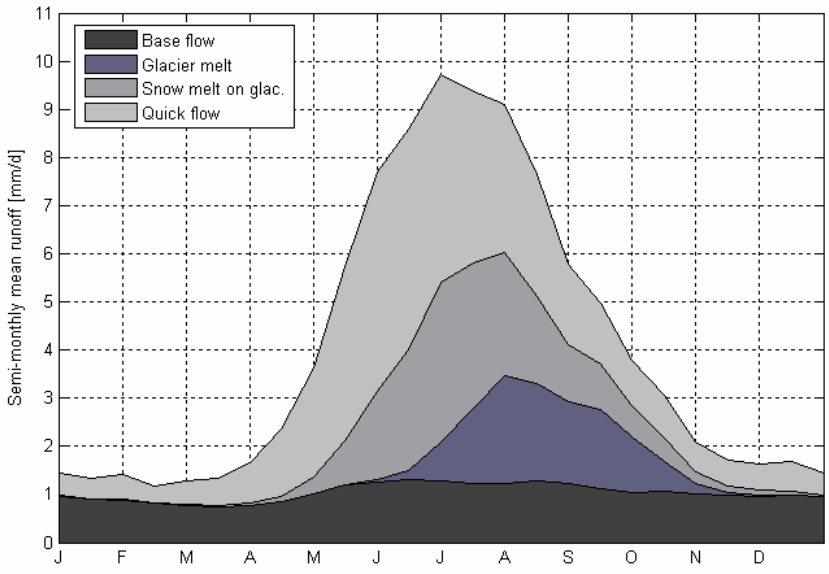

Fig. AV.5: Hydrograph components for the control period (1961-1990)

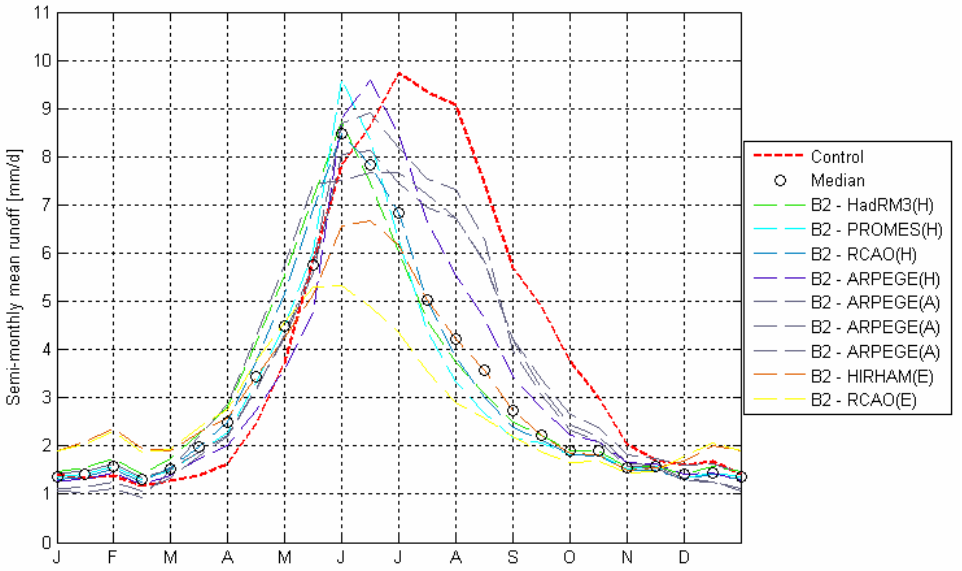

Fig. AV.7: Changes in hydrological regime for 2070-2099 – B2 scenario

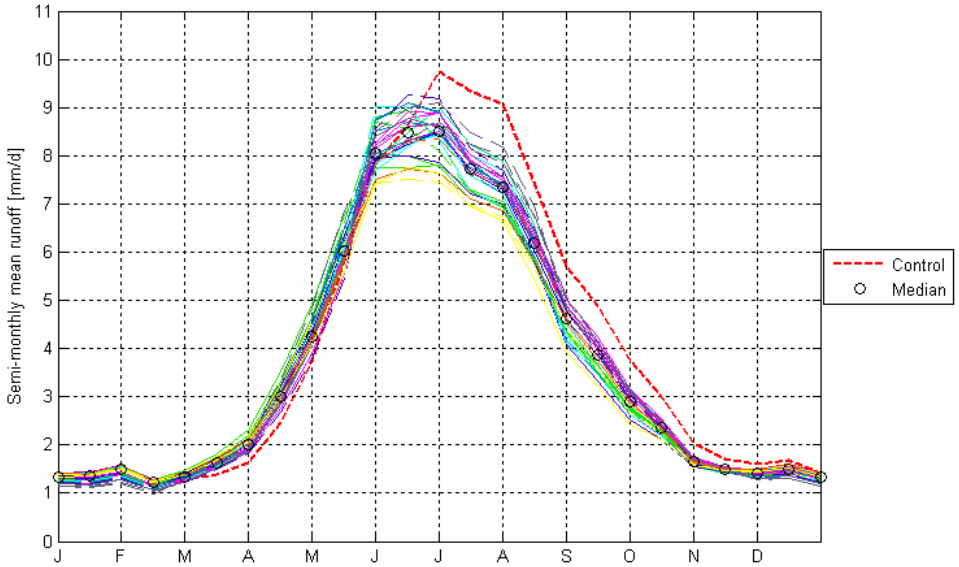

Fig. AV.6: Changes in hydrological regime for 1 °C global mean warming (scaled from A2 and B2 PRUDENCE experiments)

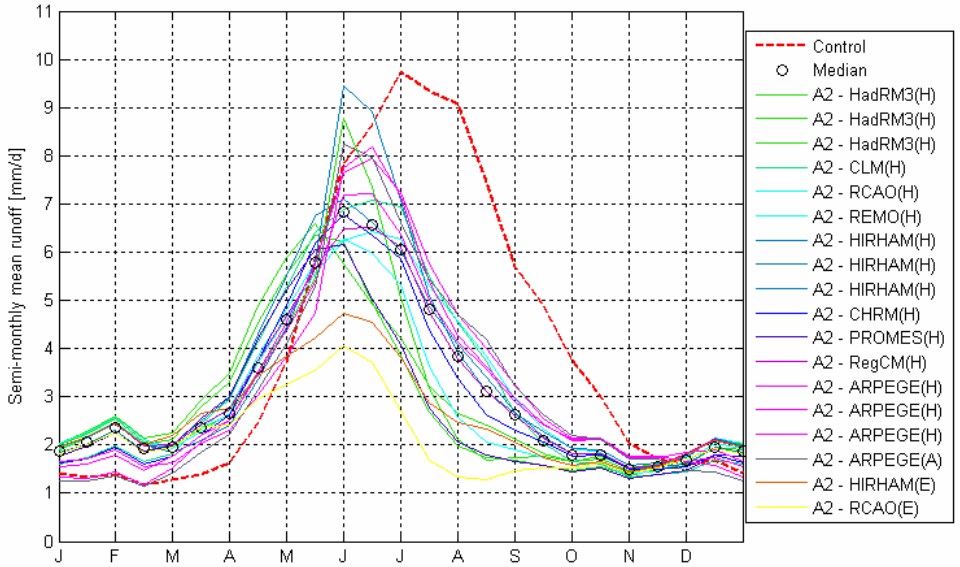

Fig. AV.8: Changes in hydrological regime for 2070-2099 – A2 scenario

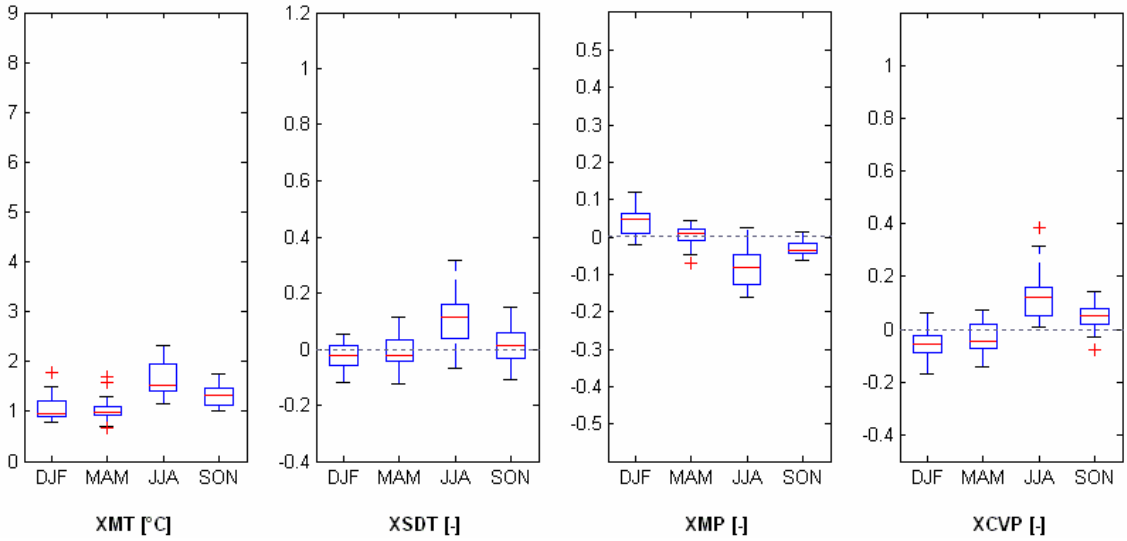

Fig. AV.9: Box plots of regional seasonal changes for 1 °C global mean warming (2020-2049) (scaled from A2 and B2 PRUDENCE experiments)

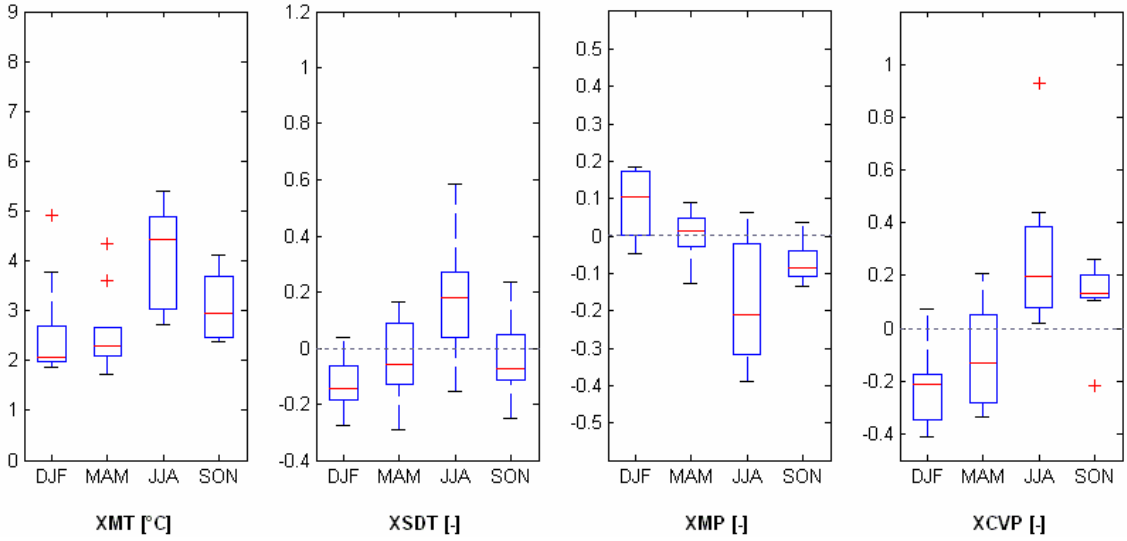

Fig. AV.10: Box plots of regional seasonal changes predicted by PRUDENCE RCM experiments for 2070-2099 – B2 scenario

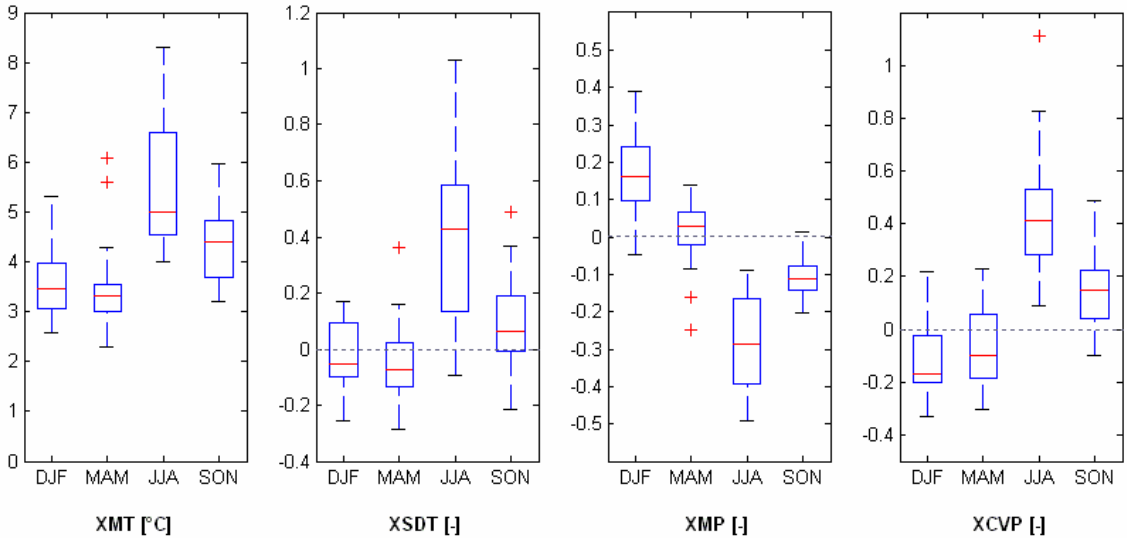

Fig. AV.11: Box plots of regional seasonal changes predicted by PRUDENCE RCM experiments for 2070-2099 – A2 scenario

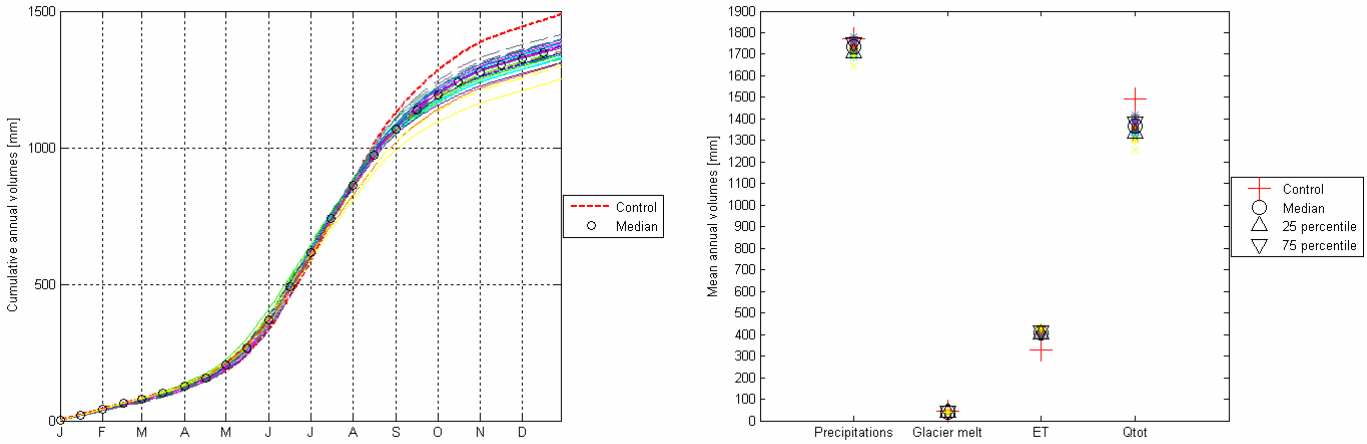

Fig. AV.12: Cumulative mean flow and water balance components for 1°C global mean warming (2020-2049) (see Fig. AV.13 and Fig. AV.14 for colors meaning)

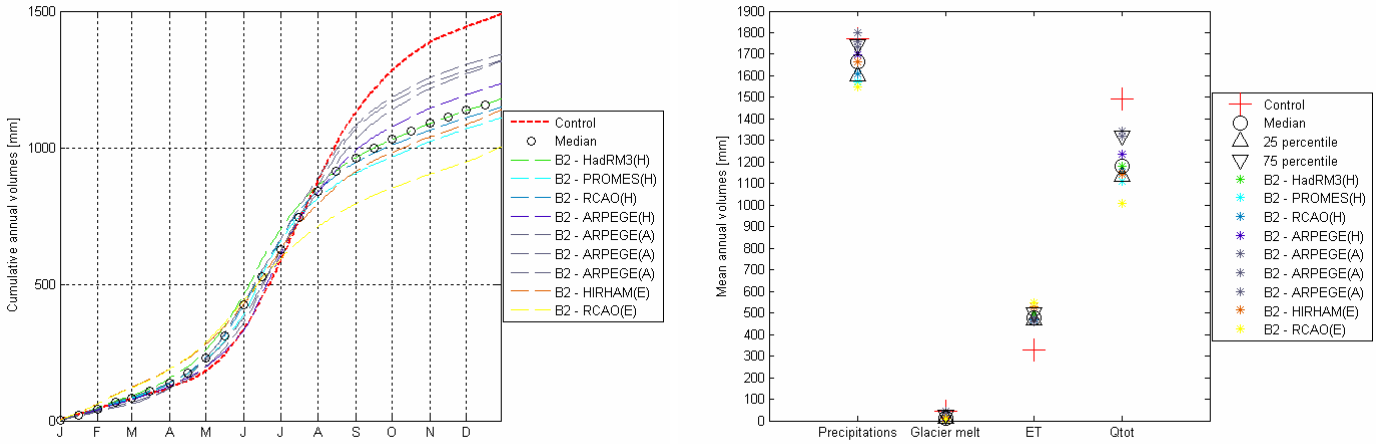

Fig. AV.13: Cumulative mean flow and water balance components for 2070-2099 – B2 scenario

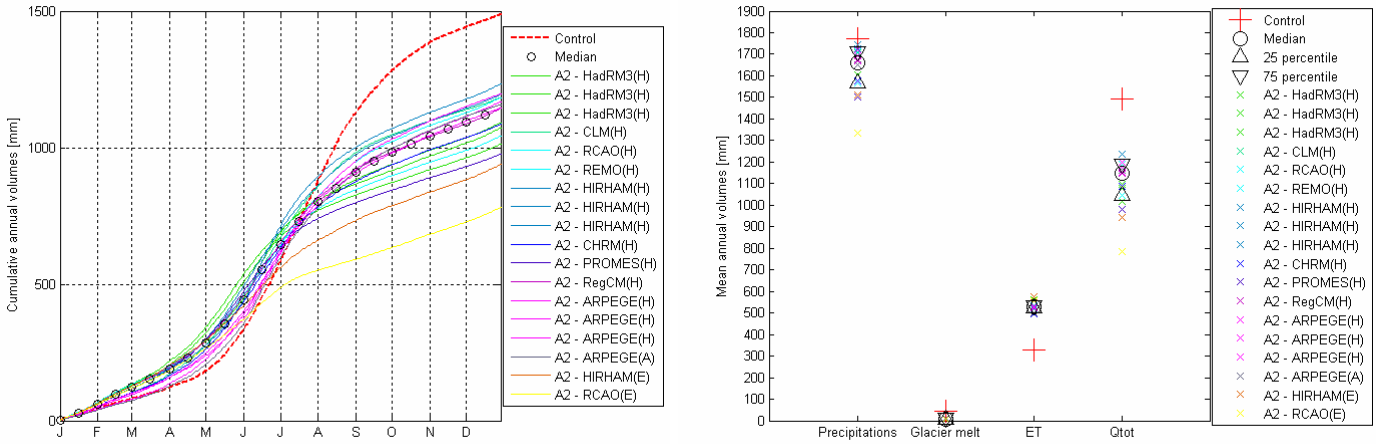

Fig. AV.14: Cumulative mean flow and water balance components for 2070-2099 – A2 scenario

Appendix 6 : The Minster catchment

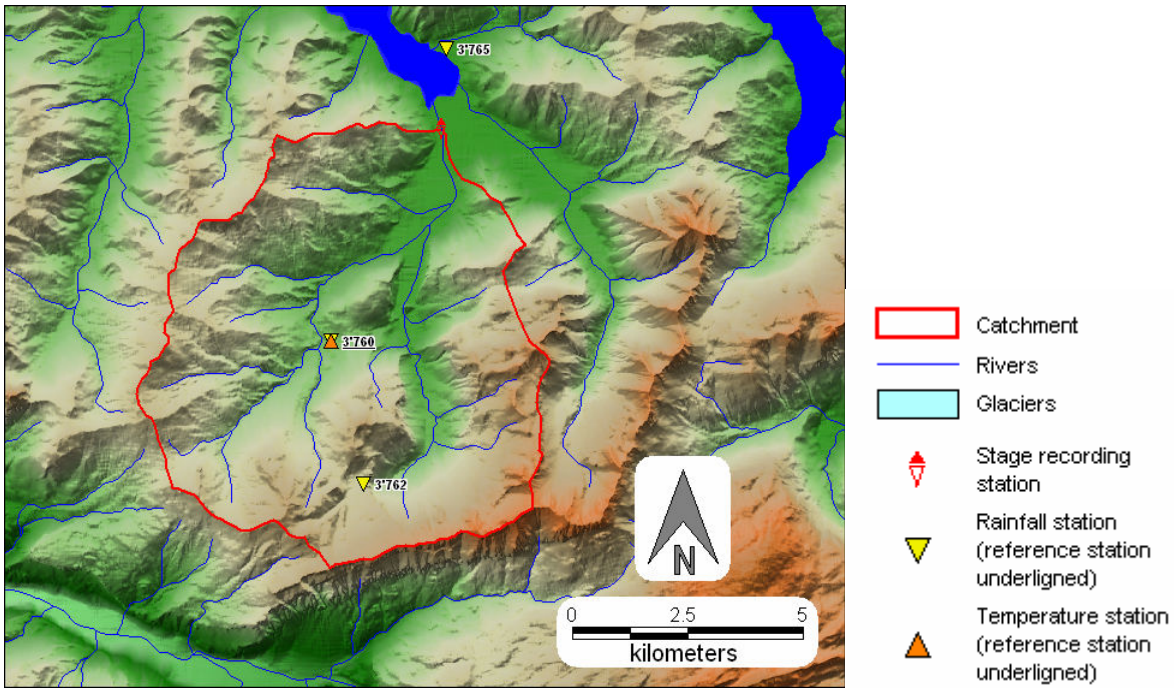

Fig. AVI.1: Catchment situation

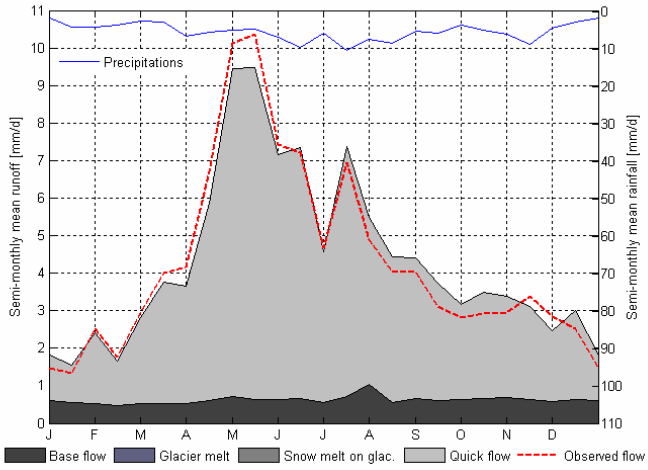

Fig. AVI.2: Calibration – Semi-monthly cycle for 1973-1980

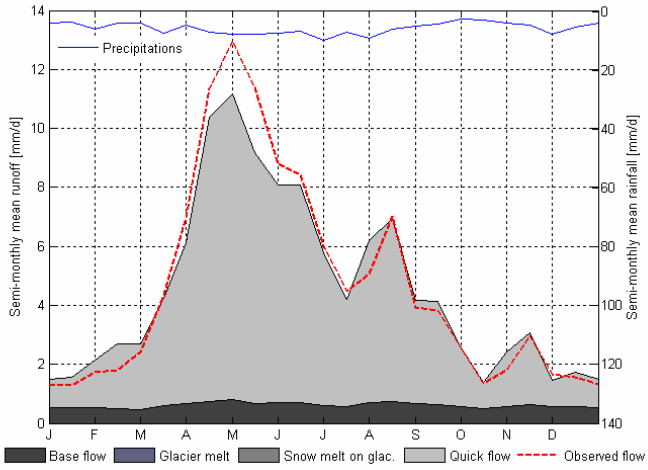

Fig. AVI.3: Validation – Semi-monthly cycle for 1963-1970

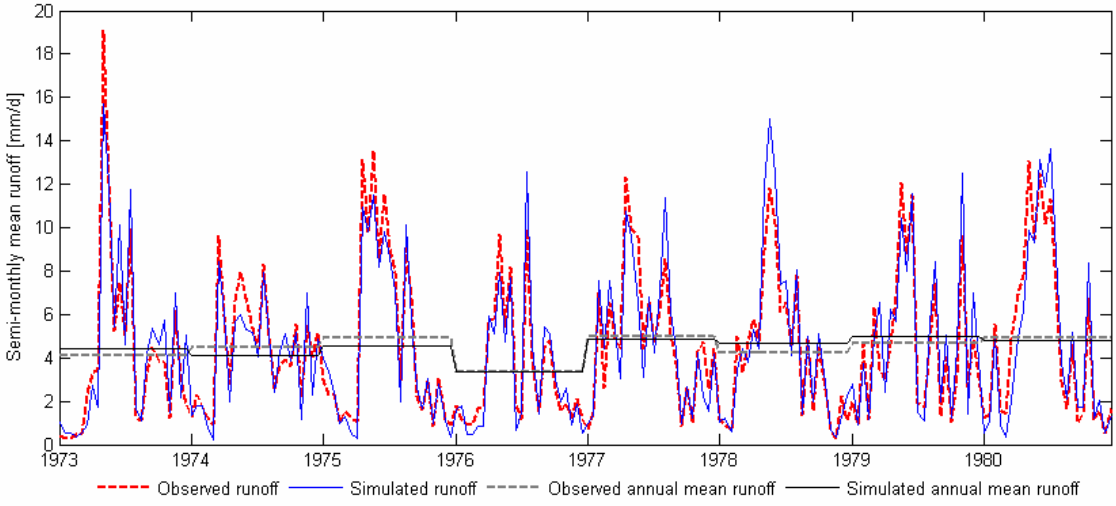

Fig. AVI.4: Calibration – Semi-monthly mean flow for 1973-1980

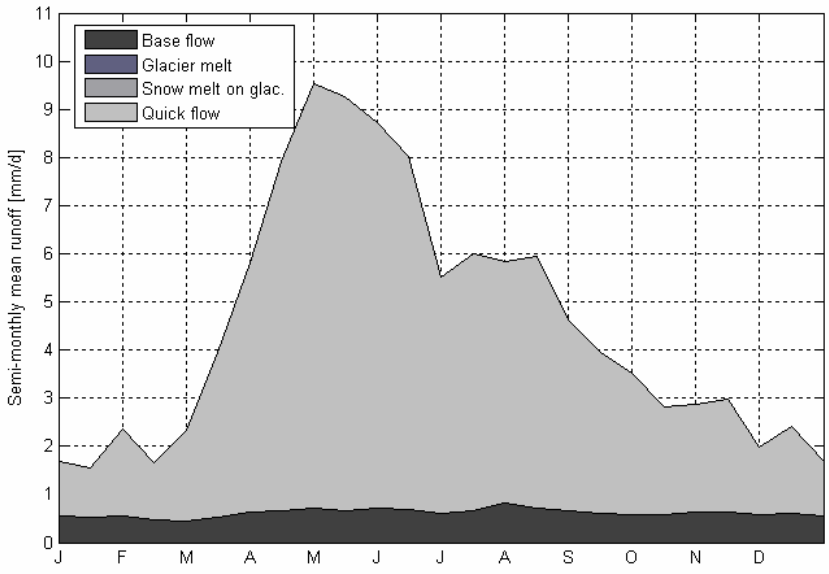

Fig. AVI.5: Hydrograph components for the control period (1961-1990)

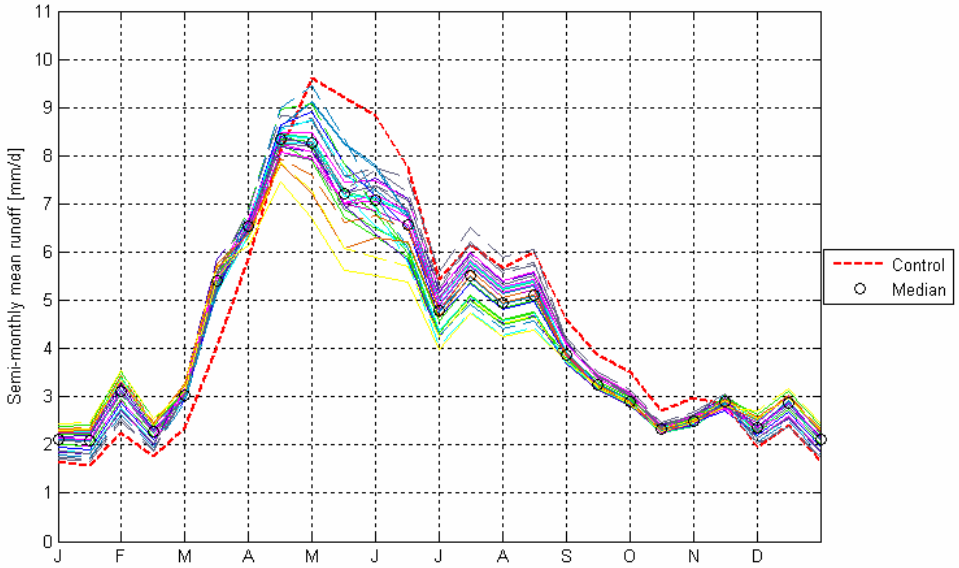

Fig. AVI.6: Changes in hydrological regime for 1°C global mean warming (scaled from A2 and B2 PRUDENCE experiments)

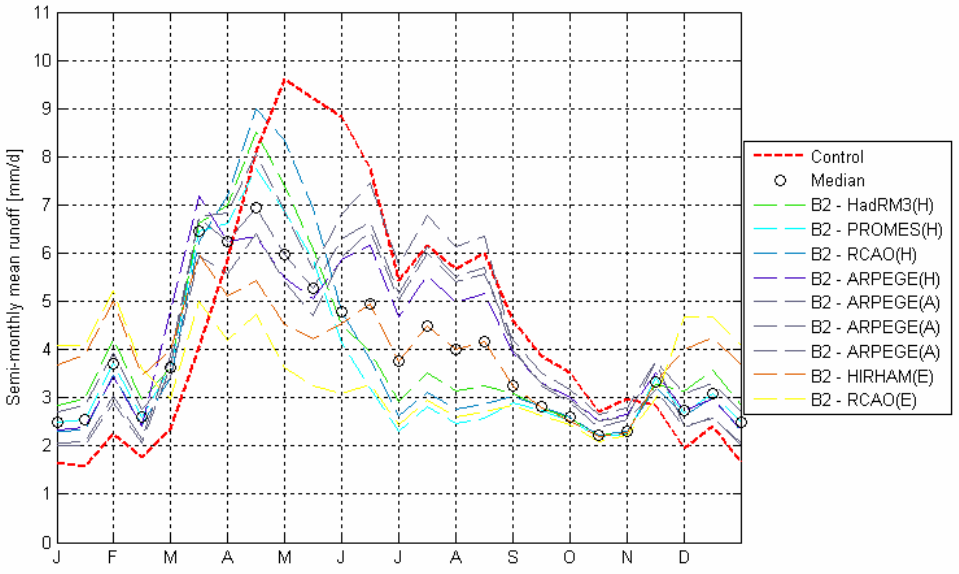

Fig. AVI.7: Changes in hydrological regime for 2070-2099 – B2 scenario

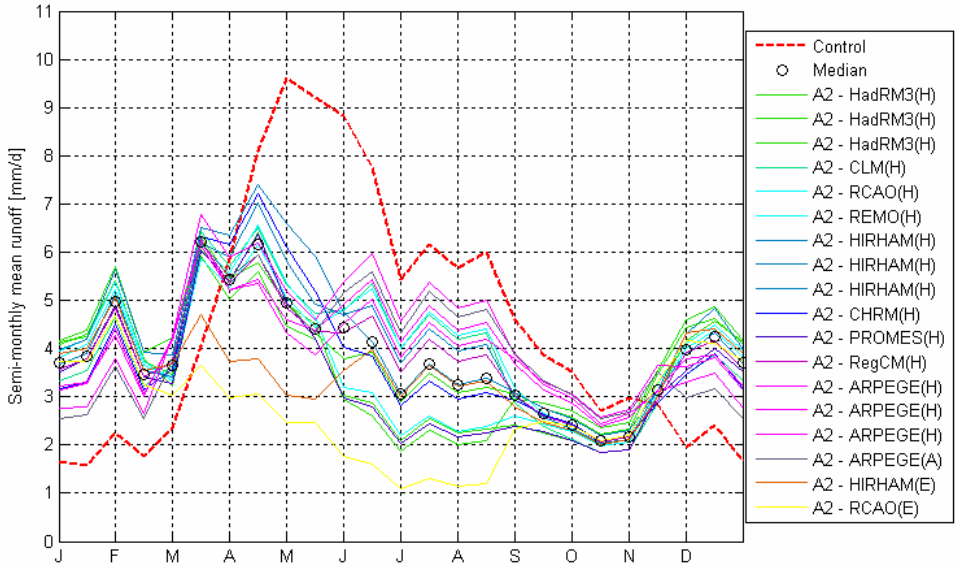

Fig. AVI.8: Changes in hydrological regime for 2070-2099 – A2 scenario

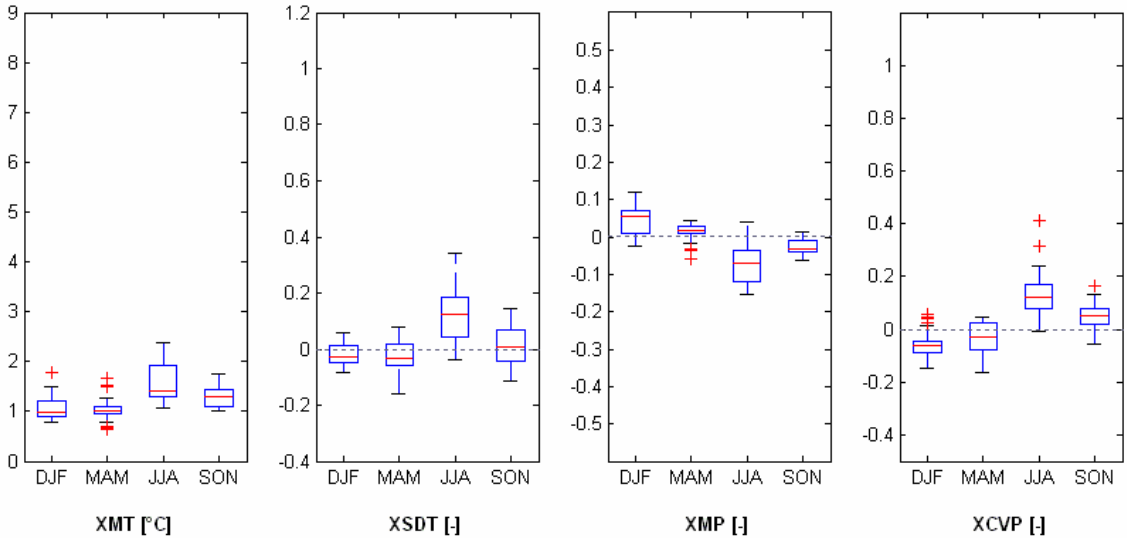

Fig. AVI.9: Box plots of regional seasonal changes for 1 °C global mean warming (2020-2049) (scaled from A2 and B2 PRUDENCE experiments)

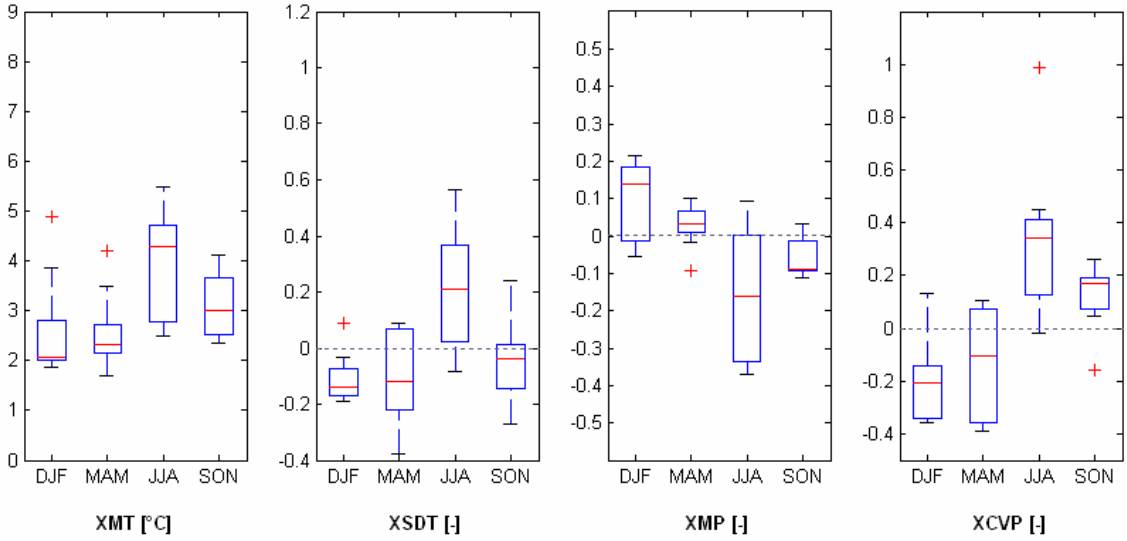

Fig. AVI.10: Box plots of regional seasonal changes predicted by PRUDENCE RCM experiments for 2070-2099 – B2 scenario

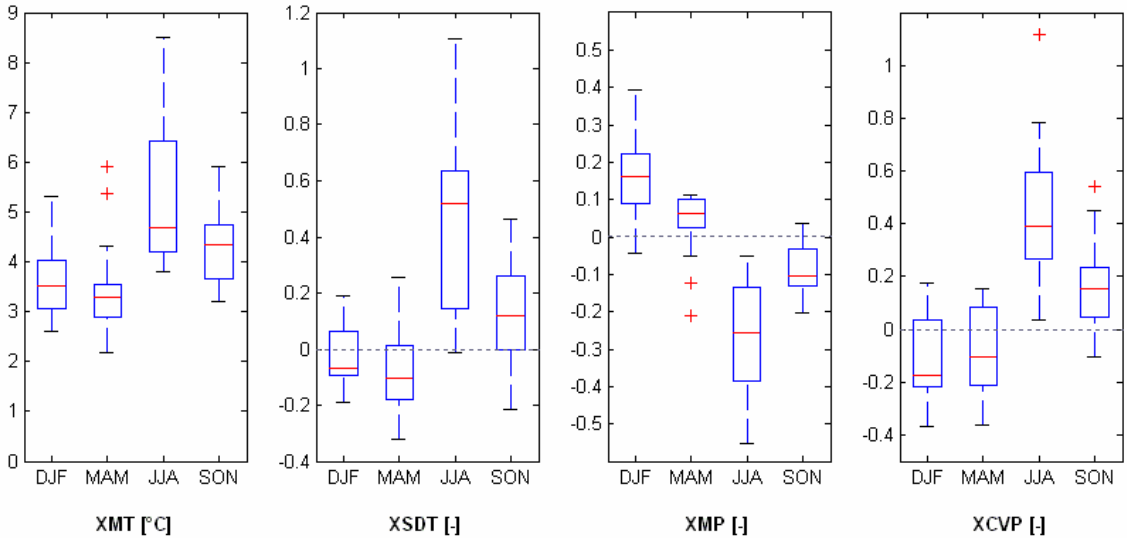

Fig. AVI.11: Box plots of regional seasonal changes predicted by PRUDENCE RCM experiments for 2070-2099 – A2 scenario

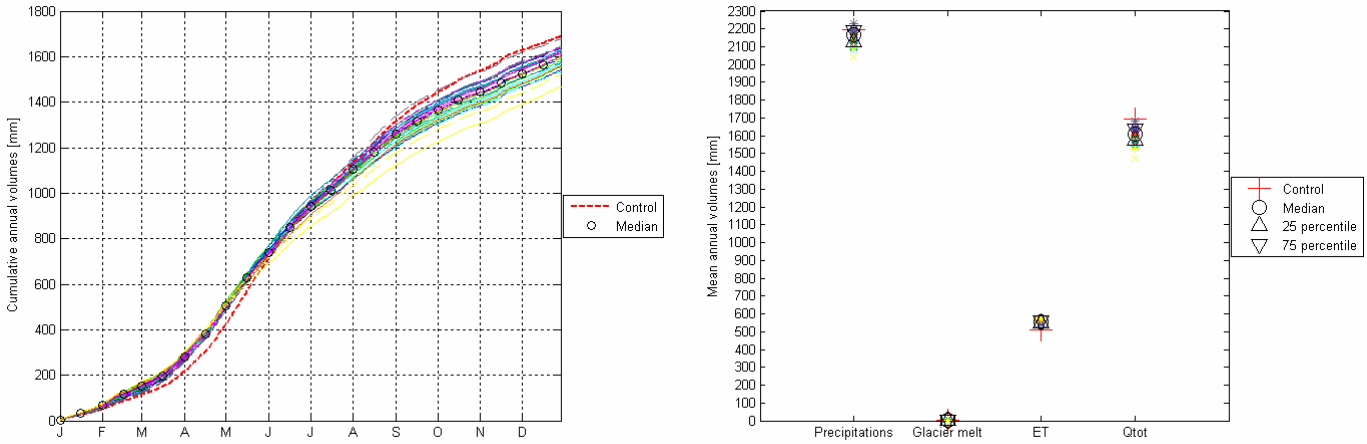

Fig. AVI.12: Cumulative mean flow and water balance components for 1°C global mean warming (2020-2049) (see Fig. AVI.13 and Fig. AVI.14 for colors meaning)

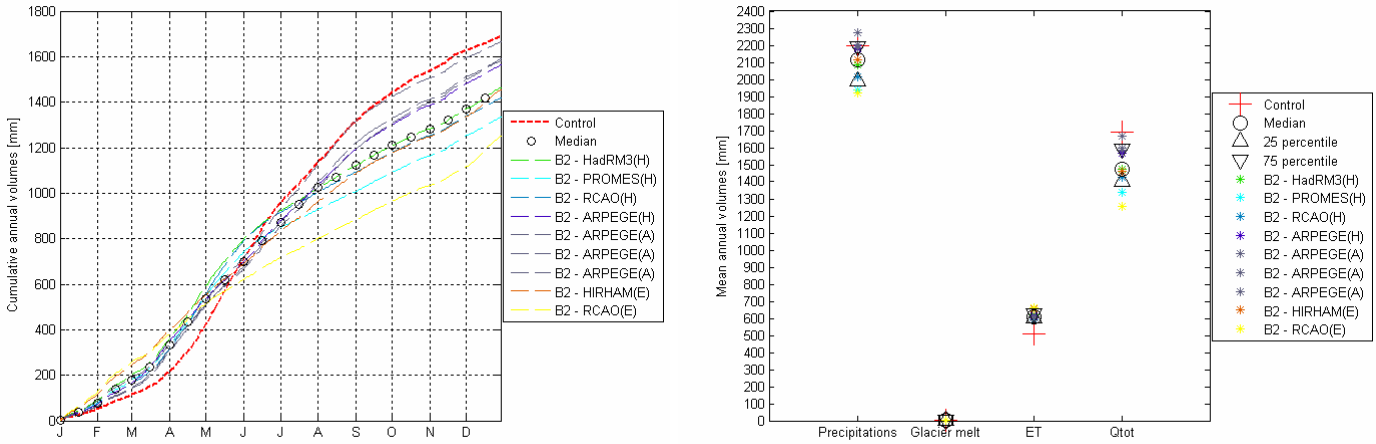

Fig. AVI.13: Cumulative mean flow and water balance components for 2070-2099 – B2 scenario

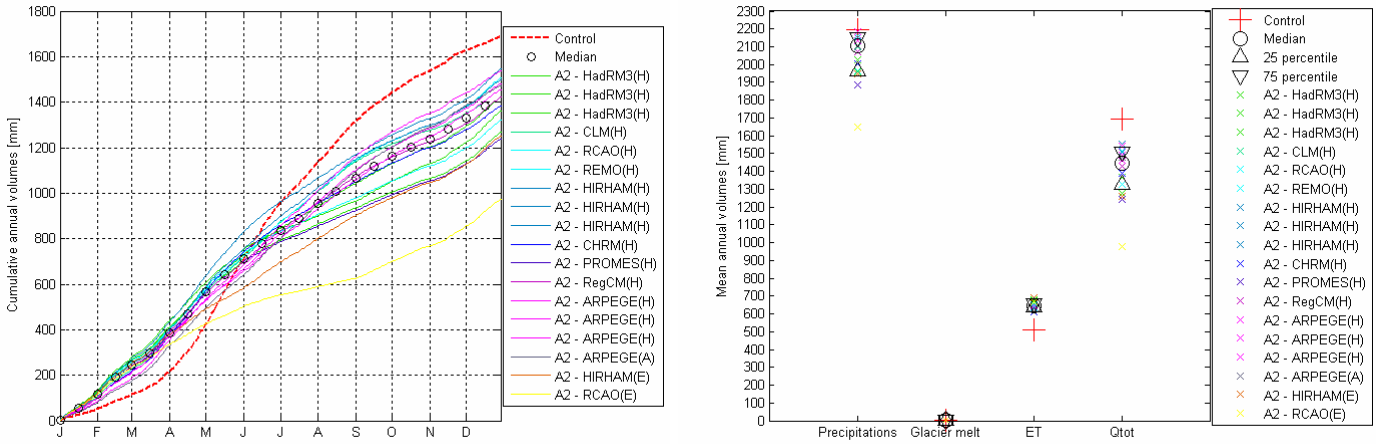

Fig. AVI.14: Cumulative mean flow and water balance components for 2070-2099 – A2 scenario

Appendix 7 : The Tamina catchment

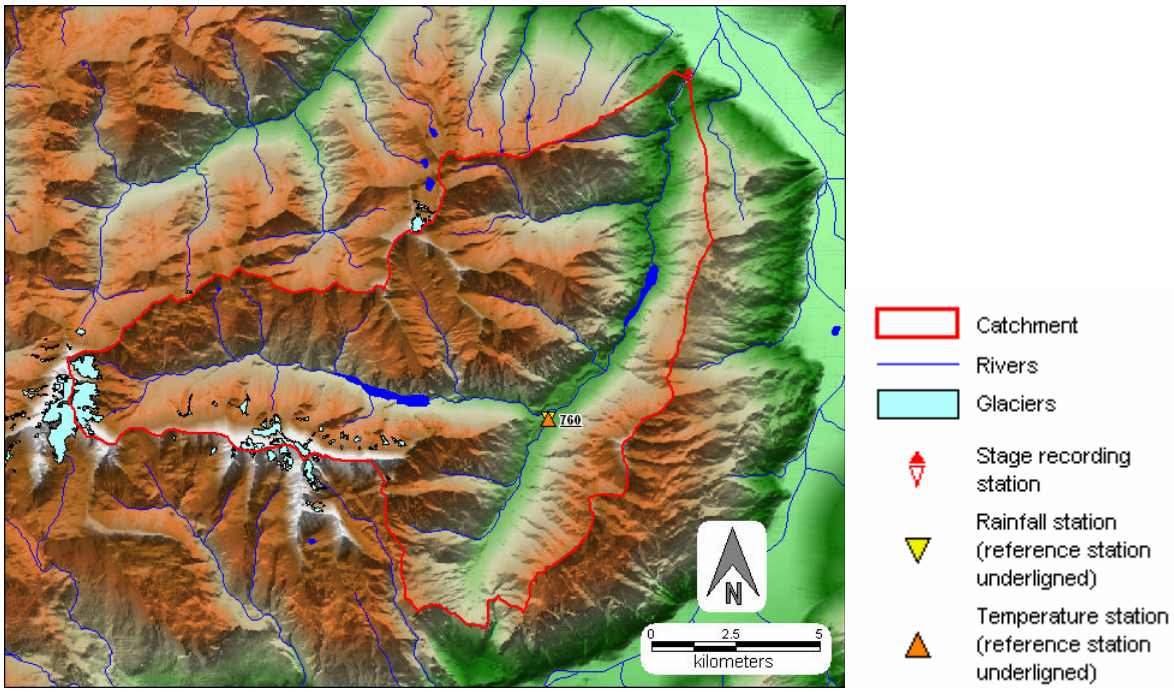

Fig. AVII.1: Catchment situation

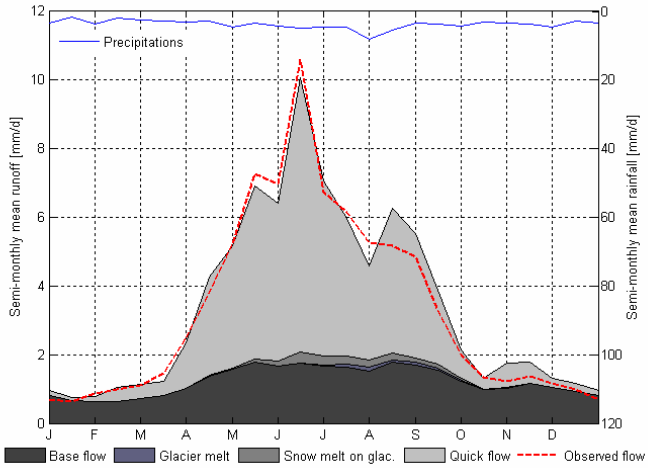

Fig. AVII.2: Calibration – Semi-monthly cycle for 1961-1967

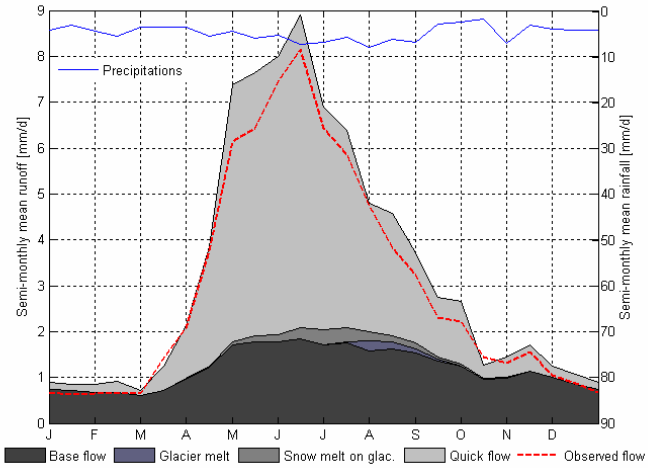

Fig. AVII.3: Validation – Semi-monthly cycle for 1968-1974

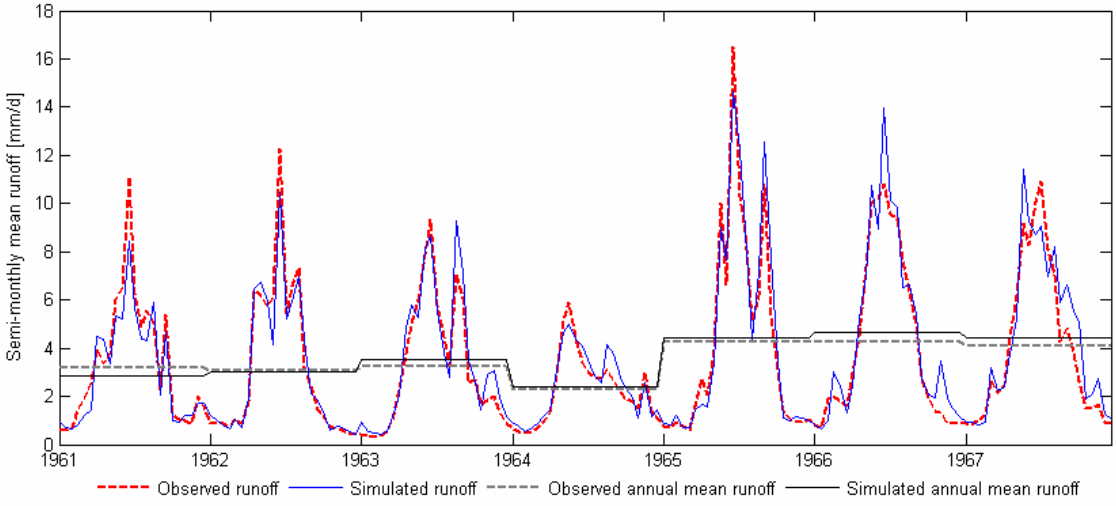

Fig. AVII.4: Calibration – Semi-monthly mean flow for 1961-1967

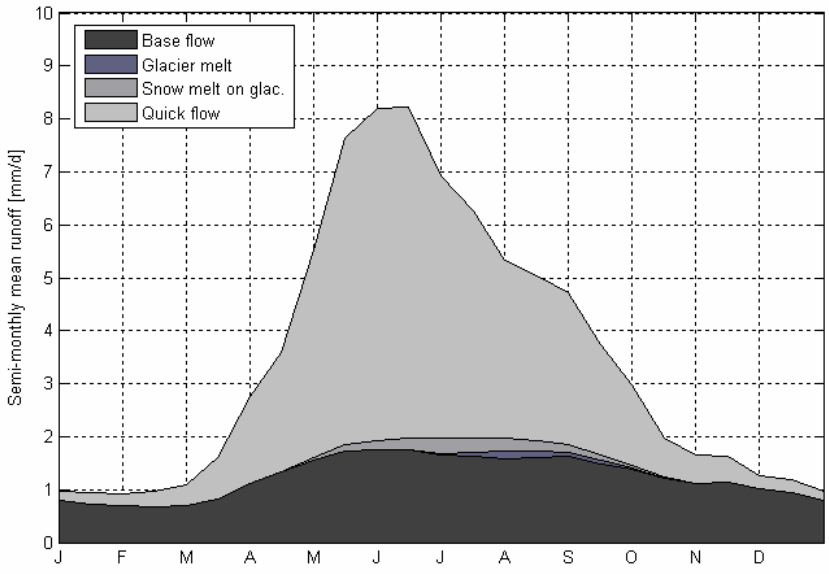

Fig. AVII.5: Hydrograph components for the control period (1961-1990)

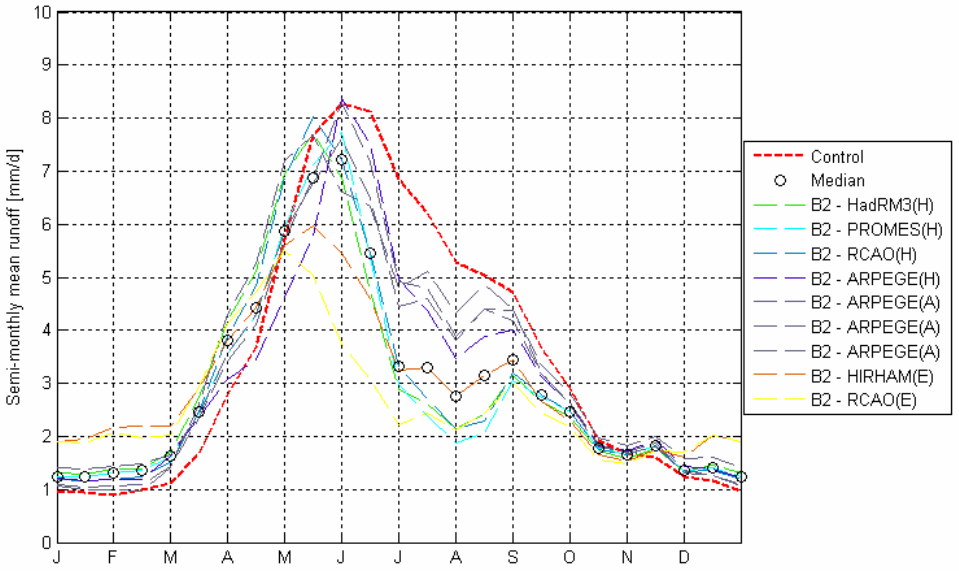

Fig. AVII.7: Changes in hydrological regime for 2070-2099 – B2 scenario

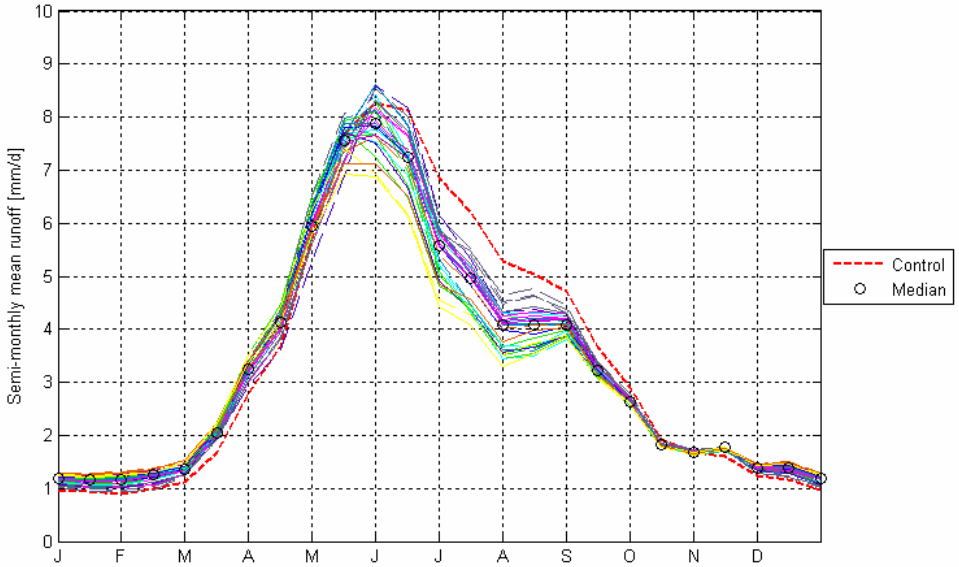

Fig. AVII.6: Changes in hydrological regime for 1 °C global mean warming (scaled from A2 and B2 PRUDENCE experiments)

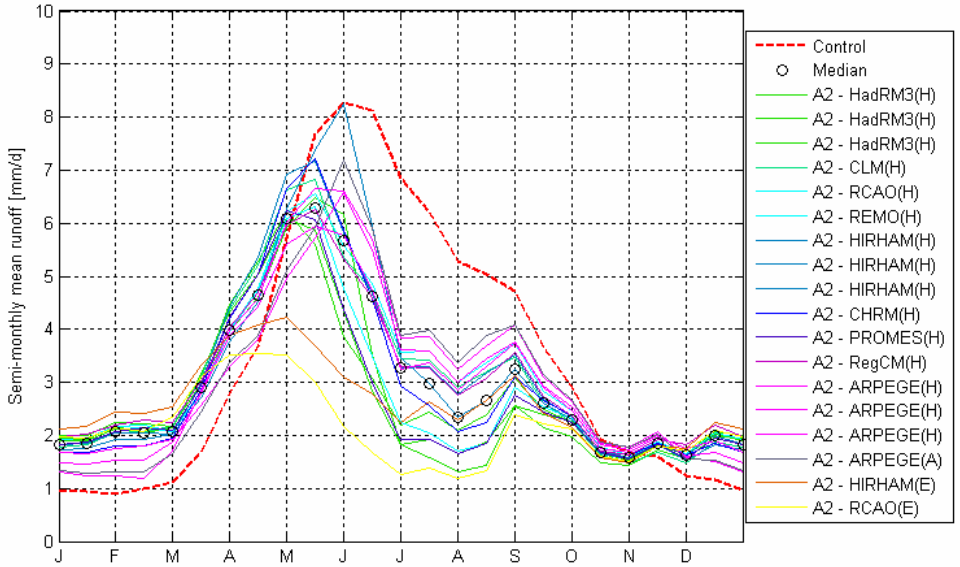

Fig. AVII.8: Changes in hydrological regime for 2070-2099 – A2 scenario

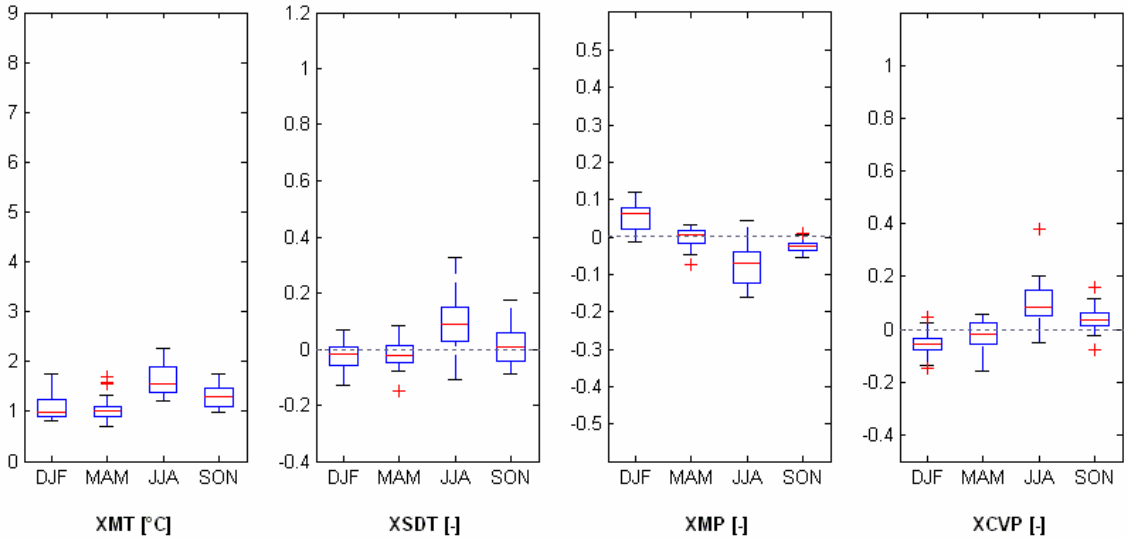

Fig. AVII.9: Box plots of regional seasonal changes for 1 °C global mean warming (2020-2049) (scaled from A2 and B2 PRUDENCE experiments)

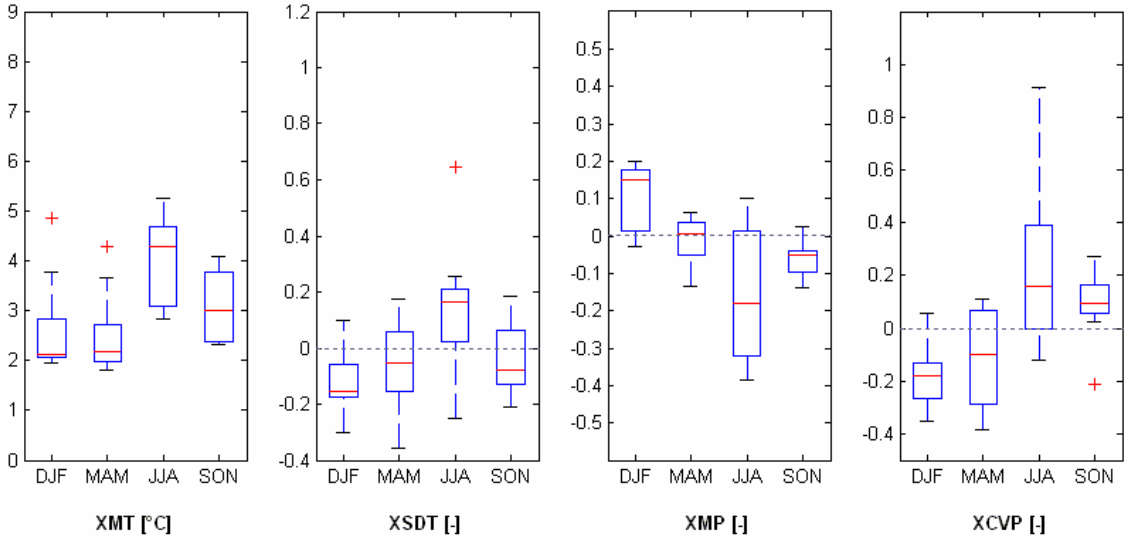

Fig. AVII.10: Box plots of regional seasonal changes predicted by PRUDENCE RCM experiments for 2070-2099 – B2 scenario

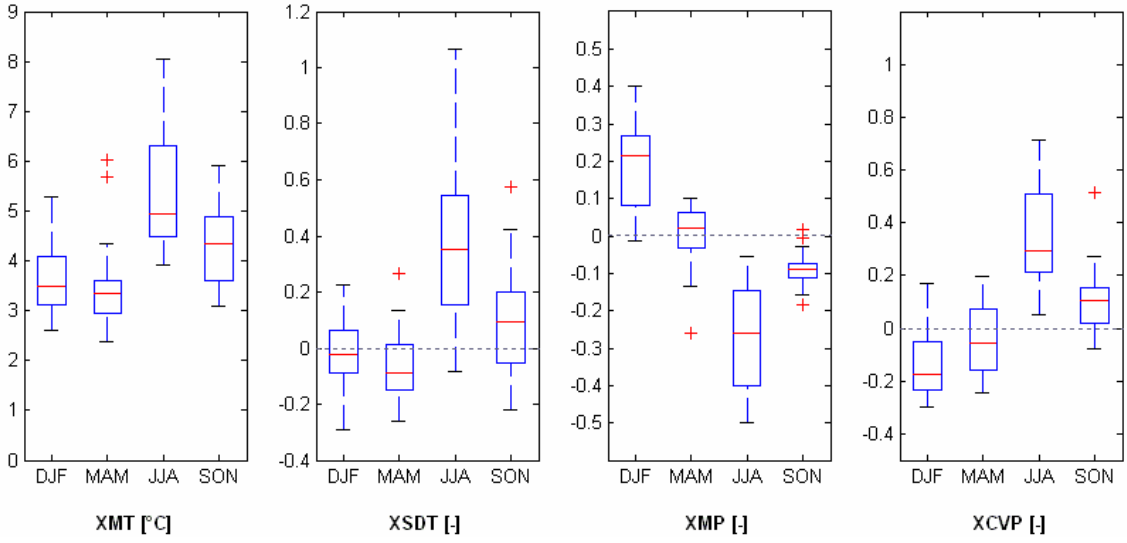

Fig. AVII.11: Box plots of regional seasonal changes predicted by PRUDENCE RCM experiments for 2070-2099 – A2 scenario

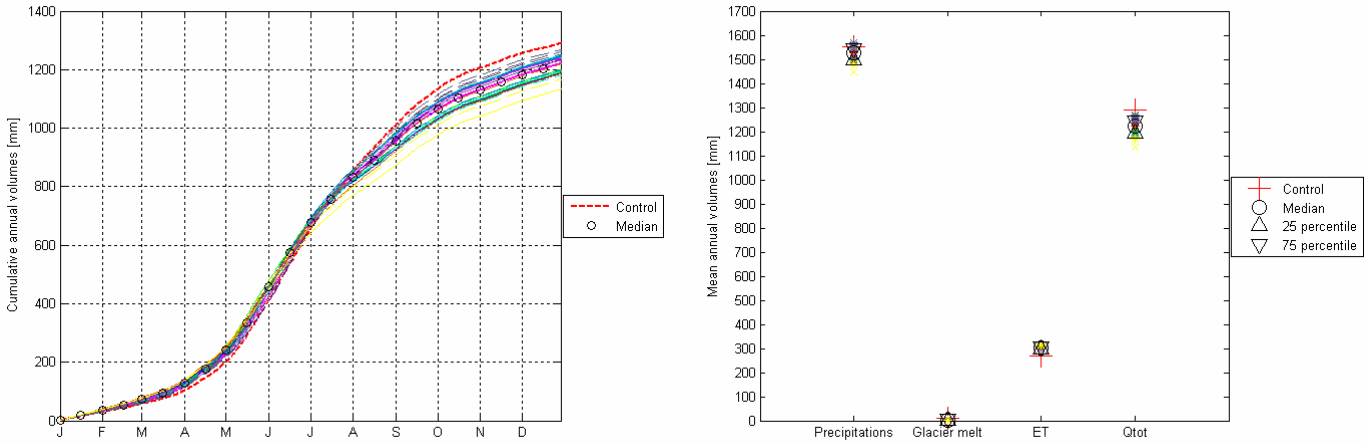

Fig. AVII.12: Cumulative mean flow and water balance components for 1°C global mean warming (2020-2049) (see Fig. AVII.13 and Fig. AVII.14 for colors meaning)

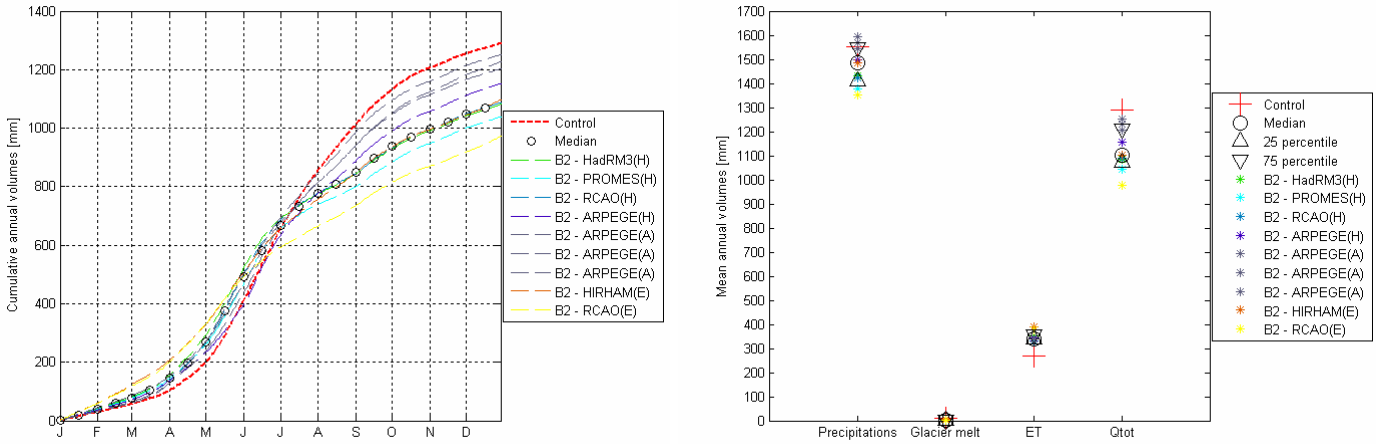

Fig. AVII.13: Cumulative mean flow and water balance components for 2070-2099 – B2 scenario

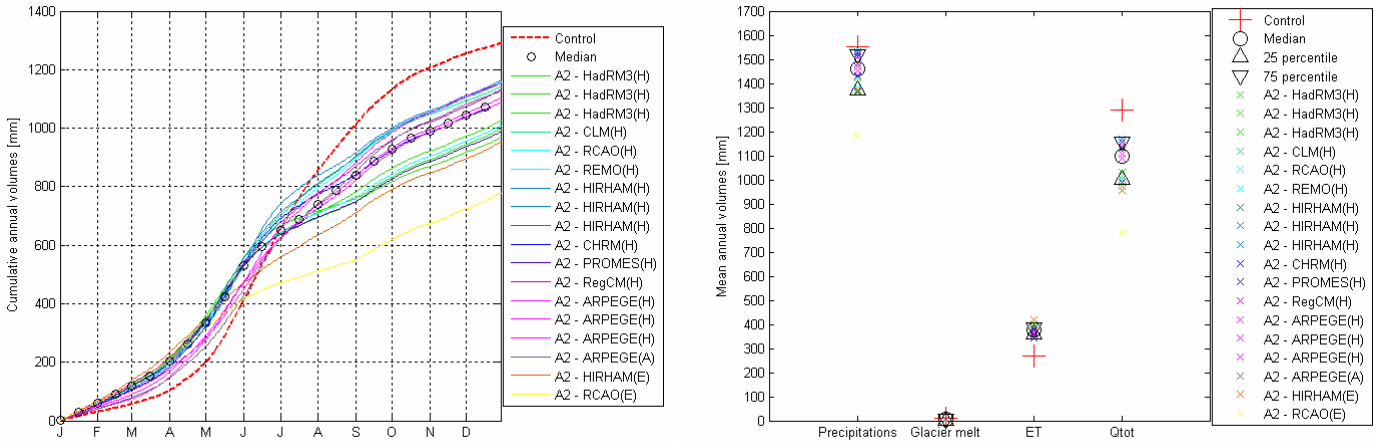

Fig. AVII.14: Cumulative mean flow and water balance components for 2070-2099 – A2 scenario

Appendix 8 : The Vorderrhein catchment

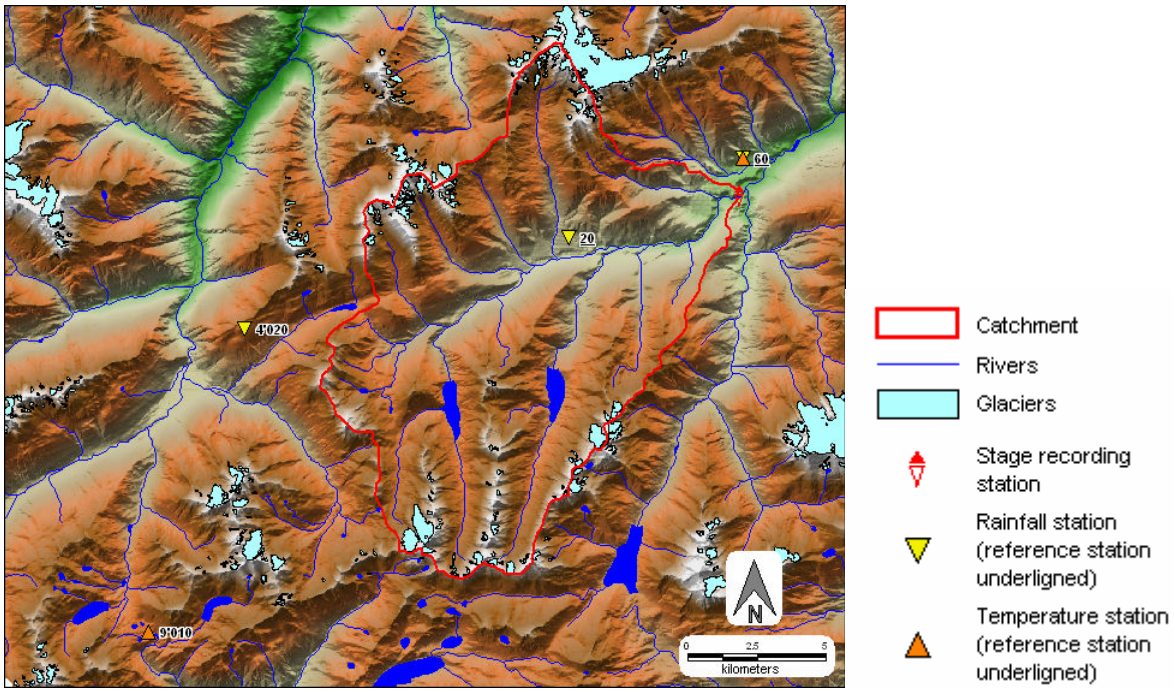

Fig. AVIII.1: Catchment situation

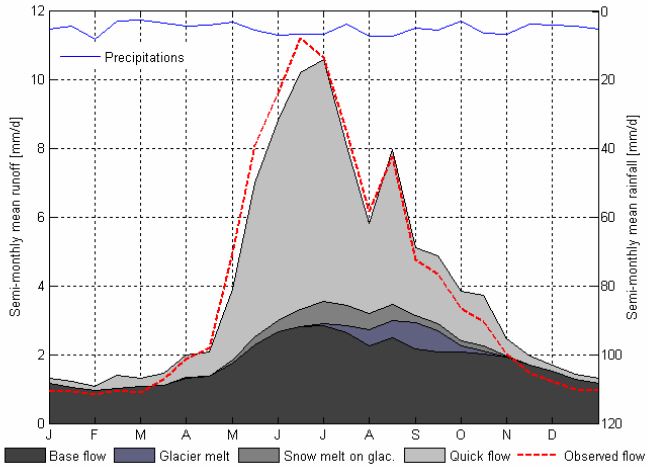

Fig. AVIII.2: Calibration – Semi-monthly cycle for 1953-1960

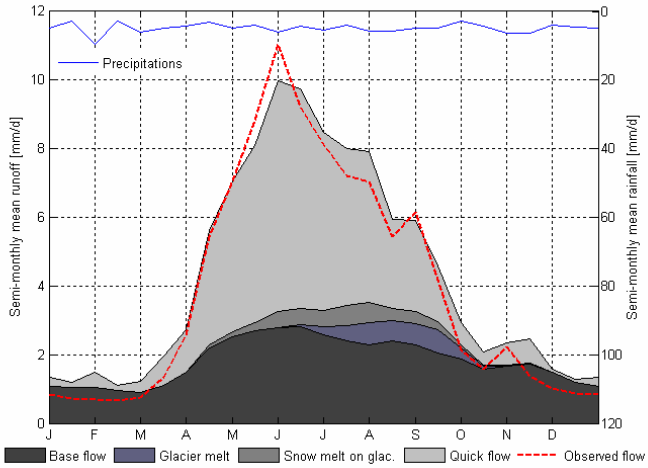

Fig. AVIII.3: Validation – Semi-monthly cycle for 1945-1950

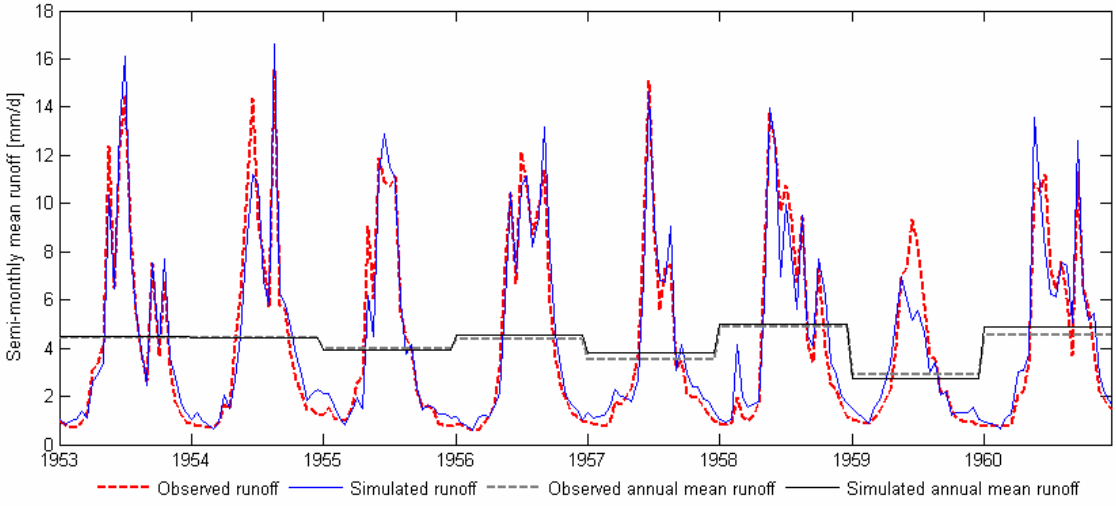

Fig. AVIII.4: Calibration – Semi-monthly mean flow for 1953-1960

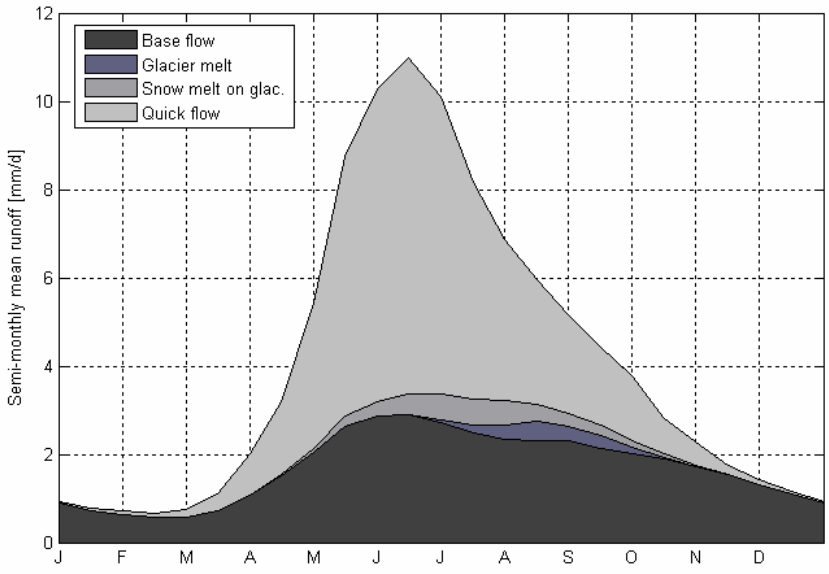

Fig. AVIII.5: Hydrograph components for the control period (1961-1990)

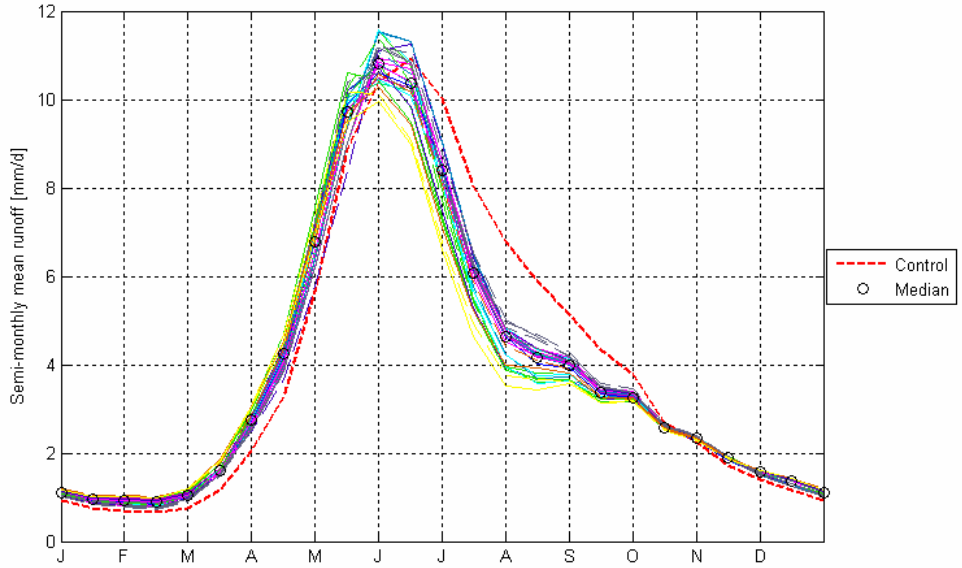

Fig. AVIII.6: Changes in hydrological regime for 1 °C global mean warming (scaled from A2 and B2 PRUDENCE experiments)

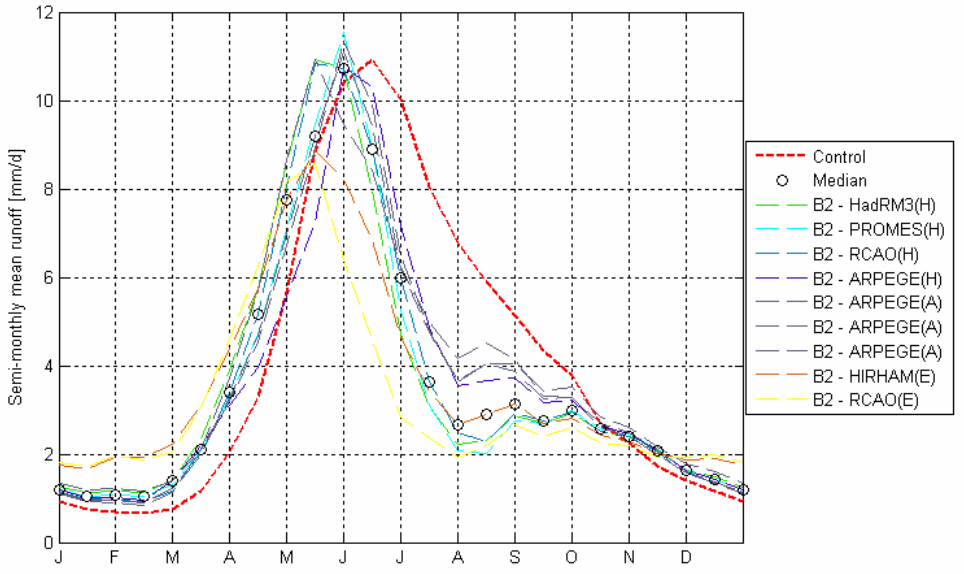

Fig. AVIII.7: Changes in hydrological regime for 2070-2099 – B2

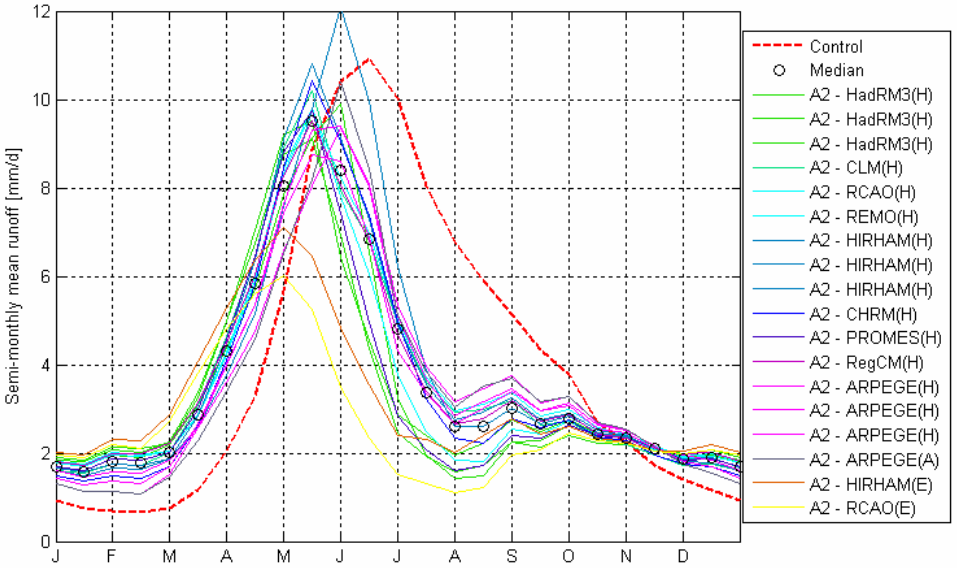

Fig. AVIII.8: Changes in hydrological regime for 2070-2099 – A2

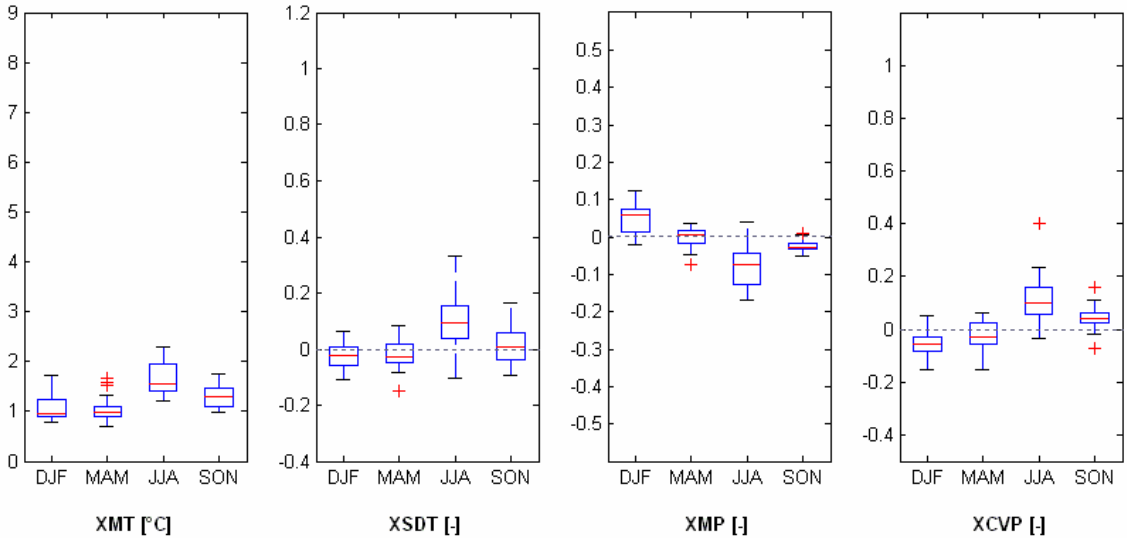

Fig. AVIII.9: Box plots of regional seasonal changes for 1 °C global mean warming (2020-2049) (scaled from A2 and B2 PRUDENCE experiments)

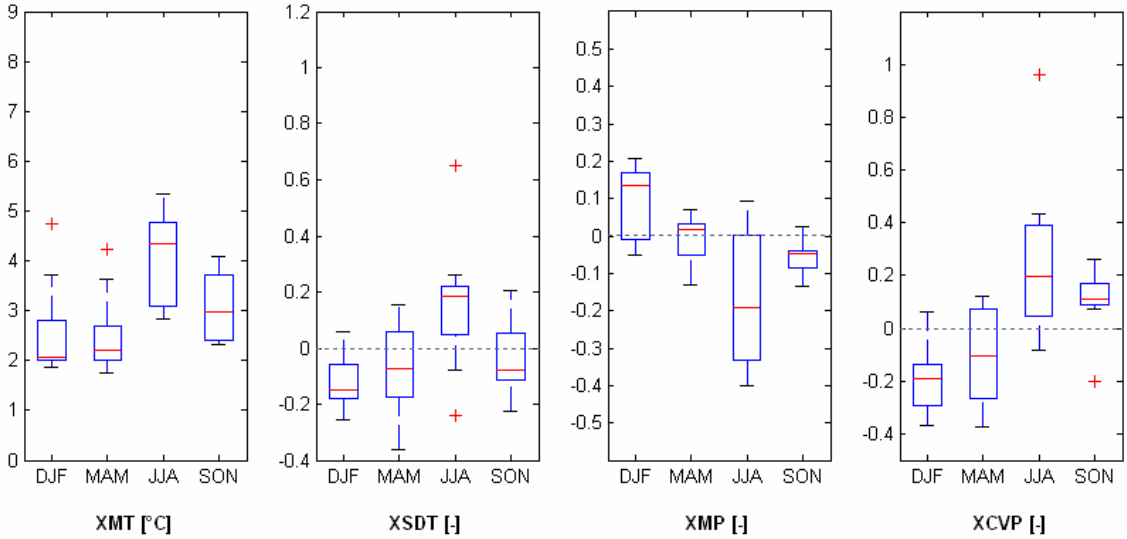

Fig. AVIII.10: Box plots of regional seasonal changes predicted by PRUDENCE RCM experiments for 2070-2099 – B2 scenario

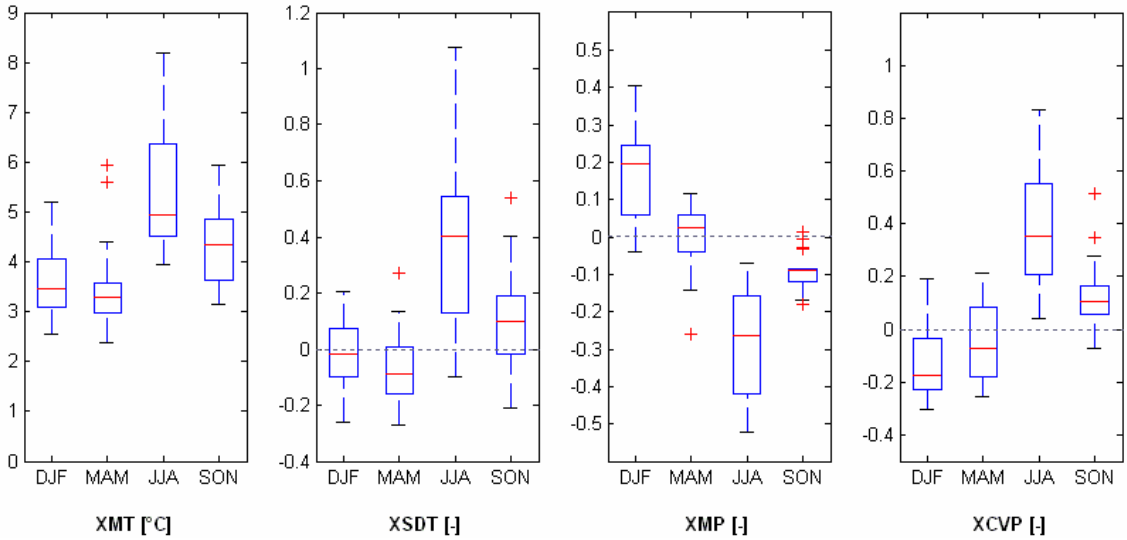

Fig. AVIII.11: Box plots of regional seasonal changes predicted by PRUDENCE RCM experiments for 2070-2099 – A2 scenario

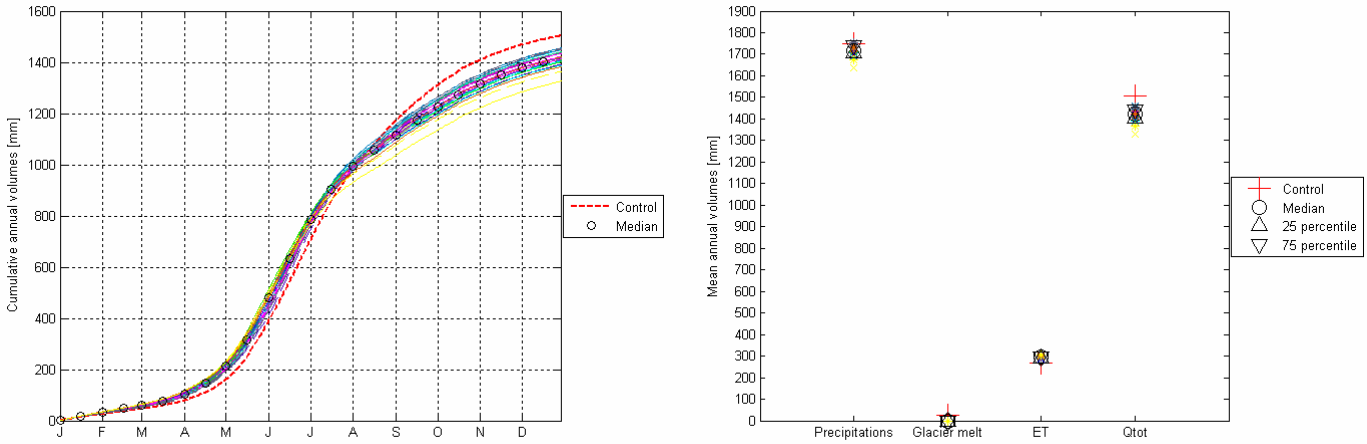

Fig. AVIII.12: Cumulative mean flow and water balance components for 1°C global mean warming (2020-2049) (see Fig. AVIII.13 and Fig. AVIII.14 for colors meaning)

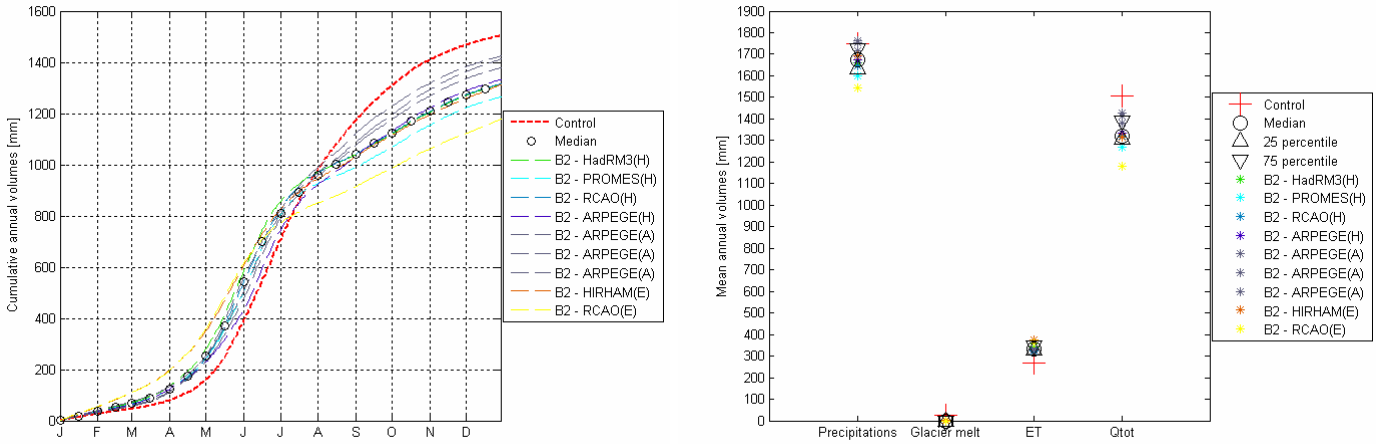

Fig. AVIII.13: Cumulative mean flow and water balance components for 2070-2099 – B2 scenario

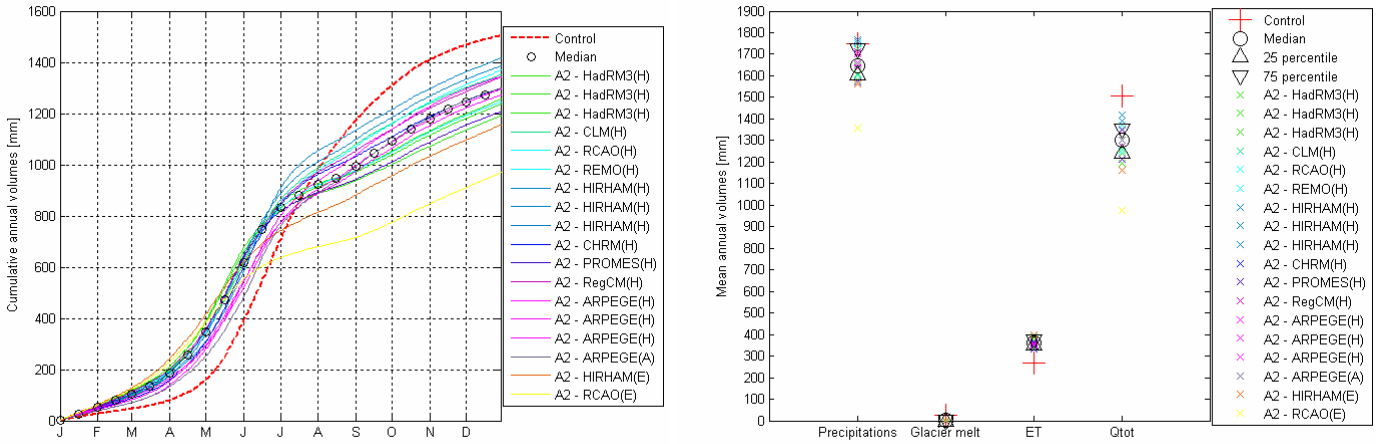

Fig. AVIII.14: Cumulative mean flow and water balance components for 2070-2099 – A2 scenario

Appendix 9 : The Dischmabach catchment

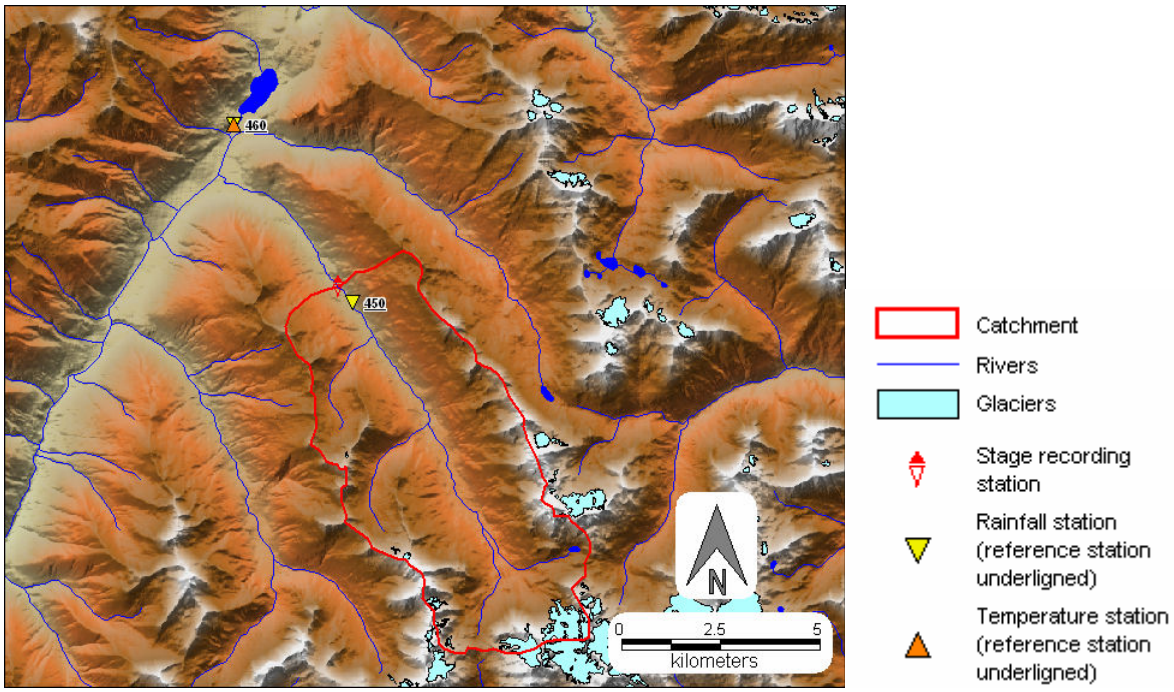

Fig. AIX.1: Catchment situation

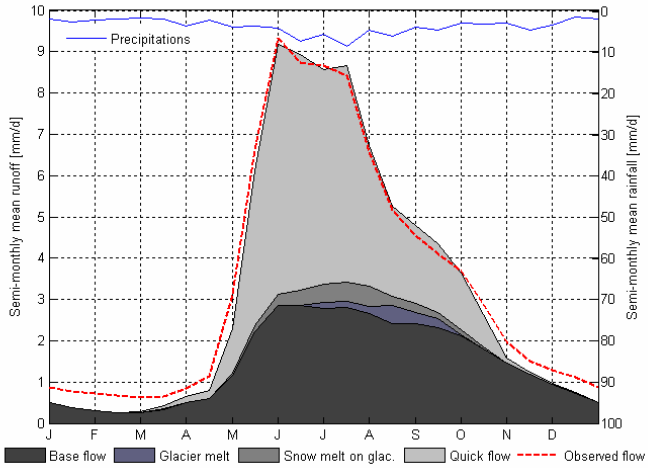

Fig. AIX.2: Calibration – Semi-monthly cycle for 1973-1980

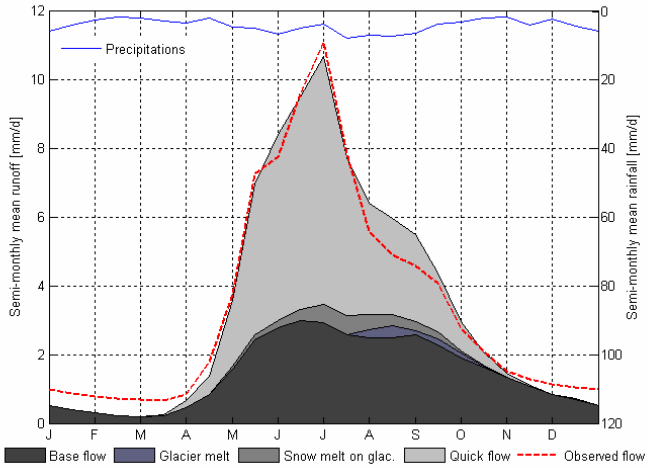

Fig. AIX.3: Validation – Semi-monthly cycle for 1983-1990

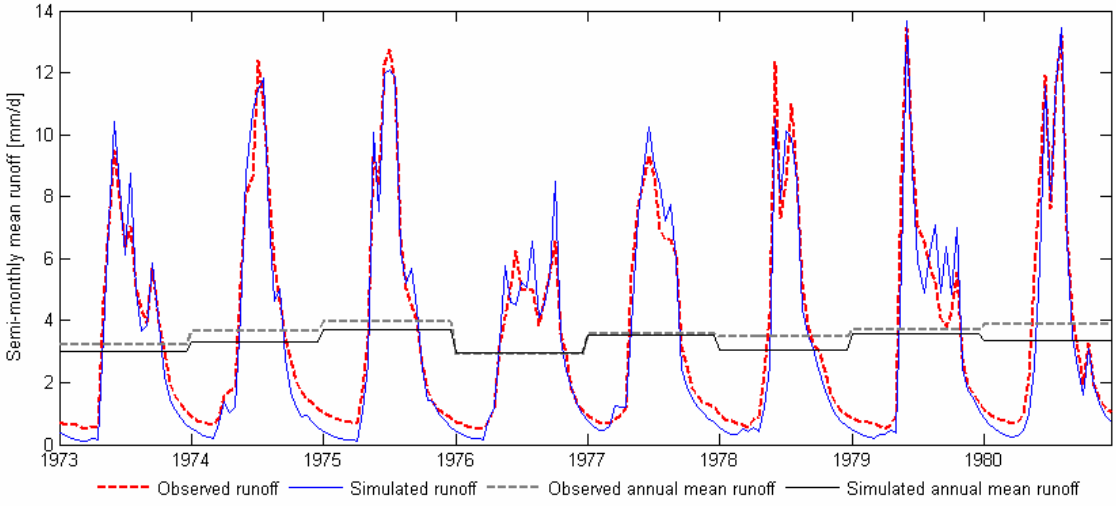

Fig. AIX.4: Calibration – Semi-monthly mean flow for 1973-1980

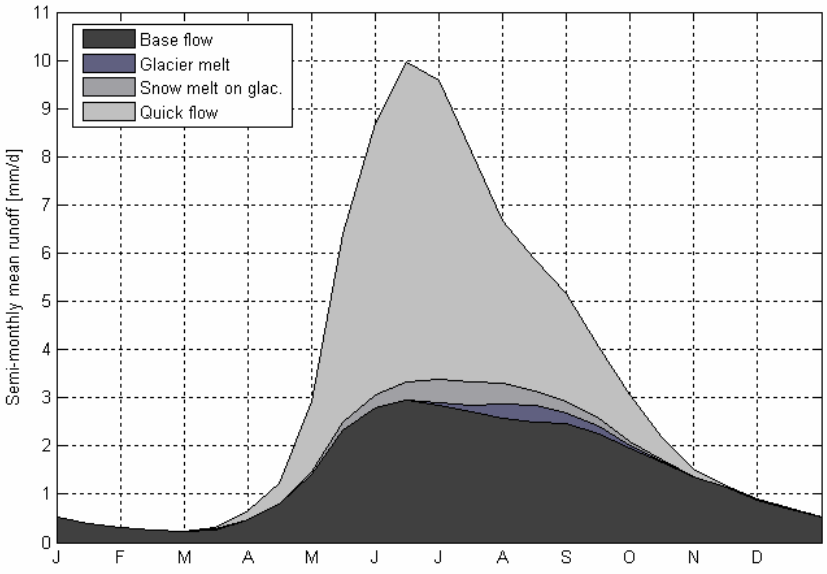

Fig. AIX.5: Hydrograph components for the control period (1961-1990)

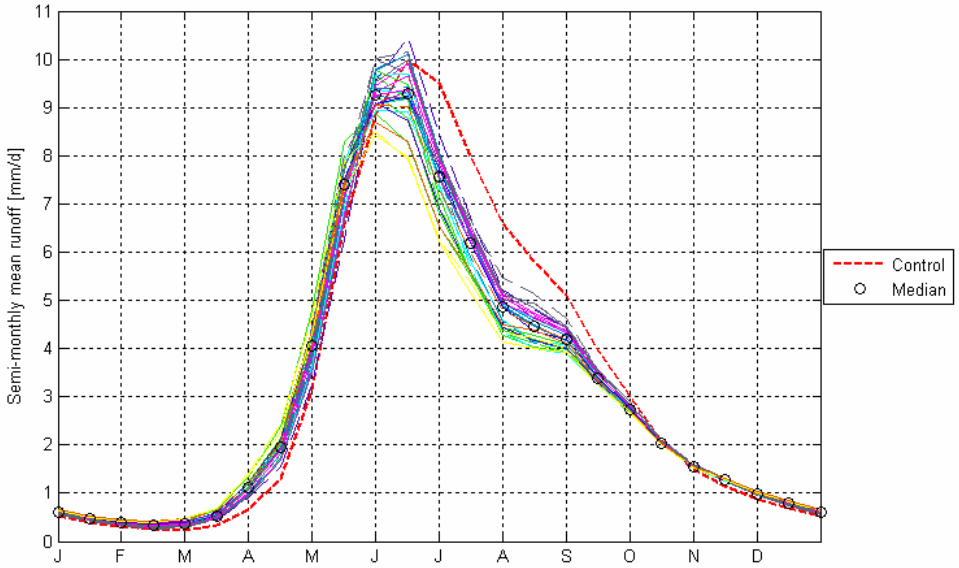

Fig. AIX.6: Changes in hydrological regime for 1°C global mean warming (scaled from A2 and B2 PRUDENCE experiments)

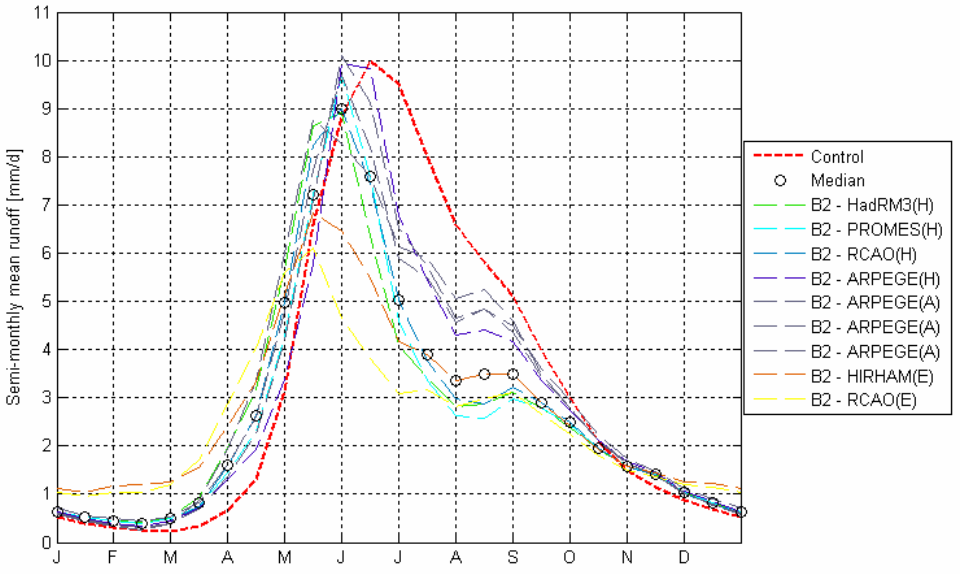

Fig. AIX.7: Changes in hydrological regime for 2070-2099 – B2 scenario

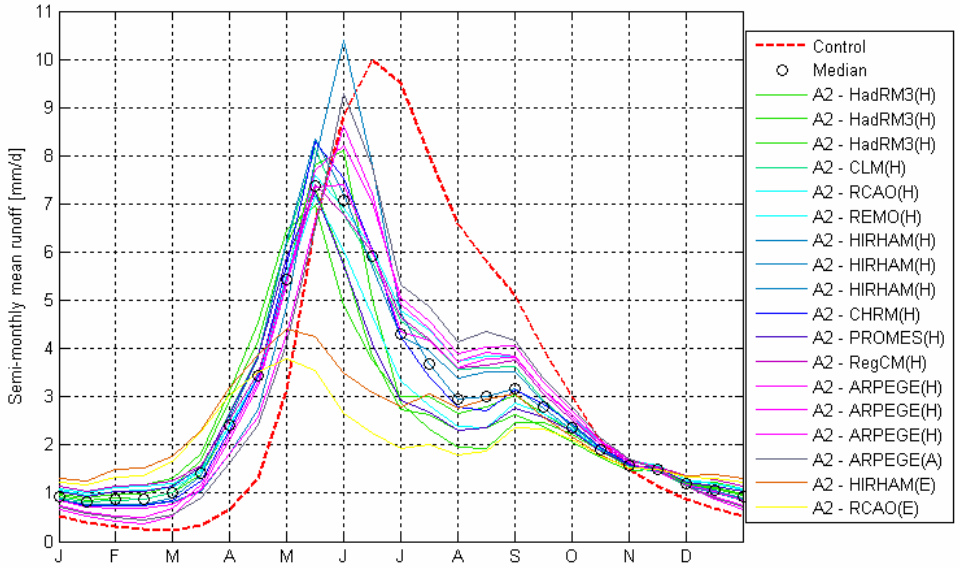

Fig. AIX.8: Changes in hydrological regime for 2070-2099 – A2 scenario

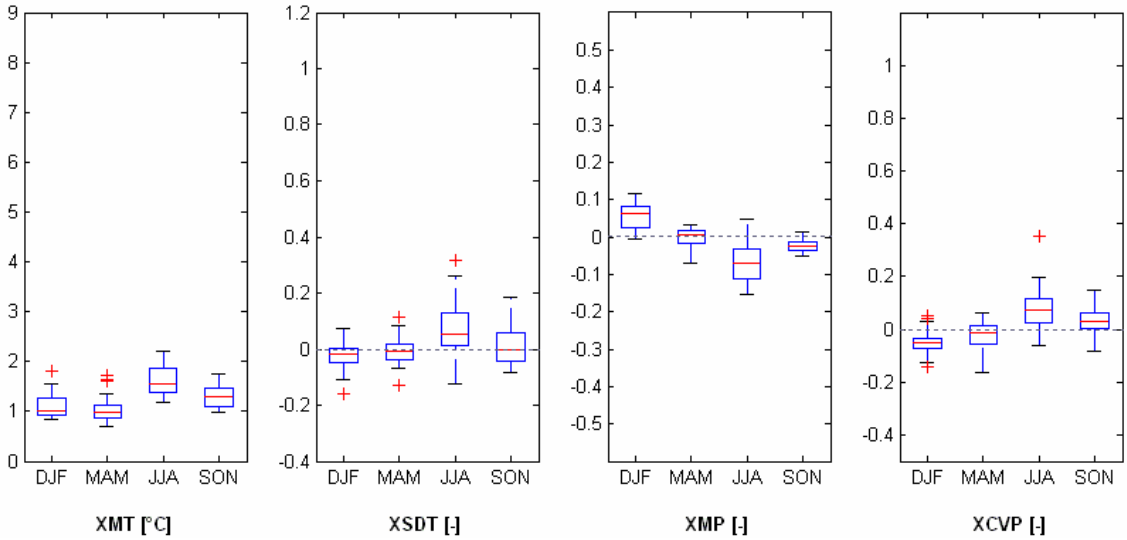

Fig. AIX.9: Box plots of regional seasonal changes for 1 °C global mean warming (2020-2049) (scaled from A2 and B2 PRUDENCE experiments)

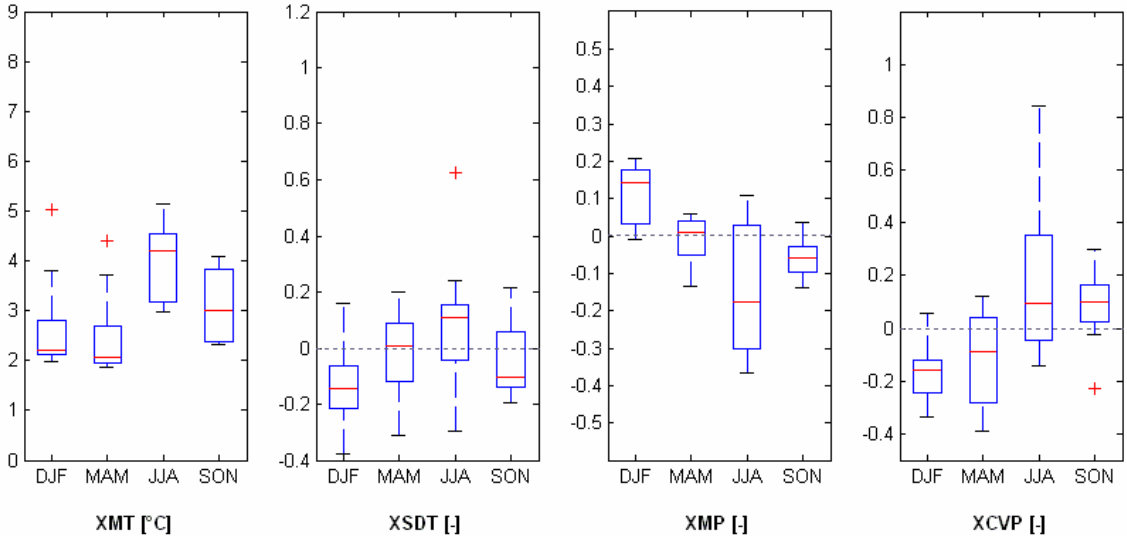

Fig. AIX.10: Box plots of regional seasonal changes predicted by PRUDENCE RCM experiments for 2070-2099 – B2 scenario

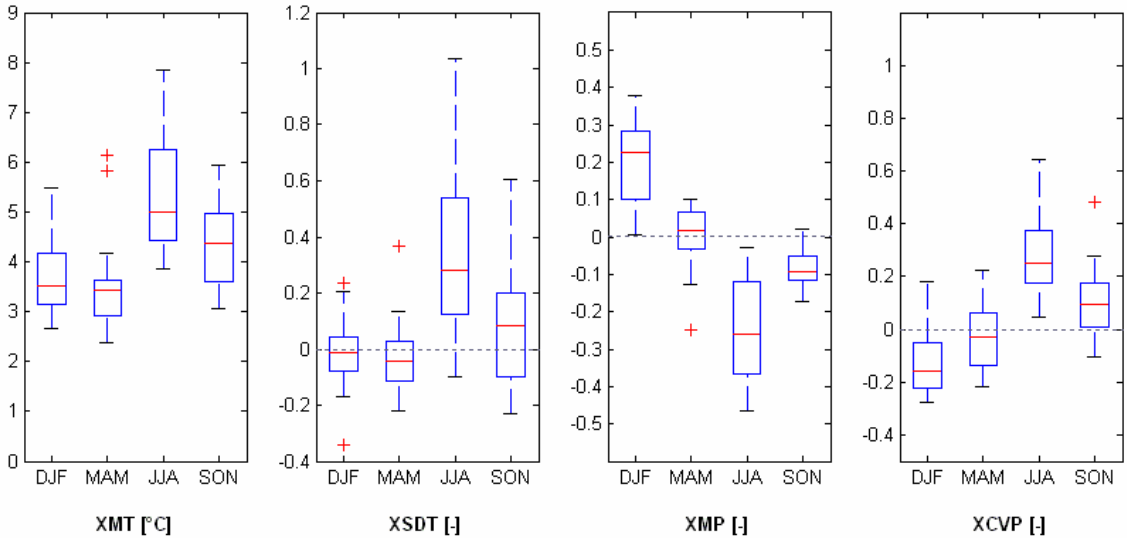

Fig. AIX.11: Box plots of regional seasonal changes predicted by PRUDENCE RCM experiments for 2070-2099 – A2 scenario

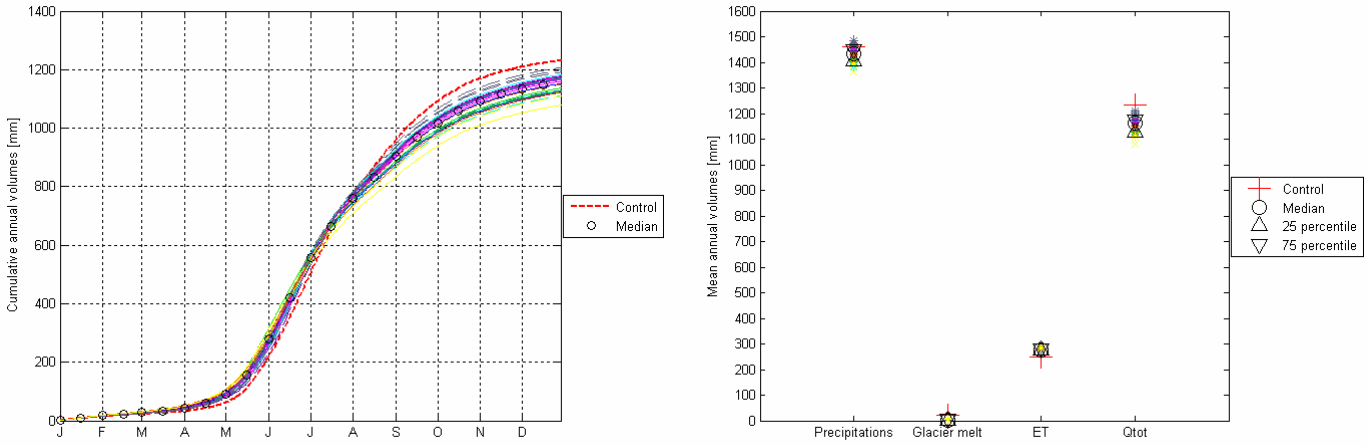

Fig. AIX.12: Cumulative mean flow and water balance components for 1°C global mean warming (2020-2049) (see Fig. AIX.13 and Fig. AIX.14 for colors meaning)

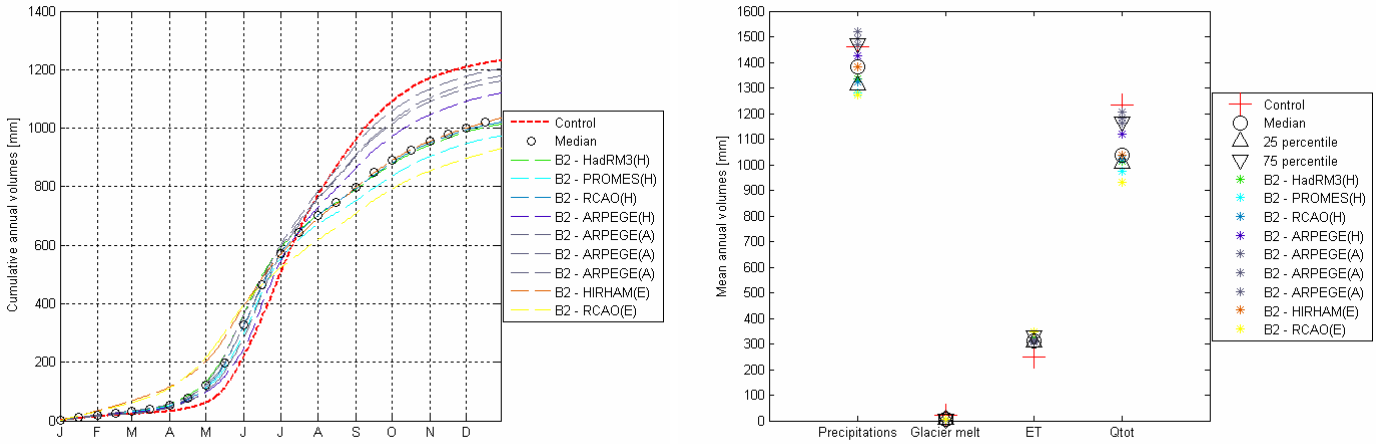

Fig. AIX.13: Cumulative mean flow and water balance components for 2070-2099 – B2 scenario

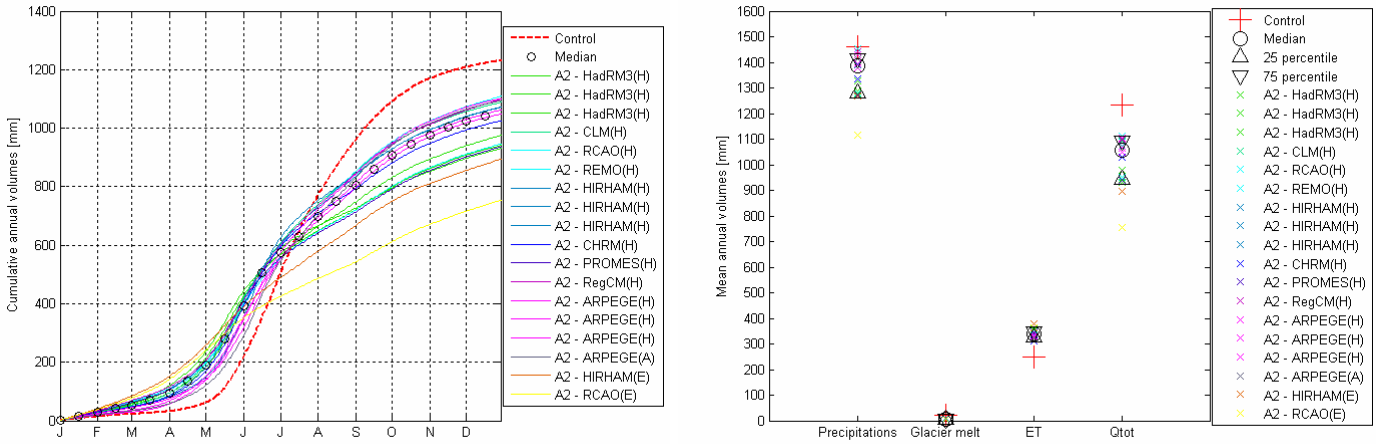

Fig. AIX.14: Cumulative mean flow and water balance components for 2070-2099 – A2 scenario

Appendix 10 : The Rosegbach catchment

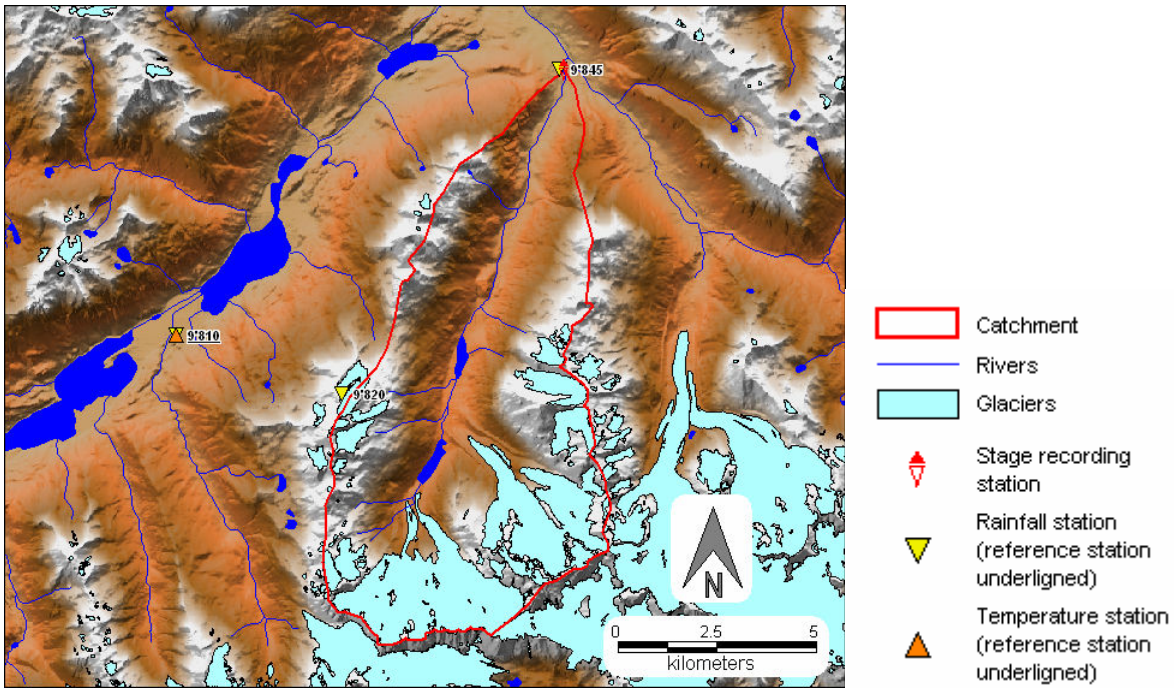

Fig. AX.1: Catchment situation

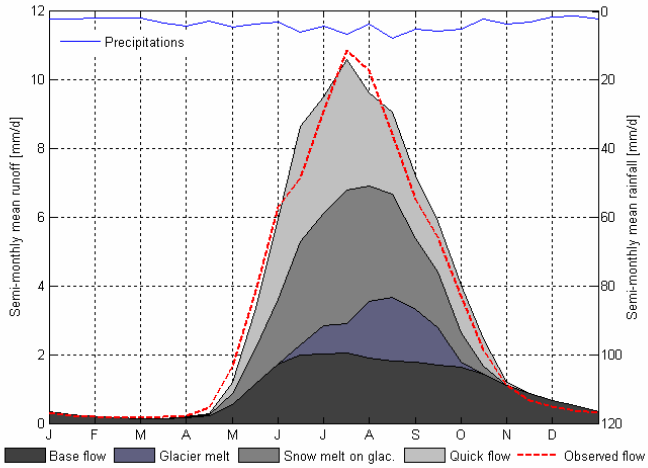

Fig. AX.2: Calibration – Semi-monthly cycle for 1973-1980

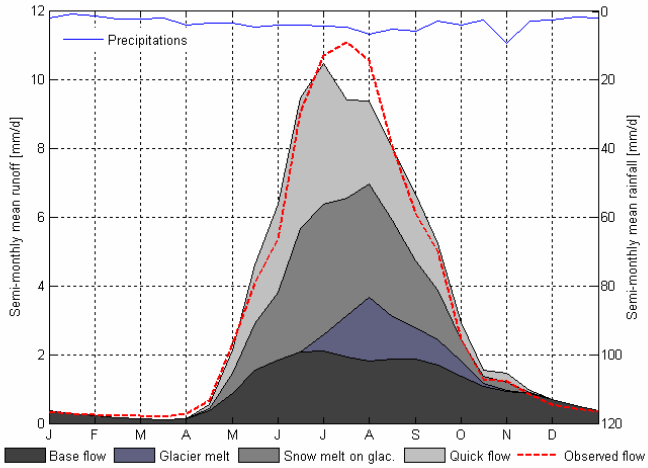

Fig. AX.3: Validation – Semi-monthly cycle for 1963-1970

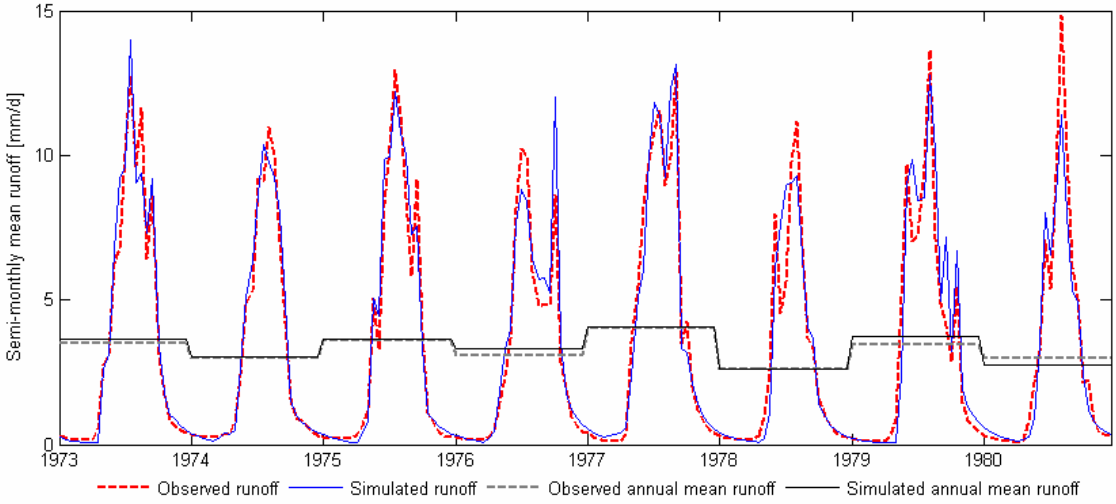

Fig. AX.4: Calibration – Semi-monthly mean flow for 1973-1980

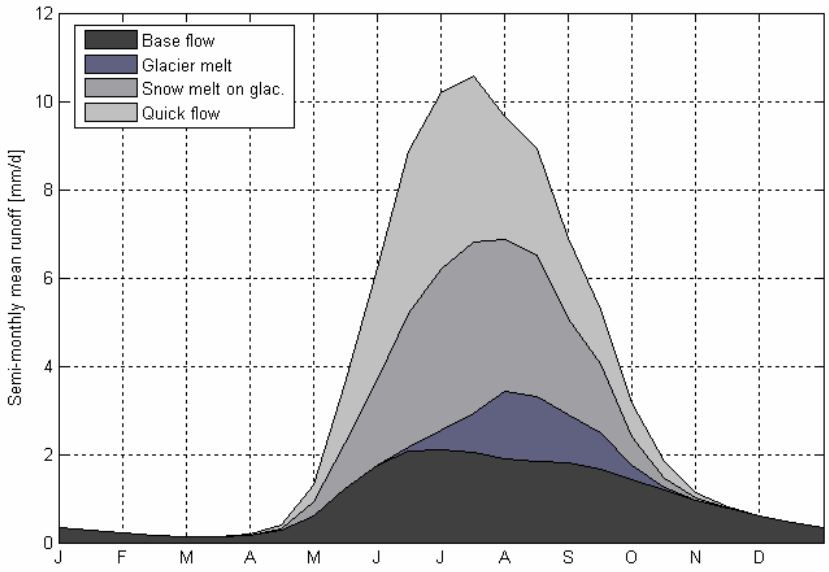

Fig. AX.5: Hydrograph components for the control period (1961-1990)

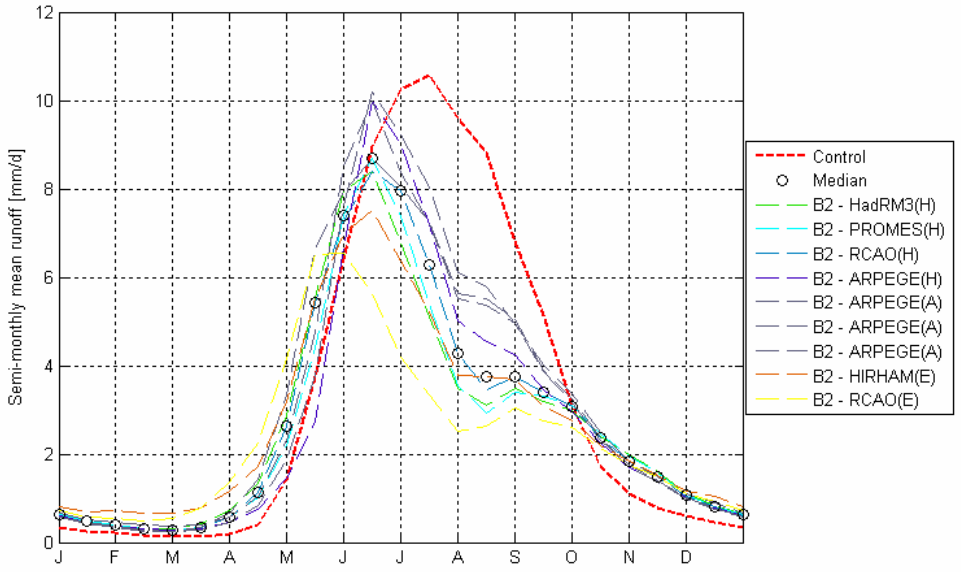

Fig. AX.7: Changes in hydrological regime for 2070-2099 – B2 scenario

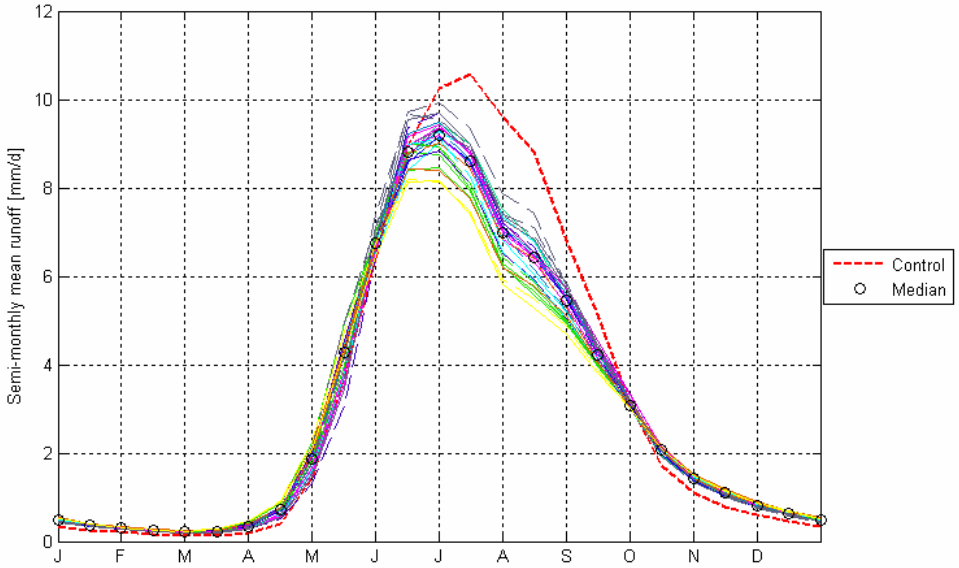

Fig. AX.6: Changes in hydrological regime for 1 ℃ global mean warming (scaled from A2 and B2 PRUDENCE experiments)

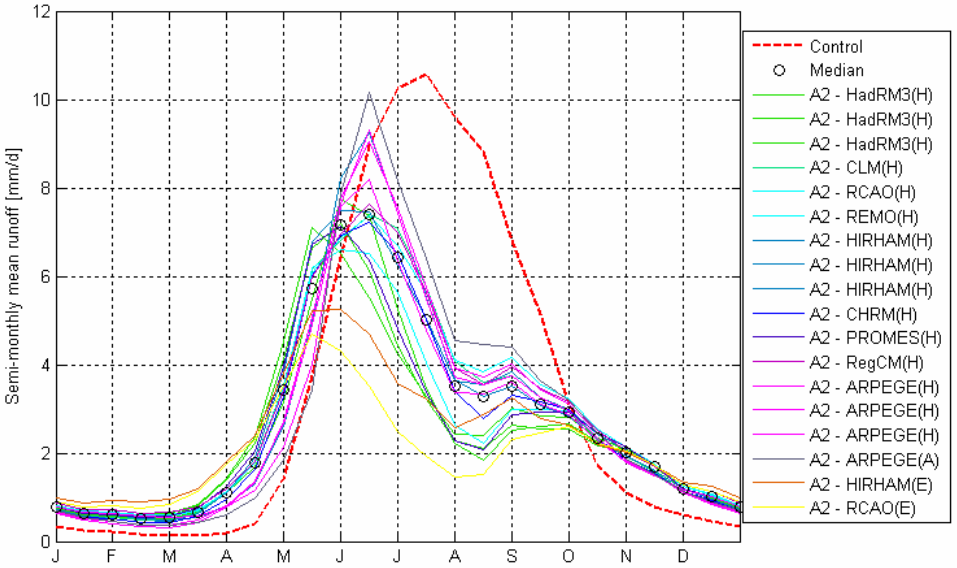

Fig. AX.8: Changes in hydrological regime for 2070-2099 – A2 scenario

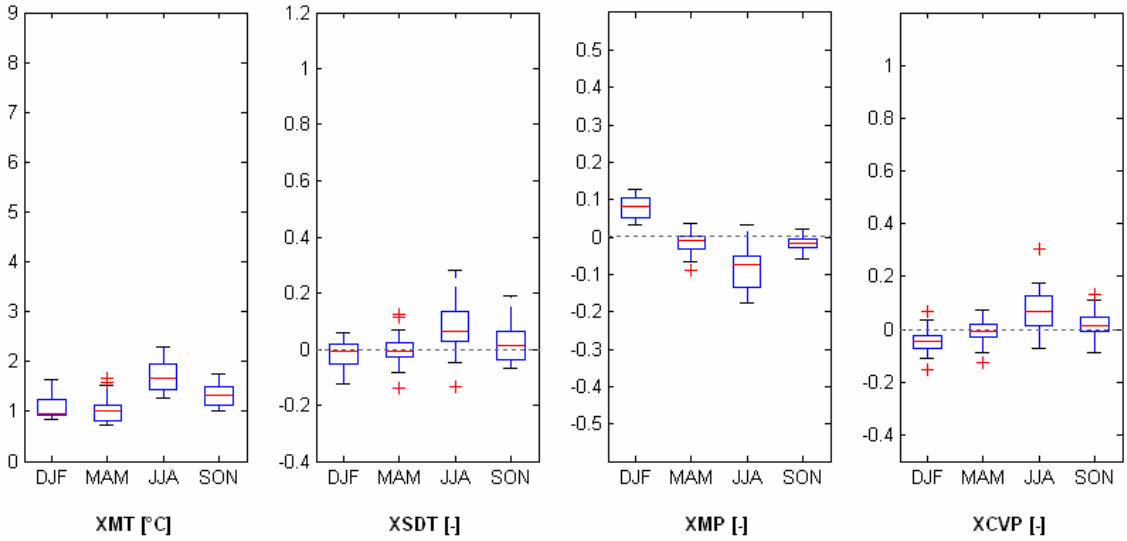

Fig. AX.9: Box plots of regional seasonal changes for 1 °C global mean warming (2020-2049) (scaled from A2 and B2 PRUDENCE experiments)

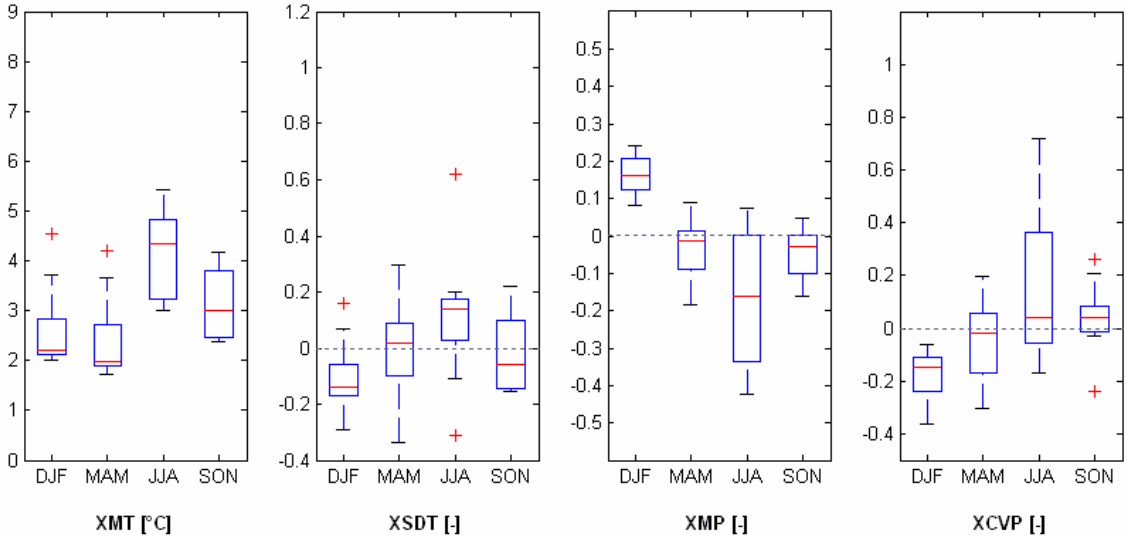

Fig. AX.10: Box plots of regional seasonal changes predicted by PRUDENCE RCM experiments for 2070-2099 – B2 scenario

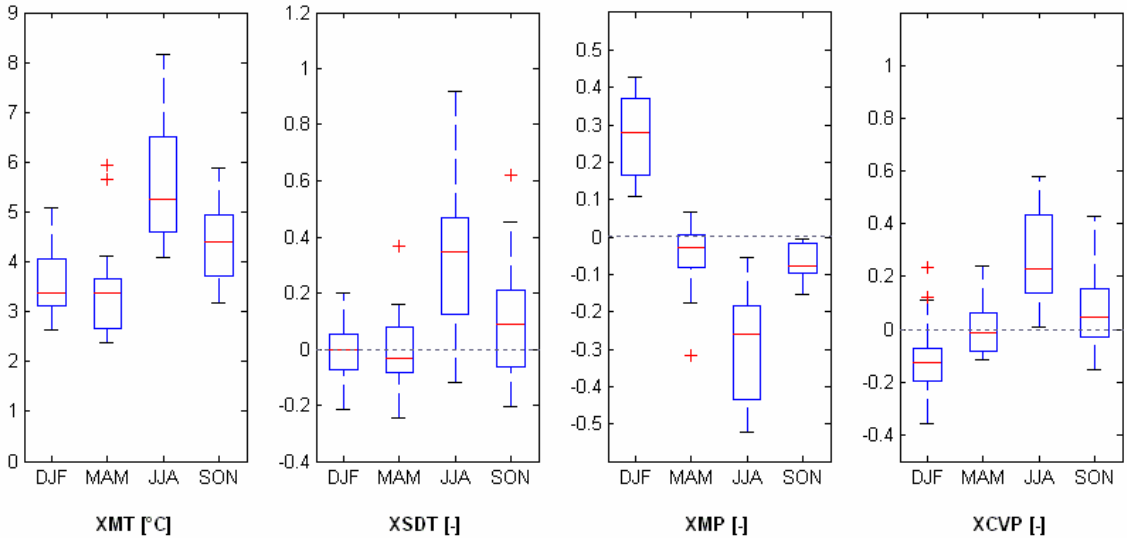

Fig. AX.11: Box plots of regional seasonal changes predicted by PRUDENCE RCM experiments for 2070-2099 – A2 scenario

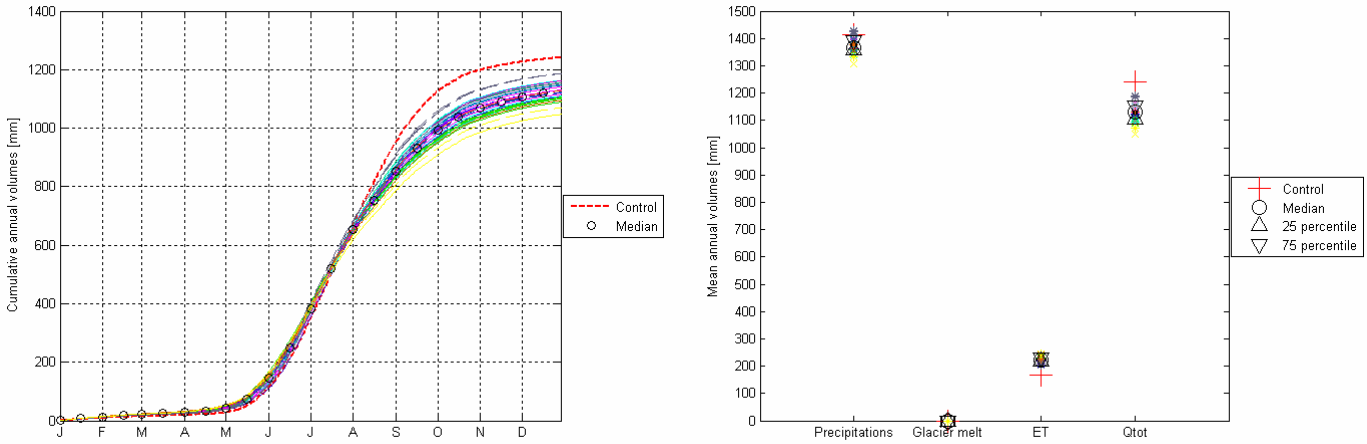

Fig. AX.12: Cumulative mean flow and water balance components for 1 °C global mean warming (2020-2049) (see Fig. AX.13 and Fig. AX.14 for colors meaning)

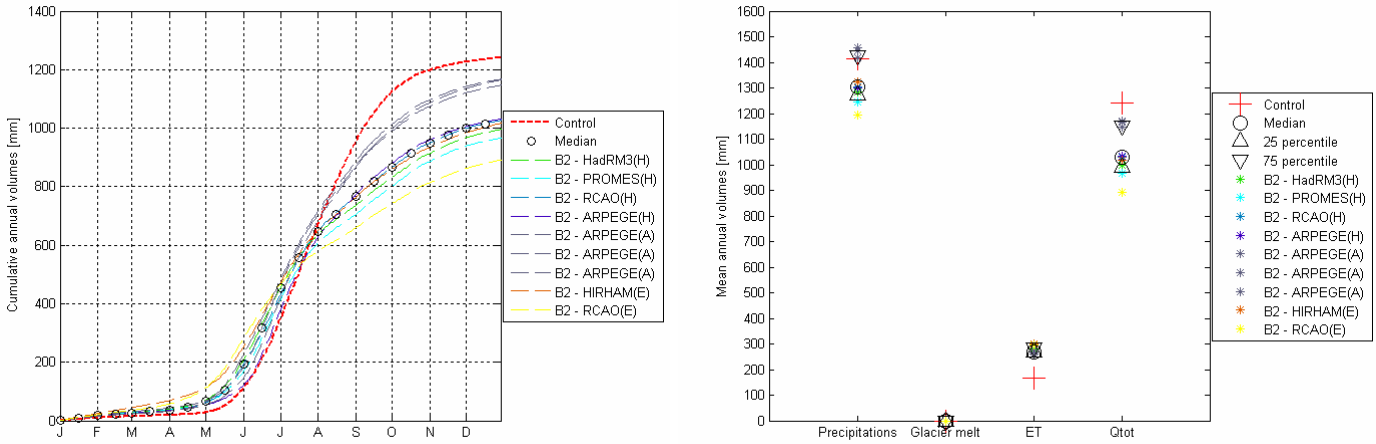

Fig. AX.13: Cumulative mean flow and water balance components for 2070-2099 – B2 scenario

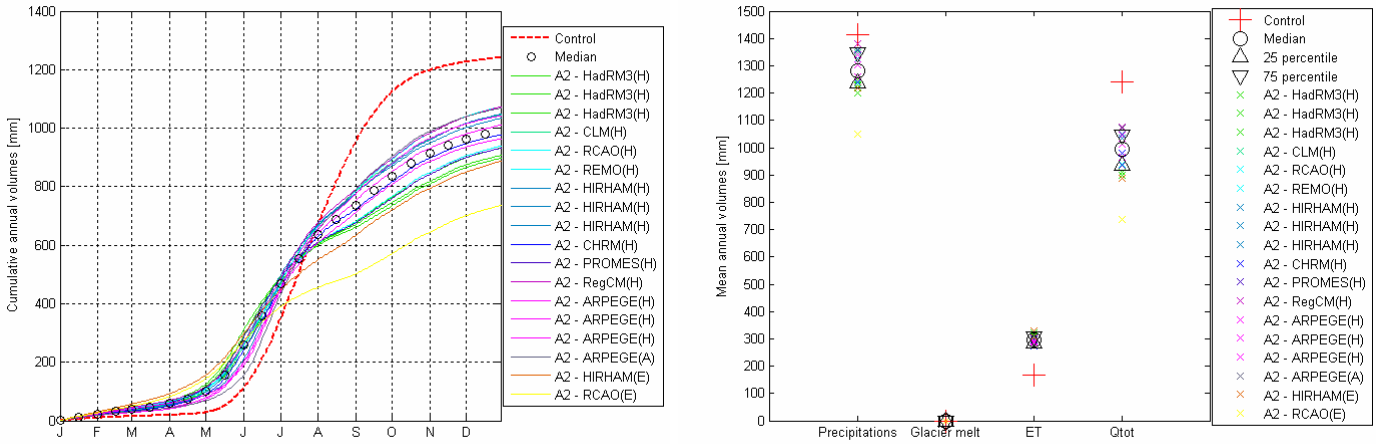

Fig. AX.14: Cumulative mean flow and water balance components for 2070-2099 – A2 scenario

Appendix 11 : The Verzasca catchment

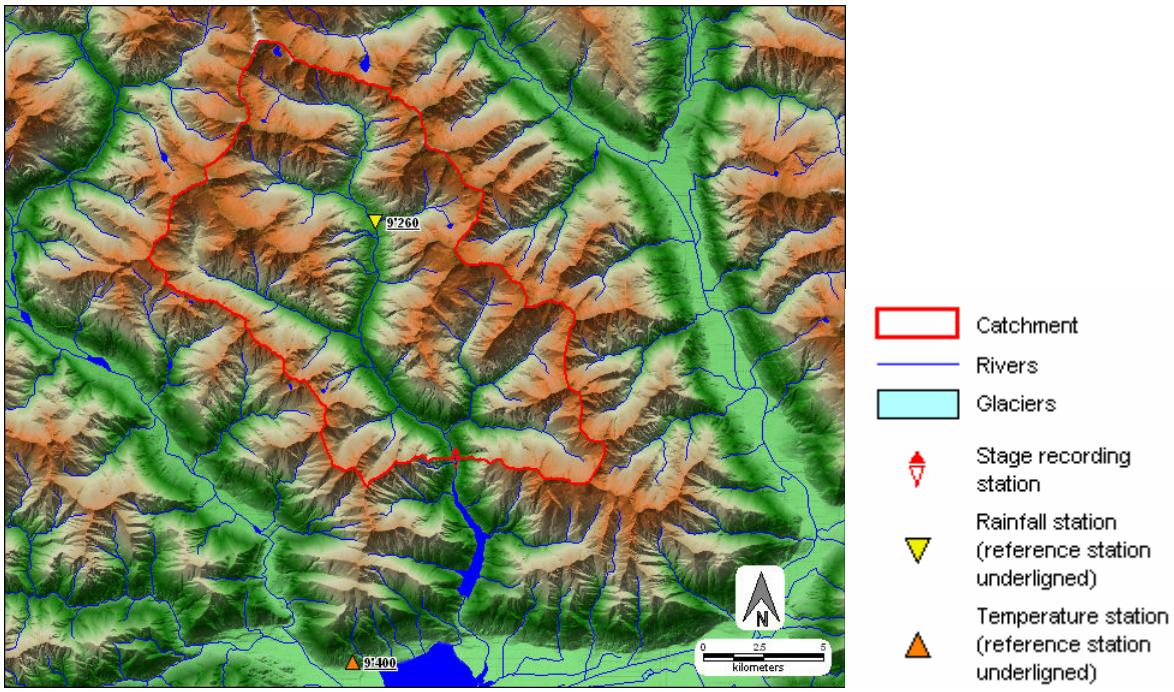

Fig. AXI.1: Catchment situation

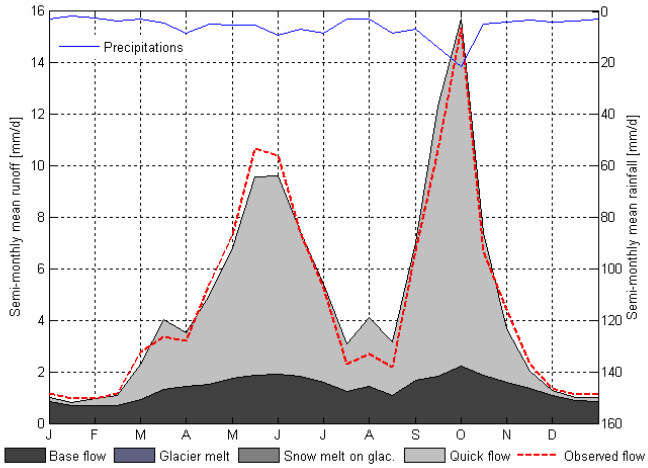

Fig. AXI.2: Calibration – Semi-monthly cycle for 1990-1996

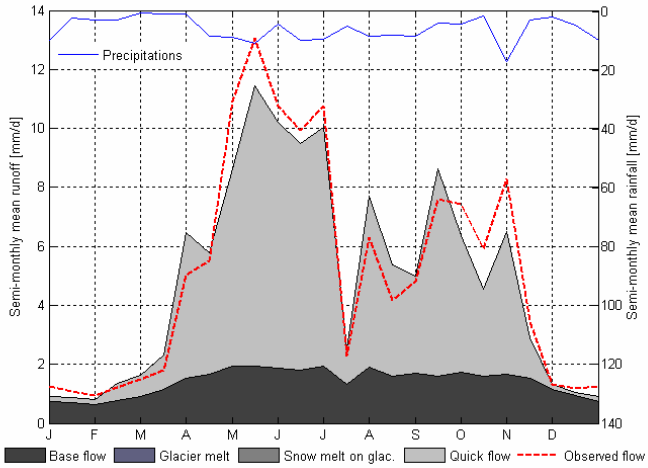

Fig. AXI.3: Validation – Semi-monthly cycle for 1996-2000

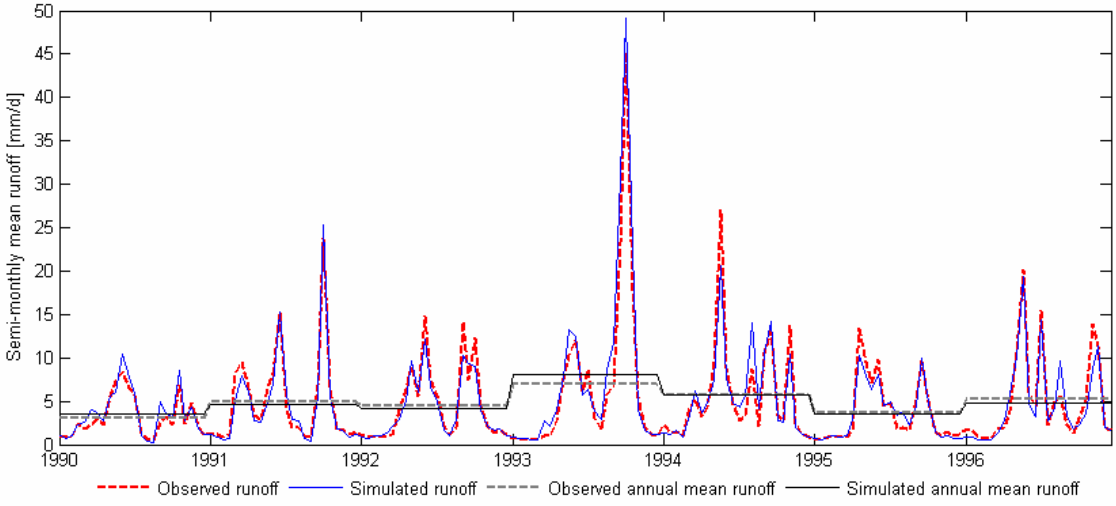

Fig. AXI.4: Calibration – Semi-monthly mean flow for 1990-1996

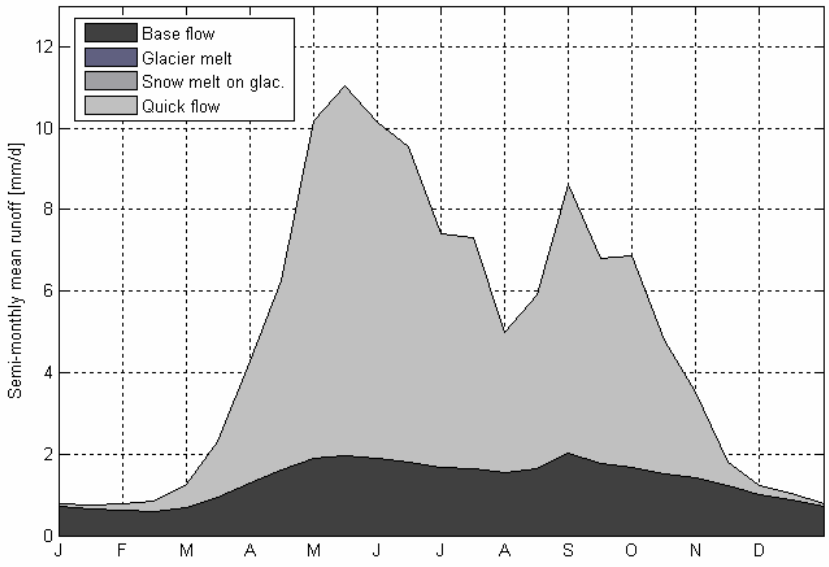

Fig. AXI.5: Hydrograph components for the control period (1961-1990)

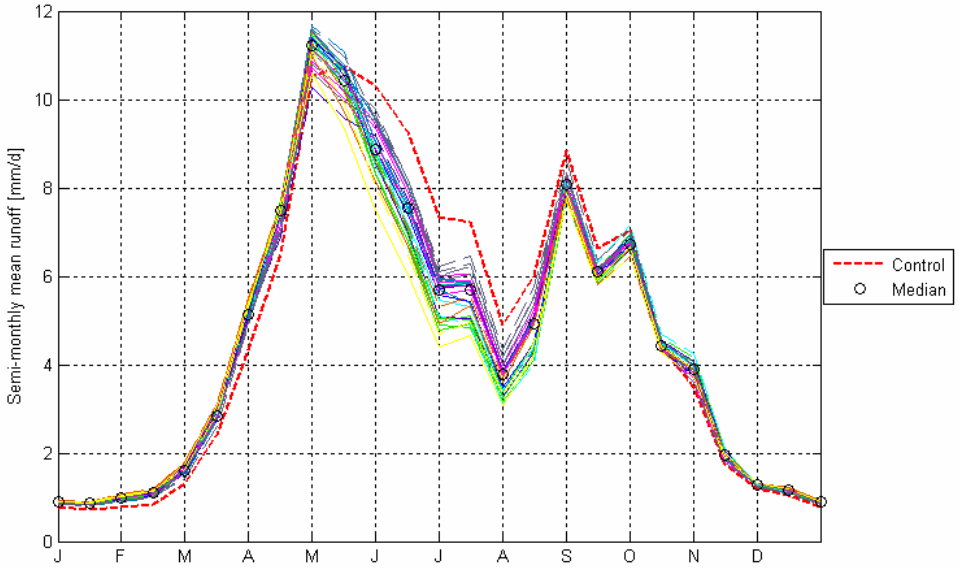

Fig. AXI.6: Changes in hydrological regime for 1°C global mean warming (scaled from A2 and B2 PRUDENCE experiments)

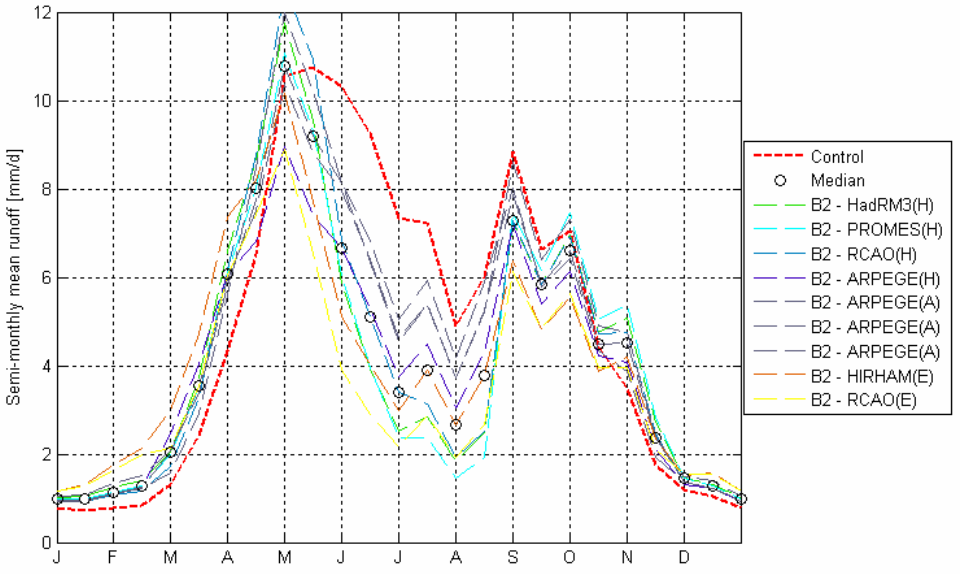

Fig. AXI.7: Changes in hydrological regime for 2070-2099 – B2 scenario

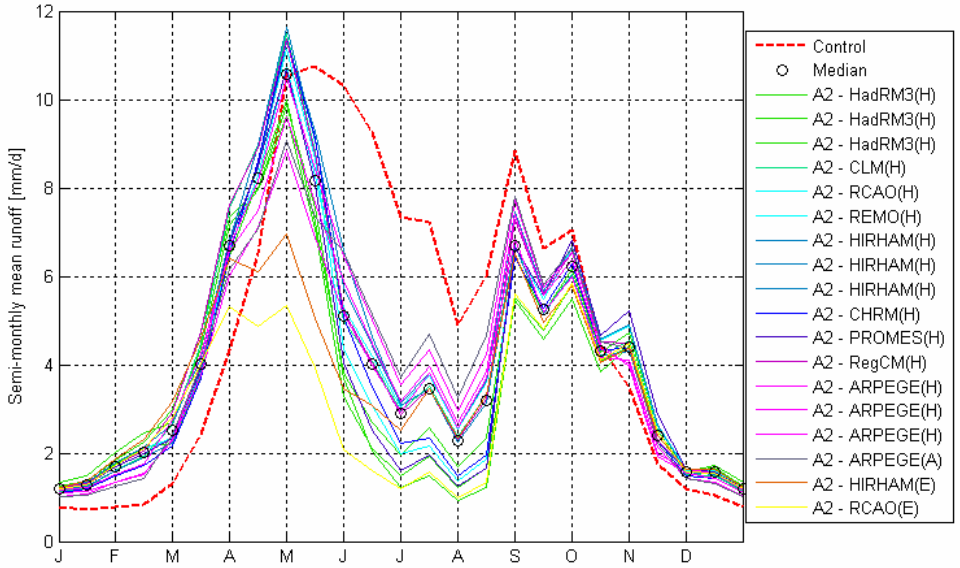

Fig. AXI.8: Changes in hydrological regime for 2070-2099 – A2 scenario

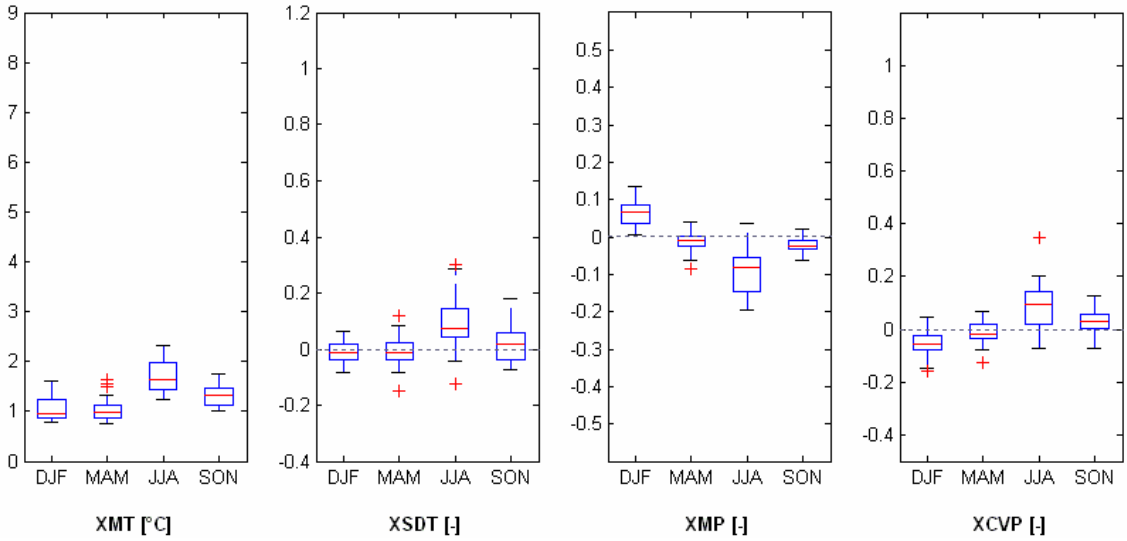

Fig. AXI.9: Box plots of regional seasonal changes for 1 °C global mean warming (2020-2049) (scaled from A2 and B2 PRUDENCE experiments)

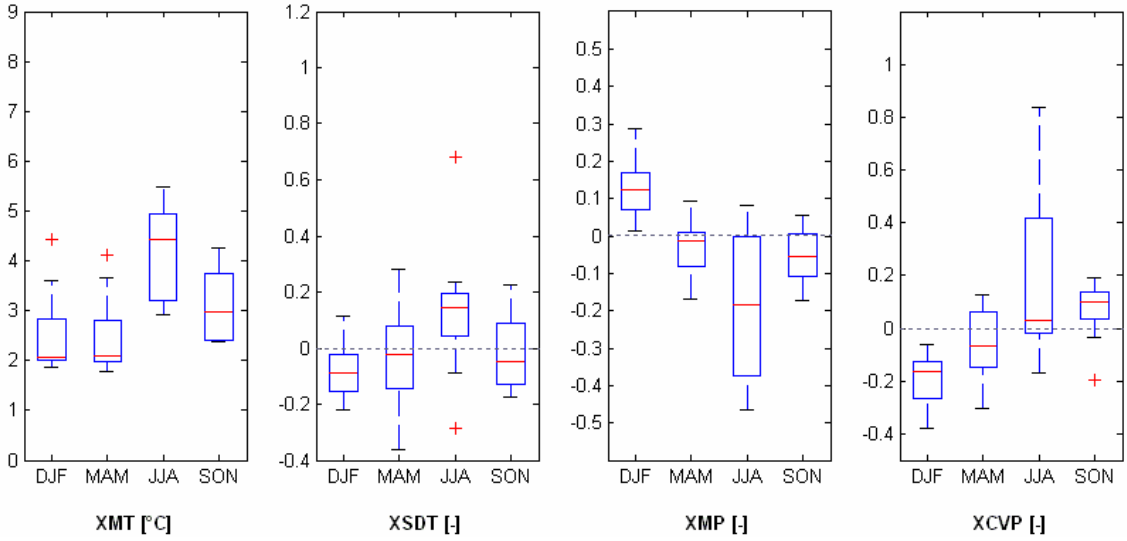

Fig. AXI.10: Box plots of regional seasonal changes predicted by PRUDENCE RCM experiments for 2070-2099 – B2 scenario

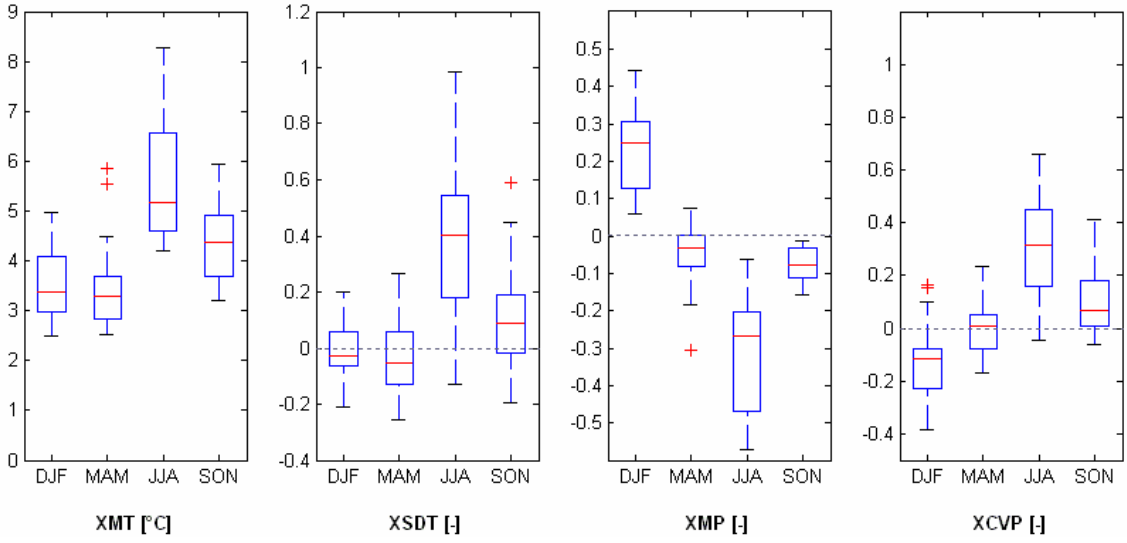

Fig. AXI.11: Box plots of regional seasonal changes predicted by PRUDENCE RCM experiments for 2070-2099 – A2 scenario

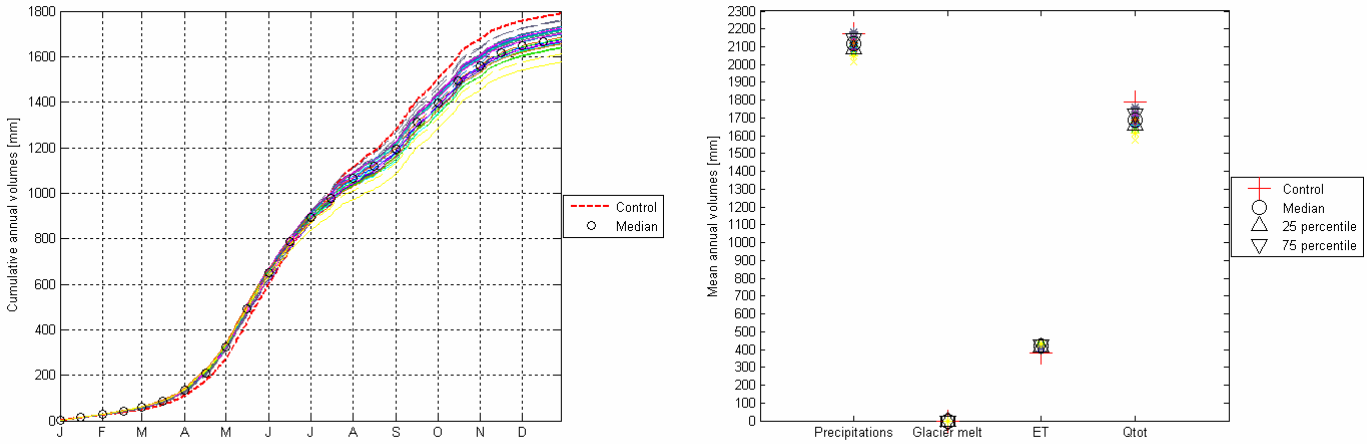

Fig. AXI.12: Cumulative mean flow and water balance components for 1°C global mean warming (2020-2049) (see Fig. AXI.13 and Fig. AXI.14 for colors meaning)

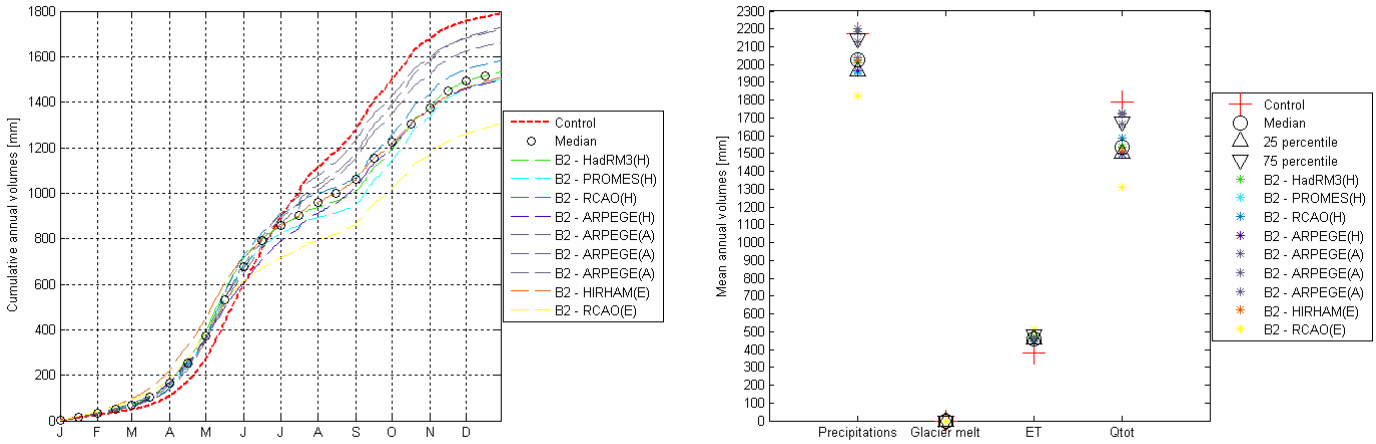

Fig. AXI.13: Cumulative mean flow and water balance components for 2070-2099 – B2 scenario

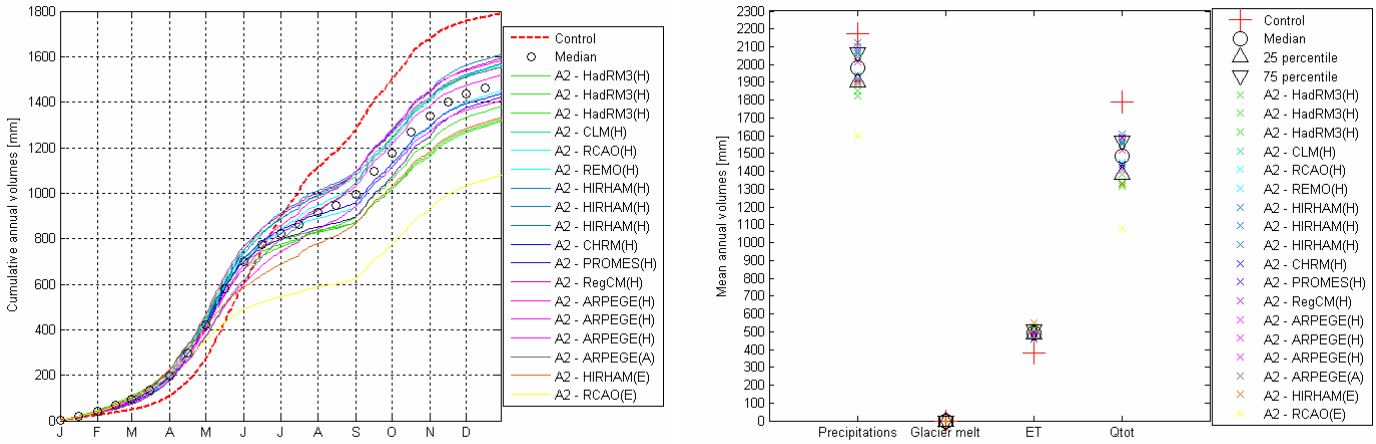

Fig. AXI.14: Cumulative mean flow and water balance components for 2070-2099 – A2 scenario